

Volume of Appendices

for

Development and Demonstration of a New Non-Equilibrium Rate-Based Process Model for the Hot Potassium Carbonate Process

by

Su Ming Pamela Ooi

Thesis submitted for the degree of
Doctor of Philosophy

in

The University of Adelaide
School of Chemical Engineering

July 2008

Table of Contents

Appendix A: Thermodynamic Model Equations	A-1
A.1 Reference States	A-2
A.2 The Electrolyte NRTL Model	A-3
A.3 Cubic Equations of State	A-8
Appendix B: Property Models for Aspen Custom Modeler®	A-10
B.1 Thermodynamic Property Models	A-11
B.2 Physical and Transport Property Models	A-17
Appendix C: Electrolyte NRTL Adjustable Parameters	A-38
C.1 Parameter Values	A-39
C.2 Data Regression Procedure	A-41
C.3 Data Regression Results	A-44
Appendix D: Aspen Custom Modeler® Simulation Results	A-49
D.1 The Different Modelling Approaches	A-50
D.2 Model Adjustments	A-52
D.3 CO ₂ Train Model Validation	A-56
Appendix E: Hypothetical K ₂ CO ₃ * HYSYS® Component Properties	A-62
E.1 Base Properties	A-63
E.2 Additional Point Properties	A-66
E.3 Temperature Dependent Properties	A-67
Appendix F: Property Models for HYSYS®	A-70
F.1 Thermodynamic Property Models	A-71
F.2 Physical and Transport Property Models	A-72
Appendix G: Enhanced PR Binary Interaction Parameters	A-84
G.1 Data Regression Procedure	A-85
G.2 Data Regression Results	A-87
Appendix H: HYSYS® Simulation Results	A-88
H.1 Preliminary Column Model Simulations	A-89
H.2 Steady-State CO ₂ Train Models	A-95
H.3 CO ₂ Train Model Validation	A-101
Appendix I: Process Control Studies of the CO ₂ Trains	A-107
I.1 Selection of Diagonal Control Structure	A-108
I.2 Selection of Diagonal Control Structure Configuration	A-111
I.3 Analysis of Diagonal Control Structure Performance	A-114
I.4 BLT Tuning	A-115
I.5 Diagonal Control Structure Dynamic Simulations	A-117

List of Figures

Figure B.1.1:	Comparison between the predicted and experimental solution heat capacities.	A-16
Figure B.2.1:	Comparison between the predicted and experimental solution mass densities.	A-20
Figure B.2.2:	Comparison between the predicted and experimental solution viscosities.	A-25
Figure B.2.3:	Comparison between the predicted and experimental solution surface tensions.	A-28
Figure B.2.4:	Comparison between the predicted and experimental solution thermal conductivities.	A-33
Figure D.1.1:	Results of the different modelling approaches for CO ₂ trains #2 to #4.	A-50
Figure D.1.2:	Results of the different modelling approaches for CO ₂ trains #5 and #6.	A-51
Figure D.2.1:	Temperature profiles for CO ₂ trains #2 to #4.	A-52
Figure D.2.2:	Temperature profiles for CO ₂ trains #5 and #6.	A-53
Figure D.2.3:	Effect of the effective interfacial area adjustment factor on the absorber CO ₂ and H ₂ S vapour phase profiles.	A-55
Figure D.3.1:	CO ₂ and H ₂ S vapour and liquid phase column profiles for the first set of plant data.	A-56
Figure D.3.2:	CO ₂ and H ₂ S vapour and liquid phase column profiles for the first set of plant data.	A-57
Figure D.3.3:	CO ₂ and H ₂ S vapour and liquid phase column profiles for the second set of plant data.	A-58
Figure D.3.4:	CO ₂ and H ₂ S vapour and liquid phase column profiles for the second set of plant data.	A-59
Figure D.3.5:	Column temperature profiles for the first set of plant data.	A-60
Figure D.3.6:	Column temperature profiles for the second set of plant data.	A-61
Figure F.2.1:	Comparison between the predicted and experimental solution mass densities.	A-74
Figure F.2.2:	Comparison between the predicted and experimental solution viscosities.	A-77
Figure F.2.3:	Comparison between the solution surface tensions predicted by the tabular model and the empirical correlation.	A-79
Figure F.2.4:	Comparison between the solution thermal conductivities predicted by the tabular model and the empirical correlation.	A-83
Figure H.1.1:	Equilibrium stage simulation results for the absorber and regenerator columns.	A-89
Figure H.1.2:	Equilibrium stage simulation results for the absorber and regenerator columns.	A-90
Figure H.1.3:	Effect of the correlated overall stage efficiencies on the steady-state absorber columns.	A-91
Figure H.1.4:	Effect of the correlated overall stage efficiencies on the steady-state absorber columns.	A-92

Figure H.1.5:	Effect of the correlated overall stage efficiencies on the steady-state behaviour of the dynamic absorber columns.	A-93
Figure H.1.6:	Effect of the correlated overall stage efficiencies on the steady-state behaviour of the dynamic absorber columns.	A-94
Figure H.2.1:	Process flow diagram for the steady-state model of CO ₂ train #2.	A-96
Figure H.2.2:	Process flow diagram for the steady-state model of CO ₂ train #3.	A-97
Figure H.2.3:	Process flow diagram for the steady-state model of CO ₂ train #4.	A-98
Figure H.2.4:	Process flow diagram for the steady-state model of CO ₂ train #5.	A-99
Figure H.2.5:	Process flow diagram for the steady-state model of CO ₂ train #6.	A-100
Figure H.3.1:	CO ₂ and H ₂ S vapour and liquid phase column profiles for the first set of plant data.	A-101
Figure H.3.2:	CO ₂ and H ₂ S vapour and liquid phase column profiles for the first set of plant data.	A-102
Figure H.3.3:	CO ₂ and H ₂ S vapour and liquid phase column profiles for the second set of plant data.	A-103
Figure H.3.4:	CO ₂ and H ₂ S vapour and liquid phase column profiles for the second set of plant data.	A-104
Figure H.3.5:	Column temperature profiles for the first set of plant data.	A-105
Figure H.3.6:	Column temperature profiles for the second set of plant data.	A-106
Figure I.5.1:	CO ₂ train #1 closed-loop step response curves at the medium gas throughput conditions.	A-121
Figure I.5.2:	CO ₂ train #7 closed-loop step response curves at the medium gas throughput conditions.	A-122
Figure I.5.3:	CO ₂ train #1 closed-loop step response curves at the low gas throughput conditions.	A-123
Figure I.5.4:	CO ₂ train #7 closed-loop step response curves at the low gas throughput conditions.	A-124

List of Tables

Table B.1.1:	Component critical properties (Poling et al., 2001).	A-11
Table B.1.2:	Ideal gas heat capacity coefficients and enthalpies of formation (Poling et al., 2001).	A-12
Table B.1.3:	Ionic species thermodynamic properties (Zemaitis et al., 1986).	A-15
Table B.1.4:	Temperature dependence of Henry's Law constants.	A-15
Table B.1.5:	Criss-Cobble entropy parameters (Criss and Cobble, 1964ab).	A-16
Table B.1.6:	Atmospheric solution heat capacity data.	A-16
Table B.1.7:	Parameter values for the Aspen Properties® heat capacity polynomial.	A-16
Table B.2.1:	Antoine equation coefficients (Rowley et al., 1998).	A-17
Table B.2.2:	Parameter values for the modified Rackett equation (Spencer and Danner, 1972).	A-19
Table B.2.3:	Atmospheric solution mass density data.	A-19
Table B.2.4:	Pair parameter values for the Clarke Aqueous Electrolyte Volume model.	A-19
Table B.2.5:	Component characteristic volumes.	A-21
Table B.2.6:	Coefficients for the DIPPR vapour viscosity model (Rowley et al., 1998).	A-23
Table B.2.7:	Coefficients for the Andrade liquid viscosity equation (Reid et al., 1977).	A-24
Table B.2.8:	Atmospheric solution viscosity data.	A-25
Table B.2.9:	Parameter values for the Jones-Dole viscosity equation.	A-25
Table B.2.10:	Coefficients for the DIPPR surface tension equation (Rowley et al., 1998).	A-27
Table B.2.11:	Atmospheric solution surface tension data.	A-28
Table B.2.12:	Surface tension correlation coefficients.	A-28
Table B.2.13:	Coefficients for the DIPPR vapour thermal conductivity model (Rowley et al., 1998).	A-30
Table B.2.14:	Coefficients for the DIPPR liquid thermal conductivity equation (Rowley et al., 1998).	A-32
Table B.2.15:	Atmospheric solution thermal conductivity data.	A-32
Table B.2.16:	Liquid phase thermal conductivity correlation coefficients.	A-32
Table B.2.17:	Normal boiling points and the corresponding liquid molar volumes (Poling et al., 2001).	A-35
Table B.2.18:	Ionic conductivities at infinite dilution.	A-37
Table B.2.19:	Diffusivities in water at 25°C.	A-37
Table C.1.1:	The Electrolyte NRTL adjustable parameters used in this work.	A-39
Table C.1.2:	The Electrolyte NRTL adjustable parameters used in this work.	A-40
Table C.3.1:	Statistical results for the CO ₂ -K ₂ CO ₃ -KHCO ₃ -H ₂ O system data regression runs.	A-45
Table C.3.2:	Suitable parameter value sets for the CO ₂ -K ₂ CO ₃ -KHCO ₃ -H ₂ O system.	A-46

Table C.3.3:	Statistical results for the CO ₂ -H ₂ S-K ₂ CO ₃ -KHCO ₃ -KHS-K ₂ S-H ₂ O system data regression runs.	A-47
Table C.3.4:	Suitable parameter value sets for the CO ₂ -H ₂ S-K ₂ CO ₃ -KHCO ₃ -KHS-K ₂ S-H ₂ O system.	A-48
Table D.2.1:	Alternative mass transfer coefficient and effective interfacial area correlations.	A-54
Table E.3.1:	Temperature dependent property correlation coefficients.	A-67
Table F.2.1:	Coefficient values for the HYSYS® liquid density tabular model.	A-73
Table F.2.2:	Coefficient values for the HYSYS® liquid viscosity tabular model.	A-77
Table F.2.3:	Coefficient values for the HYSYS® liquid surface tension tabular model.	A-79
Table F.2.4:	Coefficient values for the HYSYS® liquid thermal conductivity tabular model.	A-83
Table G.2.1:	Statistical results for the CO ₂ -K ₂ CO ₃ -H ₂ O system data regression runs.	A-87
Table G.2.2:	Statistical results for the CO ₂ -H ₂ S-K ₂ CO ₃ -H ₂ O system data regression runs.	A-87
Table I.2.1:	System poles and zeros for the SGC-RSF control structure.	A-111

APPENDIX A

THERMODYNAMIC MODEL EQUATIONS

This appendix presents the model equations for the thermodynamic models utilised in this thesis. A brief discussion of reference states is provided, followed by summaries of the Electrolyte NRTL model, the Soave-Redlich-Kwong equation of state and the Peng-Robinson equation of state.

A.1 Reference States

The difference between γ and γ^* arises from the different reference states for solvent species (i.e. water) and for solute species (e.g. CO₂). In this work, the reference state for solvents is taken to be the pure solvent species at the system temperature and pressure. This is known as the symmetric convention and it defines the activity coefficient γ_s of a solvent species s such that:

$$\gamma_s \rightarrow 1 \text{ as } x_s \rightarrow 1 \quad (\text{A.1.1})$$

where x_s is the liquid phase mole fraction of solvent species s .

For undissociated electrolytes, molecular solutes and ions, the reference state is the species at infinite dilution in pure water at the system temperature and pressure. According to this un-symmetric convention, which is denoted by an asterisk, the activity coefficient γ_j^* of a solute species j is defined so that:

$$\gamma_j^* \rightarrow 1 \text{ as } x_j \rightarrow 0 \quad (\text{A.1.2})$$

where x_j is the liquid phase mole fraction of solute species j .

The two conventions are related by:

$$\ln \gamma_j^* = \ln \gamma_j - \ln \gamma_j^\infty \quad (\text{A.1.3})$$

where γ_j^∞ is the symmetrically normalised activity coefficient of species j at infinite dilution. γ_j^∞ is achieved in the limit where the composition of species j approaches zero and all the remaining solute species k in the solution are set to zero:

$$\gamma_j^\infty = \lim_{\substack{x_j \rightarrow 0 \\ x_{k \neq j} = 0}} \gamma_j \quad (\text{A.1.4})$$

A.2 The Electrolyte NRTL Model

A summary of the theory behind the Electrolyte Non-Random Two-Liquid (NRTL) model is presented below. A more thorough discussion of the model theory and formulation can be found in the publications by Chen and co-workers (1982), Chen and Evans (1986) and Mock and co-workers (1986).

The Electrolyte NRTL model is an extension of the traditional NRTL model presented by Renon and Prausnitz (1968) for calculating liquid activity coefficients. This model is based on two fundamental assumptions (Chen et al., 1982):

1. The like-ion repulsion assumption: Due to the extremely large repulsive forces between ions of like charge, the local composition of cations around cations is zero and the local composition of anions around anions is zero.
2. The local electroneutrality assumption: The distribution of cations and anions around a central molecular species is such that the net local ionic charge is zero.

The excess Gibbs energy expression proposed by Chen and co-workers (1982) involves two types of contribution terms: one for the short-range local interactions around any central species and the other for the long-range ion-ion interactions. The short-range local contribution term is represented by the traditional NRTL model, while the long-range contribution term is represented by the un-symmetric Pitzer-Debye-Hückel (PDH) model. An un-symmetric Born correction term is applied to account for the effect of mixed solvents on the long-range contribution term. The expression for the un-symmetric excess Gibbs energy G^{E^*} is therefore:

$$\frac{G^{E^*}}{R \cdot T} = \frac{G^{E^*,PDH}}{R \cdot T} + \frac{G^{E^*,Born}}{R \cdot T} + \frac{G^{E^*,NRTL}}{R \cdot T} \quad (A.2.1)$$

where R is the gas constant and T is the absolute temperature. The un-symmetric activity coefficient is obtained from the partial differentiation of G^{E^*} with respect to the mole number n_j of species j :

$$R \cdot T \cdot \ln \gamma_j^* = \left[\frac{\partial (n_T \cdot G^{E^*})}{\partial n_j} \right]_{T,P,n_{k \neq j}} \quad (A.2.2)$$

where n_T is the total number of moles. Similarly, the symmetric activity coefficient γ_j for a species j is obtained from the partial differentiation of the symmetric excess Gibbs energy G^E :

$$R \cdot T \cdot \ln \gamma_j = \left[\frac{\partial (n_T \cdot G^E)}{\partial n_j} \right]_{T,P,n_{k \neq j}} \quad (A.2.3)$$

Substituting equation (A.2.2) into equation (A.2.1) gives the following expression for the un-symmetric activity coefficient:

$$\ln \gamma_j^* = \ln \gamma_j^{*,PDH} + \ln \gamma_j^{*,Born} + \ln \gamma_j^{*,NRTL} \quad (A.2.4)$$

For the Pitzer-Debye-Hückel model, the un-symmetric excess Gibbs energy is expressed as (Pitzer, 1980):

$$\frac{G^{E*,PDH}}{R \cdot T} = -\sum_j x_j \cdot \left(\frac{1000}{MW_{\text{solvent}}} \right)^{0.5} \cdot \frac{4 \cdot A_\phi \cdot I_x}{p} \cdot \ln(1 + p \cdot I_x^{0.5}) \quad (\text{A.2.5})$$

and the corresponding expression for the un-symmetric activity coefficient is:

$$\ln \gamma_j^{*,PDH} = -\left(\frac{1000}{MW_{\text{solvent}}} \right)^{0.5} \cdot A_\phi \cdot \left[\frac{2 \cdot z_j^2}{p} \cdot \ln(1 + p \cdot I_x^{0.5}) + \frac{z_j^2 \cdot I_x^{0.5} - 2 \cdot I_x^{1.5}}{1 + p \cdot I_x^{0.5}} \right] \quad (\text{A.2.6})$$

where MW is the molecular weight, x is the liquid phase mole fraction, p is the closest approach parameter, and z is the ionic charge. The Debye-Hückel parameter A_ϕ is defined as:

$$A_\phi = \frac{1}{3} \cdot \left(\frac{2 \cdot \pi \cdot N_o \cdot \rho_{\text{solvent}}}{1000} \right)^{0.5} \cdot \left(\frac{e^2}{\epsilon_{\text{solvent}} \cdot k \cdot T} \right)^{1.5} \quad (\text{A.2.7})$$

where N_o is Avogadro's number, ρ is the density, e is the charge of an electron, ϵ is the dielectric constant, and k is the Boltzmann constant. The mole fraction ionic strength I_x is defined as:

$$I_x = 0.5 \cdot \sum_j x_j \cdot z_j^2 \quad (\text{A.2.8})$$

In mixed solvents, there is a change of reference state due to the difference in dielectric constants. The un-symmetric Born correction term was introduced to maintain a reference state of infinite dilution in water for the ionic species (Mock et al., 1986). The Born excess Gibbs energy is defined as (Robinson and Stokes, 1965):

$$\frac{G^{E*,Born}}{R \cdot T} = \frac{e^2}{2 \cdot k \cdot T} \cdot \left(\frac{1}{\epsilon_{\text{solvent}}} - \frac{1}{\epsilon_{\text{H}_2\text{O}}} \right) \cdot \frac{\sum_j x_j \cdot z_j^2}{r_j} \cdot 10^{-2} \quad (\text{A.2.9})$$

and the corresponding un-symmetric activity coefficient is:

$$\ln \gamma_j^{*,Born} = \frac{e^2}{2 \cdot k \cdot T} \cdot \left(\frac{1}{\epsilon_{\text{solvent}}} - \frac{1}{\epsilon_{\text{H}_2\text{O}}} \right) \cdot \frac{z_j^2}{r_j} \cdot 10^{-2} \quad (\text{A.2.10})$$

where r is the Born radius. This correction accounts for the difference in Gibbs energies between ionic species in a mixed solvent and in water. Since the $\text{CO}_2\text{-H}_2\text{S-K}_2\text{CO}_3\text{-KHCO}_3\text{-KHS-K}_2\text{S-H}_2\text{O}$ system only involves a single solvent species, i.e. water, the Born terms have not been included in this work.

Unlike the above two long-range contribution terms, the short-range NRTL term is developed as a symmetric model and has to be normalised to obtain the un-symmetric model:

$$\frac{G^{E^*,\text{NRTL}}}{R \cdot T} = \frac{G^{E,\text{NRTL}}}{R \cdot T} - \sum_j x_j \cdot \ln \gamma_j^{\infty,\text{NRTL}} \quad (\text{A.2.11})$$

where $\gamma_j^{\infty,\text{NRTL}}$ is the symmetrically normalised NRTL activity coefficient at infinite dilution. The symmetric excess Gibbs energy is given as:

$$\begin{aligned} \frac{G^{E,\text{lc}}}{R \cdot T} = & \sum_m X_m \cdot \frac{\sum_j X_j \cdot G_{jm} \cdot \tau_{jm}}{\sum_k X_k \cdot G_{km}} \\ & + \sum_c X_c \cdot \sum_{a'} X_{a'} \cdot \frac{X_{a'}}{\sum_{a''} X_{a''}} \cdot \frac{\sum_j X_j \cdot G_{jc,a'c} \cdot \tau_{jc,a'c}}{\sum_k X_k \cdot G_{kc,a'c}} \\ & + \sum_a X_a \cdot \sum_{c'} X_{c'} \cdot \frac{X_{c'}}{\sum_{c''} X_{c''}} \cdot \frac{\sum_j X_j \cdot G_{ja,c'a} \cdot \tau_{ja,c'a}}{\sum_k X_k \cdot G_{ka,c'a}} \end{aligned} \quad (\text{A.2.12})$$

where

$$G_{jm} = \exp(-\alpha_{jm} \cdot \tau_{jm}) \quad G_{ca,m} = \exp(-\alpha_{ca,m} \cdot \tau_{ca,m}) \quad (\text{A.2.13})$$

$$G_{jc,ac} = \exp(-\alpha_{jc,ac} \cdot \tau_{jc,ac}) \quad G_{ja,ca} = \exp(-\alpha_{ja,ca} \cdot \tau_{ja,ca}) \quad (\text{A.2.14})$$

$$G_{cm} = \frac{\sum_a X_a \cdot G_{ca,m}}{\sum_{a'} X_{a'}} \quad G_{am} = \frac{\sum_c X_c \cdot G_{ca,m}}{\sum_{c'} X_{c'}} \quad (\text{A.2.15})$$

$$\tau_{mc,ac} = \tau_{cm} - \tau_{ca,m} + \tau_{m,ca} \quad \tau_{ma,ca} = \tau_{am} - \tau_{ca,m} + \tau_{m,ca} \quad (\text{A.2.16})$$

$$\alpha_{cm} = \frac{\sum_a X_a \cdot \alpha_{ca,m}}{\sum_{a'} X_{a'}} \quad \alpha_{am} = \frac{\sum_c X_c \cdot \alpha_{ca,m}}{\sum_{c'} X_{c'}} \quad (\text{A.2.17})$$

τ is the binary interaction energy parameter, and α is the non-randomness factor. The subscripts a, a', c, c', m and m' refer to anions, cations and molecular species, respectively, while the subscripts j and k refer to any species. The effective local mole fraction X_j of a species j is defined as:

$$X_j = x_j \cdot C_j \quad (\text{A.2.18})$$

where C_j is equal to z_j for ions and to 1 for molecular species.

The expressions for the symmetric NRTL activity coefficients are:

$$\begin{aligned}
 \ln \gamma_m^{\text{NRTL}} = & \frac{\sum_j X_j \cdot G_{jm} \cdot \tau_{jm}}{\sum_k X_k \cdot G_{km}} + \sum_{m'} \frac{X_{m'} \cdot G_{mm'}}{\sum_k X_k \cdot G_{km'}} \cdot \left(\tau_{mm'} - \frac{\sum_k X_k \cdot G_{km'} \cdot \tau_{km'}}{\sum_k X_k \cdot G_{km'}} \right) \\
 & + \sum_c \sum_{a'} \frac{X_{a'}}{\sum_{a''} X_{a''}} \cdot \frac{X_c \cdot G_{mc,a'c}}{\sum_k X_k \cdot G_{kc,a'c}} \left(\tau_{mc,a'c} - \frac{\sum_k X_k \cdot G_{kc,a'c} \cdot \tau_{kc,a'c}}{\sum_k X_k \cdot G_{kc,a'c}} \right) \\
 & + \sum_a \sum_{c'} \frac{X_{c'}}{\sum_{c''} X_{c''}} \cdot \frac{X_a \cdot G_{ma,c'a}}{\sum_k X_k \cdot G_{ka,c'a}} \left(\tau_{ma,c'a} - \frac{\sum_k X_k \cdot G_{ka,c'a} \cdot \tau_{ka,c'a}}{\sum_k X_k \cdot G_{ka,c'a}} \right)
 \end{aligned} \tag{A.2.19}$$

$$\begin{aligned}
 \frac{1}{z_c} \ln \gamma_c^{\text{NRTL}} = & \sum_m \frac{X_m \cdot G_{cm}}{\sum_k X_k \cdot G_{km}} \cdot \left(\tau_{cm} - \frac{\sum_k X_k \cdot G_{km} \cdot \tau_{km}}{\sum_k X_k \cdot G_{km}} \right) \\
 & + \sum_{a'} \frac{X_{a'}}{\sum_{a''} X_{a''}} \cdot \frac{\sum_k X_k \cdot G_{kc,a'c} \cdot \tau_{kc,a'c}}{\sum_k X_k \cdot G_{kc,a'c}} \\
 & + \sum_a \sum_{c'} \frac{X_{c'}}{\sum_{c''} X_{c''}} \cdot \frac{X_a \cdot G_{ca,c'a}}{\sum_k X_k \cdot G_{ka,c'a}} \left(\tau_{ca,c'a} - \frac{\sum_k X_k \cdot G_{ka,c'a} \cdot \tau_{ka,c'a}}{\sum_k X_k \cdot G_{ka,c'a}} \right)
 \end{aligned} \tag{A.2.20}$$

$$\begin{aligned}
 \frac{1}{z_a} \ln \gamma_a^{\text{NRTL}} = & \sum_m \frac{X_m \cdot G_{am}}{\sum_k X_k \cdot G_{km}} \cdot \left(\tau_{am} - \frac{\sum_k X_k \cdot G_{km} \cdot \tau_{km}}{\sum_k X_k \cdot G_{km}} \right) \\
 & + c \sum_{c'} \frac{X_{c'}}{\sum_{c''} X_{c''}} \cdot \frac{\sum_k X_k \cdot G_{ka,c'a} \cdot \tau_{ka,c'a}}{\sum_k X_k \cdot G_{ka,c'a}} \\
 & + \sum_c \sum_{a'} \frac{X_{a'}}{\sum_{a''} X_{a''}} \cdot \frac{X_c \cdot G_{ac,a'c}}{\sum_k X_k \cdot G_{kc,a'c}} \left(\tau_{ac,a'c} - \frac{\sum_k X_k \cdot G_{kc,a'c} \cdot \tau_{kc,a'c}}{\sum_k X_k \cdot G_{kc,a'c}} \right)
 \end{aligned} \tag{A.2.21}$$

When the solvent is pure water, the corresponding symmetrically normalised NRTL activity coefficients at infinite dilution are given by:

$$\ln \gamma_m^{\infty, \text{NRTL}} = \tau_{wm} + G_{wm} \cdot \tau_{wm} \tag{A.2.22}$$

$$\frac{1}{z_c} \ln \gamma_c^{\infty, \text{NRTL}} = G_{cw} \cdot \tau_{cw} + \frac{\sum_{a'} X_{a'} \cdot \tau_{wa,c'a}}{\sum_{a''} X_{a''}} \tag{A.2.23}$$

$$\frac{1}{z_a} \ln \gamma_a^{\infty, \text{NRTL}} = G_{aw} \cdot \tau_{aw} + \frac{\sum_{c'} X_{c'} \cdot \tau_{wc,a'c}}{\sum_{c''} X_{c''}} \tag{A.2.24}$$

where the subscript w refers to water. Following equation (A.1.3), the un-symmetric NRTL activity coefficients are calculated from:

$$\ln \gamma_m^{*,\text{NRTL}} = \ln \gamma_m^{\text{NRTL}} - \ln \gamma_m^{\infty,\text{NRTL}} \quad (\text{A.2.25})$$

$$\ln \gamma_c^{*,\text{NRTL}} = \ln \gamma_c^{\text{NRTL}} - \ln \gamma_c^{\infty,\text{NRTL}} \quad (\text{A.2.26})$$

$$\ln \gamma_a^{*,\text{NRTL}} = \ln \gamma_a^{\text{NRTL}} - \ln \gamma_a^{\infty,\text{NRTL}} \quad (\text{A.2.27})$$

In the absence of electrolytes, the Electrolyte NRTL model reduces to the NRTL model.

A.3 Cubic Equations of State

A.3.1 The Soave-Redlich-Kwong Equation of State

The pressure explicit form of the Soave-Redlich-Kwong (SRK) (Soave, 1972) cubic equation of state is:

$$P = \frac{R \cdot T}{V - b} - \frac{a}{V \cdot (V + b)} \quad (\text{A.3.1})$$

where P is the system pressure, V is the molar volume, T is the absolute system temperature, and R is the gas constant. In this work, the model parameters a and b are given by the classical mixing rules proposed by Redlich and Kwong (1949):

$$a = \sum_j \sum_k x_j \cdot x_k \cdot a_{jk} \cdot (1 - k_{jk}) \quad \text{with } k_{jk} = k_{kj} \text{ and } k_{jj} = 0 \quad (\text{A.3.2})$$

$$a_{jk} = (a_j \cdot a_k)^{0.5} \quad (\text{A.3.3})$$

$$a_j = 0.42748 \cdot \alpha_j \cdot \frac{R^2 \cdot T_{c,j}^2}{P_{c,j}} \quad (\text{A.3.4})$$

$$b = \sum_j x_j \cdot b_j \quad (\text{A.3.5})$$

$$b_j = 0.08664 \cdot \frac{R \cdot T_{c,j}}{P_{c,j}} \quad (\text{A.3.6})$$

where x is the mole fraction, k_{jk} is the binary interaction parameter for the component pair j - k , P_c is the critical pressure, and T_c is the critical temperature, while the function α_j is given by the expression proposed by Graboski and Daubert (1978):

$$\alpha_j = \left[1 + \left(0.48508 + 1.55171 \cdot \omega_j - 0.15613 \cdot \omega_j^2 \right) \cdot \left(1 - \left(\frac{T}{T_{c,j}} \right)^{0.5} \right) \right]^2 \quad (\text{A.3.7})$$

where ω is the acentricity.

The expression for the fugacity coefficient φ_j for the SRK equation of state is:

$$\begin{aligned} \ln \varphi_j = & \frac{b_j}{b} \cdot (Z - 1) - \ln \left(Z - \frac{P \cdot b}{R \cdot T} \right) \\ & - \frac{a}{b \cdot R \cdot T} \cdot \left(\frac{2}{a} \cdot \sum_k x_k \cdot a_{jk} \cdot (1 - k_{jk}) - \frac{b_j}{b} \right) \cdot \ln \left(1 + \frac{b}{V} \right) \end{aligned} \quad (\text{A.3.8})$$

where Z is the compressibility, which is represented by:

$$Z = \frac{P \cdot V}{R \cdot T} \quad (\text{A.3.9})$$

A.3.2 The Peng-Robinson Equation of State

The pressure explicit form of the Peng-Robinson (PR) (Peng and Robinson, 1976) cubic equation of state is:

$$P = \frac{R \cdot T}{V - b} - \frac{a}{V \cdot (V + b) + b \cdot (V - b)} \quad (\text{A.3.10})$$

where P is the system pressure, V is the molar volume, T is the absolute system temperature, and R is the gas constant. The parameters a and b are given by equations (A.3.2), (A.3.3) and (A.3.5) with the following component parameters a_j and b_j :

$$a_j = 0.457235 \cdot \alpha_j \cdot \frac{R^2 \cdot T_{c,j}^2}{P_{c,j}} \quad (\text{A.3.11})$$

$$b_j = 0.077796 \cdot \frac{R \cdot T_{c,j}}{P_{c,j}} \quad (\text{A.3.12})$$

where P_c is the critical pressure and T_c is the critical temperature, while α_j is given by:

$$\alpha_j = \left[1 + \left(0.37464 + 1.54226 \cdot \omega_j - 0.26992 \cdot \omega_j^2 \right) \cdot \left(1 - \left(\frac{T}{T_{c,j}} \right)^{0.5} \right) \right]^2 \quad (\text{A.3.13})$$

where ω is the acentricity. In HYSYS®, when $\omega > 0.49$, α_j is instead given by (Hyprotech Ltd, 2001a):

$$\alpha_j = \left[1 + \left(\begin{array}{l} 0.379642 + 1.48503 \cdot \omega_j \\ - 0.164423 \cdot \omega_j^2 + 1.016666 \cdot \omega_j^3 \end{array} \right) \cdot \left(1 - \left(\frac{T}{T_{c,j}} \right)^{0.5} \right) \right]^2 \quad (\text{A.3.14})$$

The expression for the fugacity coefficient φ_j for the PR equation of state is:

$$\ln \varphi_j = \frac{b_j}{b} \cdot (Z - 1) - \ln \left(Z - \frac{P \cdot b}{R \cdot T} \right) - \frac{a}{2^{1.5} \cdot b \cdot R \cdot T} \cdot \left(\frac{2}{a} \cdot \sum_k x_k \cdot a_{jk} \cdot (1 - k_{jk}) - \frac{b_j}{b} \right) \cdot \ln \left(\frac{V + (\sqrt{2} + 1) \cdot b}{V - (\sqrt{2} - 1) \cdot b} \right) \quad (\text{A.3.15})$$

where Z is the compressibility given by equation (A.3.9).

An enhanced version of the PR equation of state is the basis of the HYSYS® PR and Sour PR property packages. In the Sour PR property package, the enhanced PR equation of state is combined with the Wilson API-Sour Model (Wilson, 1980) for sour water systems. The vapour and liquid phase fugacities and the enthalpies for the vapour, liquid and aqueous phases are determined by the enhanced PR equation of state while the Wilson model accounts for the ionisation of CO_2 and H_2S in water via the aqueous phase K -values (Hyprotech Ltd, 2001a). In the absence of an aqueous phase, the Sour PR property package produces identical results to the PR property package.

APPENDIX B

PROPERTY MODELS FOR ASPEN CUSTOM MODELER®

This appendix presents the various thermodynamic and physical property models utilised in the Aspen Custom Modeler® process models for the CO₂ trains. Where necessary, model parameters are regressed from literature data.

B.1 Thermodynamic Property Models

B.1.1 Fugacity Coefficients

The fugacity coefficients used in this work were calculated from the Soave-Redlich-Kwong (SRK) equation of state, which is described in Section A.3.1 in Appendix A. This equation of state requires values for the component critical properties and the binary interaction parameters k_{jk} to provide an accurate representation of the vapour phase thermodynamics. The k_{jk} values were taken from the Aspen Properties® databanks, and the component critical properties used in this work are listed in Table B.1.1. Also given are values for the molecular weight MW, critical molar volume V_c , critical compressibility Z_c , acentricity ω , and dipole moment δ , of the components present in the raw natural gas to the Moomba CO₂ trains.

Table B.1.1: Component critical properties (Poling et al., 2001).

Component	MW (kg/kmol)	T_c (K)	P_c (bar)	V_c (cm ³ /mol)	Z_c	ω	δ (Debye)
CO ₂	44.010	304.20	73.74	93.94	0.2736	0.225	0.0
H ₂ S	34.082	373.20	89.63	98.60	0.2734	0.100	0.9
H ₂ O	18.015	647.30	220.64	55.90	0.2432	0.344	1.8
N ₂	28.014	126.20	33.98	89.64	0.2891	0.040	0.0
CH ₄	16.043	190.60	45.99	99.21	0.2882	0.008	0.0
C ₂ H ₆	30.070	305.40	48.72	148.17	0.2807	0.098	0.0
C ₃ H ₈	44.097	369.80	42.48	203.49	0.2765	0.152	0.0
n-C ₄ H ₁₀	58.123	425.20	37.96	254.92	0.2733	0.193	0.0
i-C ₄ H ₁₀	58.123	408.10	36.40	263.24	0.2754	0.176	0.1
n-C ₅ H ₁₂	72.150	469.60	33.70	303.16	0.2689	0.251	0.0
i-C ₅ H ₁₂	72.150	460.40	33.81	306.51	0.2725	0.227	0.1
n-C ₆ H ₁₄	86.177	507.40	30.25	369.44	0.2621	0.296	0.0
n-C ₇ H ₁₆	100.204	540.20	27.40	431.76	0.2612	0.351	0.0

B.1.2 Enthalpy and Heat Capacity Calculations

B.1.2.1 Vapour Phase Enthalpy and Heat Capacity

In this work, the vapour phase enthalpy h_G was calculated from the sum of the ideal gas enthalpies $h_{IG,j}$ of each vapour phase component and the residual enthalpy h_G^{res} :

$$h_G = \sum_{j=1}^{NC} y_j \cdot h_{IG,j} + h_G^{res} = \sum_{j=1}^{NC} y_j \cdot \left(\Delta h_{IG,j}^f + \int_{T_{ref}}^T C_{pIG,j} \cdot dT \right) + h_G^{res} \quad (B.1.1)$$

where Δh_{IG}^f is the ideal gas standard enthalpy of formation at the reference temperature T_{ref} (298.15 K), C_{pIG} is the ideal gas heat capacity, T is the absolute temperature, and NC is the number of vapour phase components. Coefficient values for the following ideal gas heat capacity polynomial equation (Poling et al., 2001):

$$\frac{C_{pIG}}{R} = A + B \cdot T + C \cdot T^2 + D \cdot T^3 + E \cdot T^4 \quad (B.1.2)$$

where the units of C_{pIG} depend on the value used for the gas constant R, were adapted to fit the Aspen Properties® Ideal Gas Heat Capacity polynomial (Aspen Technology Inc, 2003) which was used in this work:

$$C_{pIG} = C_1 + C_2 \cdot T + C_3 \cdot T^2 + C_4 \cdot T^3 + C_5 \cdot T^4 + C_6 \cdot T^5 \quad \text{for } C_7 < T < C_8 \quad (B.1.3)$$

Here, C_{pIG} is in kJ/kmol·K and T is in K. Table B.1.2 lists the coefficient values for equation (B.1.2), which are valid between 200 and 1000 K, along with values of $\Delta h_{IG,j}^f$.

The residual enthalpy h_G^{res} was defined according to the equation of state approach:

$$h_G^{res} = h_G - h_{IG} = R \cdot T \cdot (Z - 1) + \int_{\infty}^{V_G} \left[T \cdot \left(\frac{\partial P}{\partial T} \right)_{V_G} - P \right] \cdot dV_G \quad (B.1.4)$$

which in terms of the SRK equation of state is:

$$h_G^{res} = R \cdot T \cdot (Z - 1) - \frac{1}{b} \cdot \left(a - T \cdot \frac{da}{dT} \right) \cdot \ln \left(1 + \frac{b}{V_G} \right) \quad (B.1.5)$$

where Z is compressibility, V_G is the molar volume, and P is the pressure.

The vapour phase heat capacity C_{pG} was determined from the vapour phase enthalpy h_G :

$$C_{pG} = \left(\frac{dh_G}{dT} \right)_P \quad (B.1.6)$$

Table B.1.2: Ideal gas heat capacity coefficients and enthalpies of formation (Poling et al., 2001).

Component	A	$B \times 10^3$	$C \times 10^5$	$D \times 10^8$	$E \times 10^{11}$	Δh_{IG}^f (kJ/mol)
CO ₂	3.259	1.356	1.502	-2.374	1.056	-393.51
H ₂ S	4.266	-3.468	1.319	-1.331	0.488	-20.63
H ₂ O	4.395	-4.186	1.405	-1.564	0.632	-241.81
N ₂	3.539	-0.261	0.007	0.157	-0.099	0.00
CH ₄	4.568	-8.975	3.631	-3.407	1.091	-74.52
C ₂ H ₆	4.178	-4.427	5.660	-6.651	2.487	-83.82
C ₃ H ₈	3.847	5.131	6.011	-7.893	3.079	-104.68
n-C ₄ H ₁₀	5.547	5.536	8.057	-10.571	4.134	-125.79
i-C ₄ H ₁₀	3.351	17.883	5.477	-8.099	3.243	-134.99
n-C ₅ H ₁₂	7.554	-0.368	11.846	-14.939	5.753	-146.76
i-C ₅ H ₁₂	1.959	38.191	2.434	-5.175	2.165	-153.70
n-C ₆ H ₁₄	8.831	-0.166	14.302	-18.314	7.124	-166.92
n-C ₇ H ₁₆	9.634	4.156	15.494	-20.066	7.770	-187.80

B.1.2.2 Liquid Phase Enthalpy and Heat Capacity

In this work, the liquid phase enthalpy h_L was obtained from the mole-fraction-weighted sum of the liquid phase partial molar enthalpies $h_{L,j}$:

$$h_L = \sum_{j=1}^{NC} x_j \cdot h_{L,j} = \sum_{j=1}^{NC} x_j \cdot (h_{L,j}^{\text{ideal}} + h_{L,j}^{\text{ex}}) \approx \sum_{j=1}^{NC} x_j \cdot \left(h_{\text{aq},j}^{\text{ideal}} - R \cdot T^2 \cdot \left(\frac{\partial \ln \gamma_j^*}{\partial T} \right)_{P,x} \right) \quad (\text{B.1.7})$$

where x is the liquid phase mole fraction, NC is the number of liquid phase species, R is the gas constant, T is the system absolute temperature, γ^* is the species un-symmetric activity coefficient, and P is the system pressure. $h_{L,j}^{\text{ideal}}$ is the ideal partial molar enthalpy, which is approximated by the aqueous ideal partial molar enthalpy $h_{\text{aq},j}^{\text{ideal}}$ since $h_{\text{aq},j}^{\text{ideal}}$ is evaluated at the saturation pressure of water and not at the system pressure like $h_{L,j}^{\text{ideal}}$. A correction factor should be included to account for the enthalpy difference between the system pressure and the saturation pressure; however, at pressures below 100 bar, the pressure effect is minimal and can be ignored (Zemaitis et al., 1986). According to the un-symmetric reference state, $h_{\text{aq},j}^{\text{ideal}}$ refers to the partial molar enthalpy of pure solvent for the solvent H_2O and to the infinite dilution partial molar enthalpy for the solute species. The temperature derivative term represents the excess partial molar enthalpy $h_{L,j}^{\text{ex}}$, and was calculated from the Electrolyte NRTL model. For a detailed derivation of equation (B.1.7), please refer to the work by Zemaitis and co-workers (1986).

The aqueous ideal partial molar enthalpy $h_{\text{aq},\text{H}_2\text{O}}^{\text{ideal}}$ for H_2O was determined from the expression:

$$h_{\text{aq},\text{H}_2\text{O}}^{\text{ideal}} = \Delta h_{\text{IG},\text{H}_2\text{O}}^{\text{f}} + \int_{T_{\text{ref}}}^T C_{\text{plG},\text{H}_2\text{O}} \cdot dT + h_{\text{G},\text{H}_2\text{O}}^{\text{res}} - \Delta h_{\text{H}_2\text{O}}^{\text{vap}} \quad (\text{B.1.8})$$

where $\Delta h_{\text{IG},\text{H}_2\text{O}}^{\text{f}}$ is the ideal gas standard enthalpy of formation at the reference temperature T_{ref} (298.15 K), $C_{\text{plG},\text{H}_2\text{O}}$ is the ideal gas heat capacity, $h_{\text{G},\text{H}_2\text{O}}^{\text{res}}$ is the residual vapour enthalpy at the saturation pressure of water, and $\Delta h_{\text{H}_2\text{O}}^{\text{vap}}$ is the enthalpy of vaporisation at the saturation pressure of water. $\Delta h_{\text{H}_2\text{O}}^{\text{vap}}$ was obtained from the Watson equation (Reid et al., 1977):

$$\Delta h_{\text{H}_2\text{O}}^{\text{vap}} = \Delta h_{\text{H}_2\text{O}}^{\text{vap}}(T_1) \cdot \left(\frac{1 - T/T_{\text{c},\text{H}_2\text{O}}}{1 - T_1/T_{\text{c},\text{H}_2\text{O}}} \right)^{a+b} \left(1 - T/T_{\text{c},\text{H}_2\text{O}} \right) \quad (\text{B.1.9})$$

where $\Delta h_{\text{H}_2\text{O}}^{\text{vap}}$ is in kJ/kmol, $T_{\text{c,H}_2\text{O}}$ is the critical temperature of water in K, and T is the system temperature in K. The parameters T_1 , $\Delta h_{\text{H}_2\text{O}}^{\text{vap}}(T_1)$, a and b have the values 373.200 K, 40683.136 kJ/kmol, 0.311 and 0.000, respectively.

The infinite dilution aqueous ideal partial molar enthalpy $h_{\text{aq},j}^{\text{ideal}}$ for a solute species j was expressed as:

$$h_{\text{aq},j}^{\text{ideal}} = \Delta h_{\text{aq},j}^{\text{f}\infty} + \int_{T_{\text{ref}}}^T C_{\text{paq},j}^{\infty} \cdot dT \quad \text{for ionic solutes} \quad (\text{B.1.10})$$

$$h_{\text{aq},j}^{\text{ideal}} = \Delta h_{\text{IG},j}^{\text{f}} + \int_{T_{\text{ref}}}^T C_{\text{plG},j} \cdot dT - R \cdot T^2 \cdot \frac{d \ln H_j}{dT} \quad \text{for molecular solutes} \quad (\text{B.1.11})$$

where $\Delta h_{\text{aq},j}^{\text{f}\infty}$ is the aqueous infinite dilution standard enthalpy of formation at T_{ref} , $C_{\text{paq},j}^{\infty}$ is the aqueous infinite dilution heat capacity, $\Delta h_{\text{IG},j}^{\text{f}}$ is the ideal gas standard enthalpy of formation at T_{ref} , $C_{\text{plG},j}$ is the ideal gas heat capacity, and H_j is the Henry's Law constant at infinite dilution in water at the system temperature T . Table B.1.3 presents literature values for $\Delta h_{\text{aq},j}^{\text{f}\infty}$, and Table B.1.4 lists coefficients for determining H_j at temperatures between 25 and 150°C.

Criss and Cobble (1964ab) developed the following correlation for calculating the aqueous infinite dilution heat capacities $C_{\text{paq},j}^{\infty}$ for any ionic species j :

$$C_{\text{paq},j}^{\infty} \Big|_{25}^T = \frac{S_{T,j}^{\infty} - S_{25,j}^{\infty}}{\ln\left(\frac{T + 273.15}{298.15}\right)} \quad \text{for } j = \text{H}_3\text{O}^+ \quad (\text{B.1.12})$$

$$C_{\text{paq},j}^{\infty} \Big|_{25}^T = \frac{a_{T,j} + (b_{T,j} - 1) \cdot (S_{25,j}^{\infty} - 20.934 \cdot z_j)}{\ln\left(\frac{T + 273.15}{298.15}\right)} \quad \text{for } j \neq \text{H}_3\text{O}^+ \quad (\text{B.1.13})$$

where $C_{\text{paq},j}^{\infty} \Big|_{25}^T$ is the average value of $C_{\text{paq},j}^{\infty}$ in kJ/kmol·K between 25°C and temperature T in °C, $S_{T,j}^{\infty}$ is the infinite dilution entropy in kJ/kmol·K at T , and z_j is the ionic charge. Values for $S_{25,j}^{\infty}$ are given in Table B.1.3, while Table B.1.5 lists the temperature dependent values for $S_{T,\text{H}_3\text{O}^+}^{\infty}$ and the parameters $a_{T,j}$ and $b_{T,j}$.

Aspen Properties® also provided a polynomial for calculating $C_{\text{paq},j}^{\infty}$ (Aspen Technology Inc, 2003):

$$C_{\text{paq},j}^{\infty} = C_{1,j} + C_{2,j} \cdot T + C_{3,j} \cdot T^2 + \frac{C_{4,j}}{T} + \frac{C_{5,j}}{T^2} + \frac{C_{6,j}}{\sqrt{T}} \quad (\text{B.1.14})$$

where $C_{paq,j}^{\infty}$ is in kJ/kmol·K and T is in K. However, parameter values for the CO_3^{2-} , HCO_3^- and HS^- ions were missing from the Aspen Properties® databanks. These values had to be regressed from the literature data in Table B.1.6 using the Aspen Properties® DRS, and are listed in Table B.1.7. There was no available heat capacity data for potassium bisulfide solutions, so the parameter values for the HS^- ion were set such that the polynomial predicted the same value for the infinite dilution heat capacity at 25°C as the Criss-Cobble correlation. Figure B.1.1 compares the solution heat capacities predicted by the Aspen Properties® polynomial against the literature values. The average absolute deviation was 2.3%, compared to 10.7% for the heat capacities predicted by the Criss-Cobble correlation. Consequently, the Aspen Properties® polynomial was used in this work.

The liquid phase heat capacity C_{pL} was determined from the liquid phase enthalpy h_L :

$$C_{pL} = \left(\frac{dh_L}{dT} \right)_P \quad (B.1.15)$$

Table B.1.3: Ionic species thermodynamic properties (Zemaitis et al., 1986).

Species	$\Delta h_{aq,j}^{f\infty} \times 10^{-4}$ (kJ/kmol)	$S_{25,j}^{\infty}$ (kJ/kmol·K)
H_3O^+	-28.583	69.910
K^+	-25.238	102.50
OH^-	-22.999	-10.750
HCO_3^-	-69.199	91.200
CO_3^{2-}	-67.714	-56.900
HS^-	-1.760	62.800
S^{2-}	3.310	-14.600

Table B.1.4: Temperature dependence of Henry's Law constants.

Component	A	B	C	D
	$\ln H = A + \frac{B}{T} + C \cdot \ln T + D \cdot T$		H in bar, T in K	
CO_2^a	159.1997	-8477.711	-21.9574	0.00578075
H_2S^b	346.6251	-13236.800	-55.0551	0.05956500
N_2^c	143.4487	-6832.880	-19.1622	0
CH_4^d	239.4526	-11999.000	-33.1160	0
$C_2H_6^d$	204.0936	-10500.000	-27.8321	0
$C_3H_8^d$	246.6016	-12650.000	-33.9873	0
$n-C_4H_{10}^d$	212.5476	-11000.700	-28.9762	0
$i-C_4H_{10}^d$	247.0126	-12650.000	-33.9873	0
$n-C_5H_{12}^d$	221.5876	-11000.600	-30.4489	0
$i-C_5H_{12}^d$	244.5856	-11999.100	-33.8838	0
$n-C_6H_{14}^d$	427.2776	-21850.000	-60.1168	0
$n-C_7H_{16}^d$	339.8506	-17500.000	-47.2333	0

^a Chen (1980) ^b Austgen and co-workers (1989) ^c modified from Fernández-Prini and co-workers (2003) ^d de Hemptinne and co-workers (2000)

Table B.1.5: Criss-Cobble entropy parameters (Criss and Cobble, 1964ab).

T (°C)	K ⁺		OH ⁻ , HS ⁻ , S ²⁻		HCO ₃ ⁻		CO ₃ ²⁻		H ₃ O ⁺ S _{T,j} [∞]
	a _{T,j}	b _{T,j}	a _{T,j}	b _{T,j}	a _{T,j}	b _{T,j}	a _{T,j}	b _{T,j}	
25	0.00	1.000	0.00	1.000	0.00	1.000	0.00	1.000	-20.92 ^a
60	16.32	0.955	-21.34	0.969	-56.49	1.380	-58.58	1.217	-10.46
100	43.09	0.876	-54.39	1.000	-126.79	1.894	-129.72	1.476	8.37
150	67.78	0.792	-89.12	0.989	-836.92	2.381	-194.17	1.687	27.20

^a This value is used in equation (B.1.12) instead of the value in Table B.1.3.

Table B.1.6: Atmospheric solution heat capacity data.

Solution	Concentration	CO ₂ Loading	Temperature Range
K ₂ CO ₃ ^a	2 – 50 wt% K ₂ CO ₃	-	30 – 130°C
KHCO ₃ ^a	4 – 20 wt% KHCO ₃	-	30 – 130°C
K ₂ CO ₃ -KHCO ₃ ^b	30 wt% equivalent K ₂ CO ₃	0.2 – 0.9	70 – 120°C

^a Aseyev and Zaytsev (1996) ^b UOP Gas Processing (1998)

Table B.1.7: Parameter values for the Aspen Properties® heat capacity polynomial.

Parameter	CO ₃ ²⁻		HCO ₃ ⁻		HS ⁻	
	Value ^a	Std. Dev.	Value ^a	Std. Dev.	Value ^a	Std. Dev.
CPAQO-1	0	0 ^b	0	0 ^b	0	0 ^b
CPAQO-2	-0.1047	0.0103	0.0528	0.0101	-0.8426	0 ^b
CPAQO-3	0	0 ^b	0	0 ^b	0	0 ^b
CPAQO-4	0	0 ^b	0	0 ^b	0	0 ^b
CPAQO-5	0	0 ^b	0	0 ^b	0	0 ^b
CPAQO-6	0	0 ^b	0	0 ^b	0	0 ^b

^a Heat capacity in kJ/kmol·K. ^b Parameter was fixed so no standard deviation was determined.

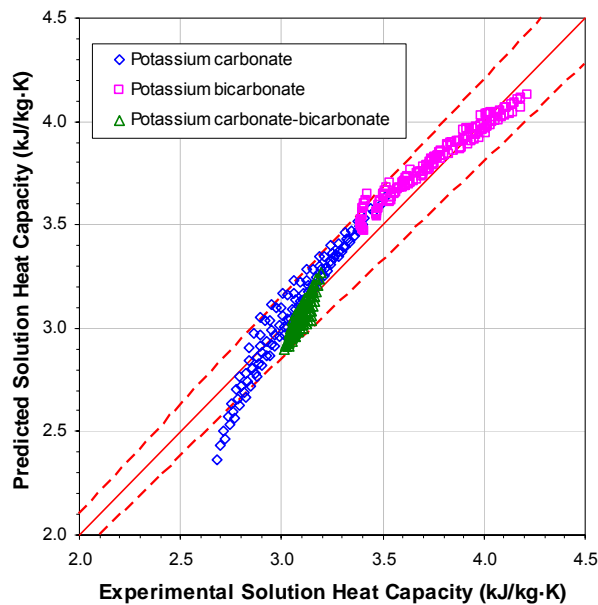


Figure B.1.1: Comparison between the predicted and experimental solution heat capacities. The dashed lines (---) represent the ± 5% lines.

B.2 Physical and Transport Property Models

B.2.1 Molecular Weight

In this work, the molecular weight MW of a phase was determined from the mole-fraction-weighted sums of the individual apparent component molecular weights:

$$MW = \sum_{j=1}^{NC} x_j \cdot MW_j \quad (\text{B.2.1})$$

where x is the apparent mole fraction and NC is the number of apparent components.

No ionic species were taken to exist in the vapour phase, so the vapour phase apparent composition was considered to be equivalent to its true composition. In the liquid phase, the speciation and chemical reactions occurring in the liquid phase were ignored and the apparent components were taken to be the vapour phase components and K_2CO_3 . The vapour phase component molecular weights are given in Table B.1.1 and the molecular weight of K_2CO_3 is 138.206 kg/kmol.

B.2.2 Vapour Pressure

The pure component vapour pressures P^s were calculated in this work using the extended Antoine equation (Rowley et al., 1998):

$$\ln P^s = A + \frac{B}{T} + C \cdot T + D \cdot \ln T + E \cdot T^F \quad (\text{B.2.2})$$

where P^s is in bar and T is the temperature in K. The relevant coefficients are listed in Table B.2.1.

Table B.2.1: Antoine equation coefficients (Rowley et al., 1998).

Component	A	B	$C \times 10^3$	D	$E \times 10^{16}$	F
CO ₂	61.3162	-3403.28	9.4907	-8.5603	2.9100	6
H ₂ S	41.2653	-3159.35	4.9926	-5.1255	0.6788	6
H ₂ O	61.0371	-7206.70	0.0000	-7.1385	4.0460×10^{10}	2
N ₂	34.6409	-984.20	23.2029	-5.4530	334.9000	6
CH ₄	31.8053	-1380.58	11.5868	-4.3964	29.1700	6
C ₂ H ₆	43.4743	-2636.62	8.5076	-5.8931	2.0660	6
C ₃ H ₈	52.0740	-3550.19	8.1898	-7.0923	0.7138	6
n-C ₄ H ₁₀	54.6370	-4301.38	6.5367	-7.2476	0.3449	6
i-C ₄ H ₁₀	51.0219	-4038.33	5.3553	-6.6422	0.4636	6
n-C ₅ H ₁₂	60.8701	-5140.97	6.1321	-8.0476	0.2090	6
i-C ₅ H ₁₂	46.3091	-4561.25	2.6262	-5.5986	0.2537	6
n-C ₆ H ₁₄	77.8480	-6285.04	8.4413	-10.6880	0.1319	6
n-C ₇ H ₁₆	77.0542	-6898.07	6.7102	-10.3076	0.1022	6

B.2.3 Density

B.2.3.1 Vapour Phase Density

The vapour phase molar density C_G is the inverse of the vapour phase molar volume V_G :

$$C_G = \frac{1}{V_G} \quad (\text{B.2.3})$$

which, in this work, was determined from the following form of the SRK equation of state:

$$V_G^3 - \frac{R \cdot T}{P} \cdot V_G^2 + \frac{a - b \cdot R \cdot T - P \cdot b^2}{P} \cdot V_G - \frac{a \cdot b}{P} = 0 \quad (\text{B.2.4})$$

where V_G is the largest positive real root. The vapour phase mass density ρ_G was calculated from C_G and vapour phase molecular weight MW_G :

$$\rho_G = C_G \cdot MW_G \quad (\text{B.2.5})$$

B.2.3.2 Liquid Phase Density

In this work, the liquid phase mass density ρ_L was determined from the relation:

$$\rho_L = C_L \cdot MW_L \quad (\text{B.2.6})$$

where MW_L is the liquid phase molecular weight and C_L is the liquid phase molar density, which was calculated from Amagat's Law (Aspen Technology Inc, 2003):

$$\frac{1}{C_L} = \sum_{j=1}^{NC} \frac{x_j}{C_{L,j}} \quad (\text{B.2.7})$$

where $C_{L,j}$ is the liquid phase molar density of component j , x is the liquid phase mole fraction, and NC is the number of liquid phase components.

The liquid phase molar densities of the solvent H_2O and the molecular solutes were obtained from the modified Rackett equation (Spencer and Danner, 1972):

$$\frac{1}{C_{L,j}} = \frac{R \cdot T_{c,j}}{P_{c,j}} \cdot Z_{RA,j} \left[1 + (1 - T/T_{c,j})^{2/7} \right] \quad (\text{B.2.8})$$

where R is the gas constant, T is the absolute temperature, T_c is the critical temperature, P_c is the critical pressure, and Z_{RA} is the Rackett parameter, for which values are presented in Table B.2.2. The liquid phase electrolyte molar densities $C_{L,ca}$ were calculated using the Clarke Aqueous Electrolyte Volume model (Chen et al., 1983):

$$\frac{1}{C_{L,ca}} = V_{ca}^{\infty} + A_{ca} \cdot \frac{\sqrt{x_{ca}}}{1 + \sqrt{x_{ca}}} \quad (\text{B.2.9})$$

where x_{ca} is the apparent electrolyte mole fraction for the electrolyte ca . Databank values for V_{ca}^{∞} and A_{ca} were available in Aspen Properties® for a number of cation-anion pairs, but not for the four key pairs of interest: (K^+, CO_3^{2-}) , (K^+, HCO_3^-) , (K^+, HS^-) and (K^+, S^{2-}) . Given the relatively negligible quantities of HS^- and S^{2-} ions present in the liquid phase for the process of interest, it was considered reasonable to neglect the effect of the (K^+, HS^-) and (K^+, S^{2-}) pairs on the liquid phase density. The parameter values for the (K^+, CO_3^{2-}) and (K^+, HCO_3^-) pairs were regressed from the literature data in Table B.2.3 using the Aspen Properties® DRS, and are presented in Table B.2.4. Figure B.2.1 compares the solution mass densities predicted by equations (B.2.6) to (B.2.9) against the literature values. The average absolute deviation between the predicted and literature values is 0.4%.

Table B.2.2: Parameter values for the modified Rackett equation (Spencer and Danner, 1972).

Component	Z_{RA}
CO ₂	0.2736
H ₂ S	0.2851
H ₂ O	0.2432
N ₂	0.2905
CH ₄	0.2876
C ₂ H ₆	0.2789
C ₃ H ₈	0.2763
n-C ₄ H ₁₀	0.2728
i-C ₄ H ₁₀	0.2750
n-C ₅ H ₁₂	0.2685
i-C ₅ H ₁₂	0.2716
n-C ₆ H ₁₄	0.2635
n-C ₇ H ₁₆	0.2611

Table B.2.3: Atmospheric solution mass density data.

Solution	Concentration	CO ₂ Loading	Temperature Range
K ₂ CO ₃ ^a	20 – 40 wt% K ₂ CO ₃	-	30 – 100°C
K ₂ CO ₃ ^b	20 – 40 wt% K ₂ CO ₃	-	30 – 90°C
KHCO ₃ ^b	1 – 30 wt% KHCO ₃	-	30 – 80°C
K ₂ CO ₃ –KHCO ₃ ^c	22 – 30 wt% K ₂ CO ₃ ^e	0 – 0.6	70 – 115°C
K ₂ CO ₃ –KHCO ₃ ^d	30 wt% K ₂ CO ₃ ^e	0 – 1	70 – 130°C

^a Armand Products Company (1998) ^b Chernen'kaya and Revenko (1975) ^c Bocard and Mayland (1962)
^d UOP Gas Processing (1998) ^e These concentrations are in terms of equivalent K₂CO₃ weight percent.

Table B.2.4: Pair parameter values for the Clarke Aqueous Electrolyte Volume model.

Parameter	Component j	Component k	Parameter Value ^a	Standard Deviation
V_{ca}^{∞}	K ⁺	CO ₃ ²⁻	0.007465	0.001818
V_{ca}^{∞}	K ⁺	HCO ₃ ⁻	0.018397	0.002006
A_{ca}	K ⁺	CO ₃ ²⁻	0.136841	0.009026
A_{ca}	K ⁺	HCO ₃ ⁻	0.077836	0.009483

^a Molar volume in m³/kmol.

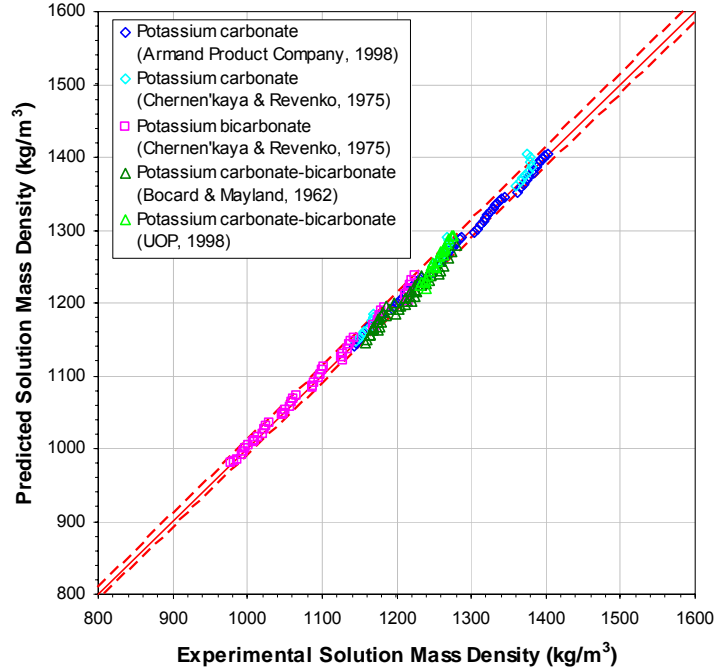


Figure B.2.1: Comparison between the predicted and experimental solution mass densities. The dashed lines (---) represent the $\pm 1\%$ lines.

B.2.3.3 Partial Molar Volume

The partial molar volume \bar{v}_j^∞ of a component j at infinite dilution in water is required to determine the effect of pressure on its Henry's Law constant. The method of Brelvi and O'Connell (1972) was used in this work to calculate \bar{v}_j^∞ :

$$\frac{\bar{v}_j^\infty}{Z_j^\circ \cdot R \cdot T} = 1 - C_{jw}^\circ \quad (\text{B.2.10})$$

where \bar{v}_j^∞ is in cm^3/mol , Z_j° is the isothermal compressibility at infinite dilution in water in $1/\text{atm}$:

$$\ln \left(1 + \frac{V_{L,H_2O}^s}{Z_j^\circ \cdot R \cdot T} \right) = -0.42704 \cdot (\tilde{v}_j - 1) + 2.089 \cdot (\tilde{v}_j - 1)^2 - 0.42367 \cdot (\tilde{v}_j - 1)^3 \quad (\text{B.2.11})$$

C_{jw}° is the reduced volume integral of component j at infinite dilution in water:

$$\ln \left(-C_{jw}^\circ \cdot \left(\frac{V_w^*}{V_j^*} \right)^{0.62} \right) = -2.4467 + 2.12074 \cdot \tilde{v}_j \quad \text{for } 2.0 \leq \tilde{v}_j \leq 2.785 \quad (\text{B.2.12})$$

$$\ln \left(-C_{jw}^\circ \cdot \left(\frac{V_w^*}{V_j^*} \right)^{0.62} \right) = 3.02214 - 1.87085 \cdot \tilde{v}_j + 0.71955 \cdot \tilde{v}_j^2 \quad \text{for } 2.785 \leq \tilde{v}_j \leq 3.2 \quad (\text{B.2.13})$$

T is the system temperature in K, R is the gas constant (82.06 atm·cm³/mol·K), V_{L,H_2O}^s is the liquid phase molar volume of water in at its saturation pressure in cm³/mol, v_j^* is the characteristic volume for which values are listed in Table B.2.5, and \tilde{v}_j is the dimensionless reduced molar volume:

$$\tilde{v}_j = \frac{v_j^*}{V_{L,H_2O}^s} \quad (\text{B.2.14})$$

Table B.2.5: Component characteristic volumes.

Component	v^* (cm ³ /mol)
CO ₂ ^a	93.94
H ₂ S ^a	88.74
H ₂ O ^a	46.40
N ₂ ^b	89.64
CH ₄ ^b	99.21
C ₂ H ₆ ^b	148.17
C ₃ H ₈ ^b	203.49
n-C ₄ H ₁₀ ^b	254.92
i-C ₄ H ₁₀ ^b	263.24
n-C ₅ H ₁₂ ^b	303.16
i-C ₅ H ₁₂ ^b	306.51
n-C ₆ H ₁₄ ^b	369.44
n-C ₇ H ₁₆ ^b	431.76

^a Austgen and co-workers (1989)

^b Zemaitiis and co-workers (1986)

B.2.4 Viscosity

B.2.4.1 Vapour Phase Viscosity

In this work, the vapour phase viscosity μ_G was determined in two steps. First, the low pressure vapour phase viscosity μ_G^{LP} was determined from the Wilke method (Wilke, 1950):

$$\mu_G^{LP} = \frac{\sum_{j=1}^{NC} y_j \cdot \mu_{G,j}^{LP}}{\sum_{k=1}^{NC} y_k \cdot \phi_{jk}} \quad (\text{B.2.15})$$

$$\phi_{jk} = \frac{\left[1 + \left(\frac{\mu_{G,j}^{LP}}{\mu_{G,k}^{LP}} \right)^{0.5} \cdot \left(\frac{MW_k}{MW_j} \right)^{0.25} \right]^2}{\left[8 \cdot \left(1 + \frac{MW_j}{MW_k} \right) \right]^{0.5}} \quad (\text{B.2.16})$$

where y_j and y_k are the vapour phase mole fractions of components j and k, $\mu_{G,j}^{LP}$ and $\mu_{G,k}^{LP}$ are the component low pressure vapour phase viscosities, MW_j and MW_k are the component molecular

weights, and NC is the number of vapour phase components. The Dean-Stiel pressure correction (Dean and Stiel, 1965) was then applied to μ_G^{LP} to give μ_G :

$$\mu_G - \mu_G^{LP} = \frac{1.08 \times 10^{-4}}{\xi} \cdot \left(e^{1.439 \cdot V_{c,G}/V_G} - e^{-1.111 \cdot (V_{c,G}/V_G)^{1.858}} \right) \quad (B.2.17)$$

$$\xi = \frac{T_{c,G}^{1/6}}{MW_G^{1/2} \cdot P_{c,G}^{2/3}} \quad (B.2.18)$$

where μ_G and μ_G^{LP} are in cP, MW_G is the vapour phase molecular weight in kg/kmol, V_G is the vapour phase molar volume, $V_{c,G}$ is the vapour phase critical molar volume, $T_{c,G}$ is the vapour phase critical temperature in K, and $P_{c,G}$ is the vapour phase critical pressure in atm. The vapour phase critical properties were obtained as follows:

$$V_{c,G} = \sum_{j=1}^{NC} y_j \cdot V_{c,j} \quad (B.2.19)$$

$$T_{c,G} = \sum_{j=1}^{NC} y_j \cdot T_{c,j} \quad (B.2.20)$$

$$Z_{c,G} = \sum_{j=1}^{NC} y_j \cdot Z_{c,j} \quad (B.2.21)$$

$$P_{c,G} = \frac{Z_{c,G} \cdot R \cdot T_{c,G}}{V_{c,G}} \quad (B.2.22)$$

where R is the gas constant, $Z_{c,G}$ is the vapour phase critical compressibility, and $V_{c,j}$, $T_{c,j}$ and $Z_{c,j}$ are the component critical molar volume, temperature and compressibility, respectively.

The component low pressure vapour phase viscosities $\mu_{G,j}^{LP}$ were calculated using the DIPPR vapour viscosity model (Rowley et al., 1998):

$$\mu_{G,j}^{LP} = \frac{A \cdot T^B}{1 + C/T + D/T^2} \quad (B.2.23)$$

where $\mu_{G,j}^{LP}$ is in cP and T is the system temperature in K. The relevant coefficients are given in Table B.2.6.

Table B.2.6: Coefficients for the DIPPR vapour viscosity model (Rowley et al., 1998).

Component	$A \times 10^4$	$B \times 10^1$	$C \times 10^{-1}$	$D \times 10^{-4}$
CO ₂	21.4800	4.6000	29.0000	0
H ₂ S	0.5860	10.1680	37.2400	-6.4310
H ₂ O	6.1839	6.7779	84.7230	-7.3930
N ₂	6.5592	6.0810	5.4714	0
CH ₄	5.2546	5.9006	10.5670	0
C ₂ H ₆	2.5906	6.7988	9.8902	0
C ₃ H ₈	2.4993	6.8612	17.9340	-0.8255
n-C ₄ H ₁₀	2.2980	6.9442	22.7660	-1.4610
i-C ₄ H ₁₀	1.0871	7.8135	7.0639	0
n-C ₅ H ₁₂	0.6341	8.4758	4.1718	0
i-C ₅ H ₁₂	0.2434	9.7376	-9.1597	1.8720
n-C ₆ H ₁₄	1.7514	7.0737	15.7140	0
n-C ₇ H ₁₆	0.6672	8.2837	8.5752	0

B.2.4.2 Liquid Phase Viscosity

In this work, the liquid phase viscosity μ_L was determined from the Jones-Dole equation (Jones and Dole, 1929):

$$\mu_L = \mu_{L,\text{solvent}} \cdot \left(1 + \sum_{ca} \Delta\mu_{ca} \right) \quad (\text{B.2.24})$$

where $\mu_{L,\text{solvent}}$ is the viscosity of the solvent, which was determined from the mole-fraction-weighted sum of the component liquid viscosities $\mu_{L,j}$ for H₂O and any molecular species present in the liquid phase:

$$\mu_{L,\text{solvent}} = \sum_{j=1}^{NC} x_j \cdot \mu_{L,j} \quad (\text{B.2.25})$$

x is the liquid phase mole fraction and NC is the number of molecular species present in the liquid phase. The values of $\mu_{L,j}$ were calculated from the Andrade equation (Reid et al., 1977) with the coefficients given in Table B.2.7:

$$\ln \mu_{L,j} = A_j + \frac{B_j}{T} \quad (\text{B.2.26})$$

where $\mu_{L,j}$ is in cP and T is in K.

The contribution term $\Delta\mu_{ca}$ was determined using the Breslau-Miller equation (Breslau and Miller, 1972; Breslau et al., 1974):

$$\Delta\mu_{ca} = 2.5 \cdot V_e \cdot C_{L,ca} + 10.05 \cdot (V_e \cdot C_{L,ca})^2 \quad (\text{B.2.27})$$

where $C_{L,ca}$ is the molar concentration of the apparent electrolyte ca :

$$C_{L,ca} = x_{ca} \cdot C_L \quad (B.2.28)$$

V_e is the effective volume in L/mol:

$$V_e = \frac{B_{ca} - 0.002}{2.60} \quad \text{for electrolytes involving univalent ions} \quad (B.2.29)$$

$$V_e = \frac{B_{ca} - 0.011}{5.06} \quad \text{for other electrolytes} \quad (B.2.30)$$

$$B_{ca} = b_{c,1} + b_{c,2} \cdot T + b_{a,1} + b_{a,2} \cdot T \quad (B.2.31)$$

x_{ca} is the apparent electrolyte mole fraction, C_L is the liquid phase molar density, and T is the system absolute temperature.

Databank values for the parameters $b_{c,1}$, $b_{c,2}$, $b_{a,1}$ and $b_{a,2}$ were available in Aspen Properties® for a number of cations and anions, but not for the K^+ , HCO_3^- , CO_3^{2-} , HS^- and S^{2-} ions. Given the relatively negligible quantities of HS^- and S^{2-} ions present in the liquid phase for the process of interest, it was considered reasonable to neglect the effect of these two ions on the liquid phase viscosity. The parameter values for the K^+ , HCO_3^- and CO_3^{2-} ions were regressed from the literature data in Table B.2.8 using the Aspen Properties® DRS, and are given in Table B.2.9. Figure B.2.1 compares the solution viscosities predicted by equations (B.2.24) to (B.2.31) against the literature values. The average absolute deviation between the predicted and literature values is 3.1%.

Table B.2.7: Coefficients for the Andrade liquid viscosity equation (Reid et al., 1977).

Component	A	$B \times 10^{-2}$
CO ₂	-7.1857	13.3108
H ₂ S	-4.7681	7.8930
H ₂ O	-5.3527	15.1568
N ₂	-4.5064	2.0792
CH ₄	-4.5628	2.6282
C ₂ H ₆	-3.7730	3.6058
C ₃ H ₈	-3.8432	5.1272
n-C ₄ H ₁₀	-3.8210	6.1212
i-C ₄ H ₁₀	-4.0926	6.9656
n-C ₅ H ₁₂	-3.9579	7.2223
i-C ₅ H ₁₂	-4.4148	8.4579
n-C ₆ H ₁₄	-4.0338	8.3535
n-C ₇ H ₁₆	-4.3246	10.0561

Table B.2.8: Atmospheric solution viscosity data.

Solution	Concentration	CO ₂ Loading	Temperature Range
K ₂ CO ₃ ^a	20 – 40 wt% K ₂ CO ₃	-	35 – 90°C
K ₂ CO ₃ ^b	20 – 25 wt% K ₂ CO ₃	-	75 – 90°C
K ₂ CO ₃ ^c	28 – 40 wt% K ₂ CO ₃	-	30 – 60°C
K ₂ CO ₃ ^d	22 – 30 wt% K ₂ CO ₃	-	70 – 130°C
KHCO ₃ ^a	10 – 30 wt% KHCO ₃	-	35 – 75°C
K ₂ CO ₃ –KHCO ₃ ^e	30 wt% K ₂ CO ₃ ^f	0.6	70 – 130°C

^a Chernen'kaya and Revenko (1975) ^b Correia and co-workers (1980) ^c Gonçalves and Kestin (1981)
^d Bocard and Mayland (1962) ^e UOP Gas Processing (1998) ^f This concentration is in terms of equivalent K₂CO₃ weight percent .

Table B.2.9: Parameter values for the Jones-Dole viscosity equation.

Parameter	K ⁺		HCO ₃ ⁻		CO ₃ ²⁻	
	Value	Std. Dev.	Value	Std. Dev.	Value	Std. Dev.
b _{c,1} ^a	13.0705	4.7165	-	-	-	-
b _{c,2} ^b	-0.0295	0.0113	-	-	-	-
b _{a,1} ^a	-	-	-12.7297	4.7312	-25.1305	9.3835
b _{a,2} ^b	-	-	0.02893	0.01138	0.0576	0.0225

^a Parameter in m³/kmol. ^b Parameter in m³/kmol·K.

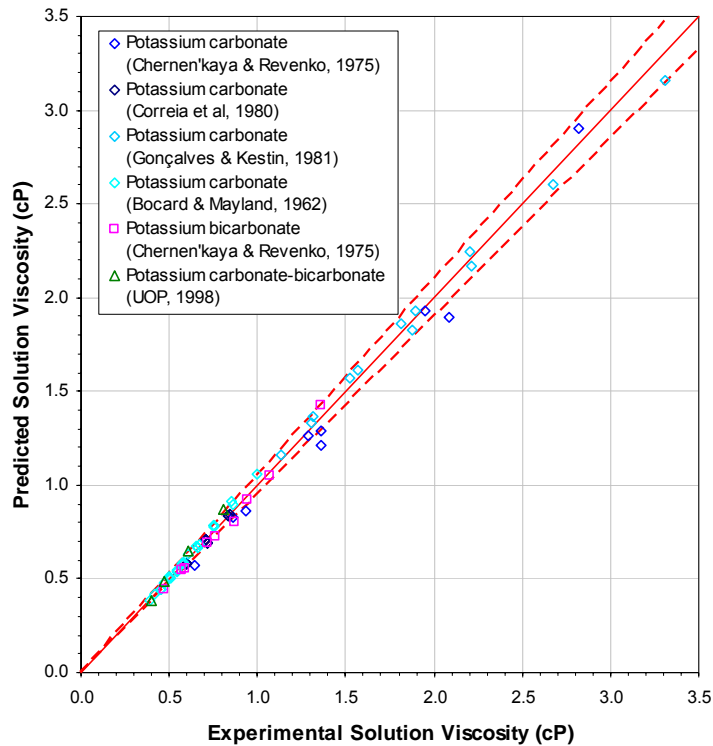


Figure B.2.2: Comparison between the predicted and experimental solution viscosities. The dashed lines (---) represent the ± 5% lines.

B.2.5 Surface Tension

In Aspen Properties®, the Onsager-Samaras model (Onsager and Samaras, 1934) is used to determine the liquid phase surface tension σ_L for an electrolyte system:

$$\sigma_L = \sigma_{L,\text{solvent}} + \sum_{ca} x_{ca} \cdot \Delta\sigma_{ca} \quad (\text{B.2.32})$$

where $\sigma_{L,\text{solvent}}$ is the surface tension of the solvent, which is determined from the mole-fraction-weighted sum of the component surface tensions $\sigma_{L,j}$ for H₂O and any molecular species present in the liquid phase:

$$\sigma_{L,\text{solvent}} = \sum_{j=1}^{NC} x_j \cdot \sigma_{L,j} \quad (\text{B.2.33})$$

x is the liquid phase mole fraction and NC is the number of molecular species present in the liquid phase. The component surface tensions $\sigma_{L,j}$ are calculated from the DIPPR surface tension equation (Rowley et al., 1998):

$$\sigma_{L,j} = A_j \cdot \left(1 - \frac{T}{T_{c,j}}\right)^{B_j + C_j \cdot \frac{T}{T_{c,j}} + D_j \left(\frac{T}{T_{c,j}}\right)^2 + E_j \left(\frac{T}{T_{c,j}}\right)^3} \quad (\text{B.2.34})$$

where $\sigma_{L,j}$ is in N/m, the temperature T and the component critical temperature $T_{c,j}$ are in K, and the relevant coefficients are given in Table B.2.10.

The contribution term $\Delta\sigma_{ca}$ is defined as (Horvath, 1985):

$$\Delta\sigma_{ca} = \frac{80.0}{\varepsilon_{\text{H}_2\text{O}}} \cdot C_{L,ca} \cdot \log \left(\frac{1.13 \times 10^{-13} \cdot (\varepsilon_{\text{H}_2\text{O}} \cdot T)^3}{C_{L,ca}} \right) \quad (\text{B.2.35})$$

where $\varepsilon_{\text{H}_2\text{O}}$ is the dielectric constant of water (Harned and Owen, 1958):

$$\varepsilon_{\text{H}_2\text{O}} = 78.540 + 31989.380 \cdot \left(\frac{1}{T} - \frac{1}{298.15} \right) \quad (\text{B.2.36})$$

$C_{L,ca}$ is the molar concentration of the apparent electrolyte ca , and T is the system temperature in K.

When equations (B.2.32) to (B.2.36) were applied to carbonate-bicarbonate solutions, the predicted surface tensions were found to be inconsistent with the literature data in Table B.2.11. Since there were no adjustable parameters which could be regressed to give a better fit to the data, it was decided to extrapolate the literature data to develop an empirical surface tension correlation of the form:

$$\sigma_L = \left(A_0 + A_1 \cdot \text{wf}_{\text{K}_2\text{CO}_3} + A_2 \cdot \text{wf}_{\text{K}_2\text{CO}_3}^2 \right) \cdot \left[(B_0 + B_1 \cdot T + B_2 \cdot T^2) \cdot (F_{\text{CO}_2} - 0.35)^2 + (C_0 + C_1 \cdot T) \right] \quad (\text{B.2.37})$$

where σ_L is in N/m, T is the temperature in °C, $\text{wf}_{\text{K}_2\text{CO}_3}$ is the equivalent K_2CO_3 weight fraction, and F_{CO_2} is the CO_2 loading. The correlation coefficients were determined via the simple unweighted least squares method in a Microsoft® Excel spreadsheet, and the resulting values are given in Table B.2.12. Since the surface tension of water is not affected by pressure within the pressure range of interest (Haar et al., 1984), σ_L was assumed to be similarly unaffected by pressure.

The above correlation is valid for temperatures between 20° and 130°C, equivalent K_2CO_3 concentrations of 20 to 40 wt% and CO_2 loadings between 0 and 1. These conditions encompass the typical absorber and regenerator operating conditions for the Moomba CO_2 trains. It was considered reasonable to neglect the effect of the H_2S loading on the surface tension since relatively negligible quantities of H_2S are absorbed in the CO_2 trains. The typical H_2S loading is of the order of 10^{-4} , which is several orders of magnitude less than the CO_2 loading for the CO_2 trains. Similarly, it was also considered reasonable to disregard the presence of other gases (such as N_2 , CH_4 and other hydrocarbons) as negligible amounts of these gases are dissolved into the liquid phase.

Figure B.2.3 compares the surface tension values predicted by equation (B.2.37) against the literature values. The average absolute deviation is 0.4%, compared to 7.6% for the values predicted by the Onsager-Samaras model and the DIPPR equation. As a result, the empirical correlation was used in this work.

Table B.2.10: Coefficients for the DIPPR surface tension equation (Rowley et al., 1998).

Component	$A \times 10^2$	B	C	D	E
CO_2	8.0710	1.2662	0	0	0
H_2S	7.4256	1.2997	0	0	0
H_2O	18.5480	2.7170	-3.5540	2.0470	0
N_2	2.9010	1.2485	0	0	0
CH_4	3.6557	1.1466	0	0	0
C_2H_6	4.8643	1.1981	0	0	0
C_3H_8	5.0920	1.2197	0	0	0
n- C_4H_{10}	5.1960	1.2181	0	0	0
i- C_4H_{10}	5.1359	1.2532	0	0	0
n- C_5H_{12}	5.2020	1.2041	0	0	0
i- C_5H_{12}	5.0876	1.2066	0	0	0
n- C_6H_{14}	5.5003	1.2674	0	0	0
n- C_7H_{16}	5.4143	1.2512	0	0	0

Table B.2.11: Atmospheric solution surface tension data.

Solution	Concentration	CO ₂ Loading	Temperature Range
K ₂ CO ₃ ^a	0 – 50 wt% K ₂ CO ₃	-	20°C
K ₂ CO ₃ –KHCO ₃ ^b	27 – 30 wt% K ₂ CO ₃ ^d	0 – 0.35	20 – 130°C
Na ₂ CO ₃ –NaHCO ₃ ^c	20 wt% Na ₂ CO ₃ ^e	0 – 0.9	25°C

^a Armand Products Company (1998) ^b UOP Gas Processing (1998) ^c Bedekar (1955) ^d These concentrations are in terms of equivalent K₂CO₃ weight percent. ^e This concentration is in terms of equivalent Na₂CO₃ weight percent.

Table B.2.12: Surface tension correlation coefficients.

Coefficient	Value
A ₀	8.7129×10 ⁻¹
A ₁	0
A ₂	1.4250
B ₀	2.3859×10 ⁻²
B ₁	4.9160×10 ⁻⁵
B ₂	6.0020×10 ⁻⁷
C ₀	8.2563×10 ⁻²
C ₁	-1.4361×10 ⁻⁴

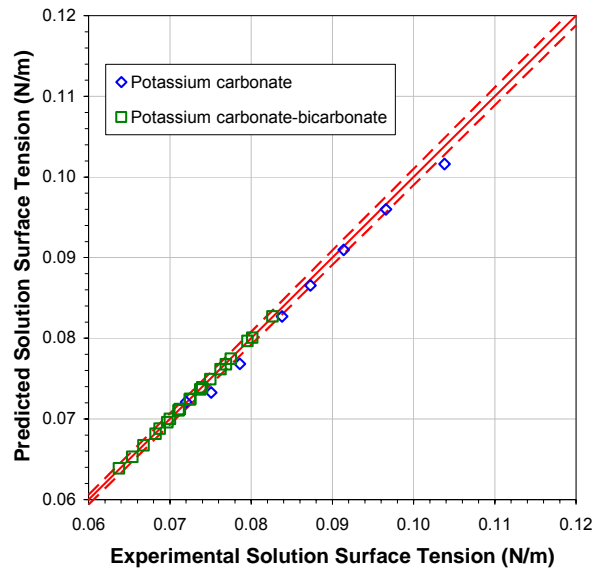


Figure B.2.3: Comparison between the predicted and experimental solution surface tensions. The dashed lines (---) represent the ± 1% lines.

B.2.6 Thermal Conductivity

B.2.6.1 Vapour Phase Thermal Conductivity

Like the vapour phase viscosity, the vapour phase thermal conductivity λ_G was determined in two steps in this work. First, the low pressure vapour phase thermal conductivity λ_G^{LP} was determined from the Wassiljewa-Mason-Saxena method (Mason and Saxena, 1958):

$$\lambda_G^{LP} = \frac{\sum_{j=1}^{NC} y_j \cdot \lambda_{G,j}^{LP}}{\sum_{k=1}^{NC} y_k \cdot \phi_{jk}} \quad (\text{B.2.38})$$

$$\phi_{jk} = \frac{\left[1 + \left(\frac{\mu_{G,j}^{LP}}{\mu_{G,k}^{LP}} \right)^{0.5} \cdot \left(\frac{MW_k}{MW_j} \right)^{0.25} \right]^2}{\left[8 \cdot \left(1 + \frac{MW_j}{MW_k} \right) \right]^{0.5}} \quad (\text{B.2.39})$$

where $\lambda_{G,j}^{LP}$ is the component low pressure thermal conductivity, y_j and y_k are the component vapour phase mole fractions, $\mu_{G,j}^{LP}$ and $\mu_{G,k}^{LP}$ are the component low pressure vapour phase viscosities, MW_j and MW_k are the component molecular weights, and NC is the number of vapour phase components. The Stiel-Thodos pressure correction (Stiel and Thodos, 1964) was then applied to λ_G^{LP} to give λ_G :

$$\left(\lambda_G - \lambda_G^{LP} \right) \cdot \Gamma \cdot Z_{c,G}^5 = 1.22 \times 10^{-2} \cdot \left(e^{0.535 \cdot V_{c,G}/V_G} - 1 \right) \quad \text{for } \frac{V_{c,G}}{V_G} < 0.5 \quad (\text{B.2.40})$$

$$\left(\lambda_G - \lambda_G^{LP} \right) \cdot \Gamma \cdot Z_{c,G}^5 = 1.14 \times 10^{-2} \cdot \left(e^{0.67 \cdot V_{c,G}/V_G} - 1.069 \right) \quad \text{for } 0.5 < \frac{V_{c,G}}{V_G} < 2.0 \quad (\text{B.2.41})$$

$$\left(\lambda_G - \lambda_G^{LP} \right) \cdot \Gamma \cdot Z_{c,G}^5 = 2.60 \times 10^{-3} \cdot \left(e^{1.155 \cdot V_{c,G}/V_G} + 2.016 \right) \quad \text{for } 2.0 < \frac{V_{c,G}}{V_G} < 2.8 \quad (\text{B.2.42})$$

$$\Gamma = 210 \cdot \left(\frac{T_{c,G} \cdot MW_G^3}{P_{c,G}^4} \right)^{1/6} \quad (\text{B.2.43})$$

$Z_{c,G}$, $V_{c,G}$, $T_{c,G}$ and $P_{c,G}$ are the vapour phase critical compressibility, critical molar volume, critical temperature in K and critical pressure in bar, respectively, and the parameter Γ is in $\text{m} \cdot \text{K}/\text{W}$. V_G is the vapour phase molar volume, and MW_G is the vapour phase molecular weight in kg/kmol . The vapour phase critical properties were obtained as follows (Poling et al., 2001):

$$V_{c,G} = \sum_{j=1}^{NC} \sum_{k=1}^{NC} y_j \cdot y_k \cdot V_{c,jk} \quad (\text{B.2.44})$$

$$T_{c,G} = \frac{\sum_{j=1}^{NC} \sum_{k=1}^{NC} y_j \cdot y_k \cdot V_{c,jk} \cdot T_{c,jk}}{V_{c,G}} \quad (\text{B.2.45})$$

$$\omega_G = \sum_{j=1}^{NC} y_j \cdot \omega_j \quad (\text{B.2.46})$$

$$Z_{c,G} = 0.291 - 0.08 \cdot \omega_G \quad (\text{B.2.47})$$

$$P_{c,G} = \frac{Z_{c,G} \cdot R \cdot T_{c,G}}{V_{c,G}} \quad (\text{B.2.48})$$

$$V_{c,jk} = \frac{(V_{c,j}^{1/3} + V_{c,k}^{1/3})^3}{8} \quad (\text{B.2.49})$$

$$T_{c,jk} = (T_{c,j} \cdot T_{c,k})^{0.5} \quad (\text{B.2.50})$$

where ω_G is the vapour phase acentricity, R is the gas constant, $V_{c,j}$ and $V_{c,k}$ are the component critical molar volumes, $T_{c,j}$ and $T_{c,k}$ are the component critical temperatures, ω_j is the component acentricity, and $Z_{c,j}$ is the component critical compressibility.

The component low pressure vapour phase thermal conductivities $\lambda_{G,j}^{LP}$ are calculated using the DIPPR vapour thermal conductivity model (Rowley et al., 1998):

$$\lambda_{G,j}^{LP} = \frac{A_j \cdot T^{B_j}}{1 + \frac{C_j}{T} + \frac{D_j}{T^2}} \quad (\text{B.2.51})$$

where $\lambda_{G,j}^{LP}$ is in W/m·K and T is the system temperature in K. The relevant coefficients are given in Table B.2.13.

Table B.2.13: Coefficients for the DIPPR vapour thermal conductivity model (Rowley et al., 1998).

Component	A	B	$C \times 10^{-2}$	$D \times 10^{-6}$
CO ₂	3.6900	-0.38380	9.64000	1.86000
H ₂ S	1.3810×10^{-7}	1.83790	-3.52090	4.60410×10^{-2}
H ₂ O	2.1606×10^{-3}	0.76839	39.40500	-0.44534
N ₂	3.3143×10^{-4}	0.77220	0.16323	3.73720×10^{-4}
CH ₄	6.3252×10^3	0.43041	7.7040×10^6	-3.87250×10^4
C ₂ H ₆	7.3869×10^{-5}	1.16890	5.00730	0
C ₃ H ₈	-1.1200	0.10972	-98.34600	-7.53580
n-C ₄ H ₁₀	5.1094×10^{-2}	0.45253	54.55500	1.97980
i-C ₄ H ₁₀	8.9772×10^{-2}	0.18501	6.39230	1.11470
n-C ₅ H ₁₂	-6.8440×10^2	0.76400	-1.0550×10^7	0
i-C ₅ H ₁₂	8.9680×10^{-4}	0.77420	4.56000	0.23064
n-C ₆ H ₁₄	-6.5050×10^2	0.80530	-1.4121×10^7	0
n-C ₇ H ₁₆	-7.0028×10^{-2}	0.38068	-70.4990	-2.40050

B.2.6.2 Liquid Phase Thermal Conductivity

In Aspen Properties®, the liquid phase thermal conductivity λ_L for an electrolyte system is determined from the Riedel equation (Riedel, 1951):

$$\lambda_L = \frac{\lambda_{L,\text{solvent}}}{\lambda_{L,\text{solvent}}(293\text{K})} \cdot \left(\lambda_{L,\text{solvent}}(293\text{K}) + \sum_{\text{ca}} (a_c + a_a) \cdot C_{L,\text{ca}} \right) \quad (\text{B.2.52})$$

where $\lambda_{L,\text{solvent}}$ is the solvent thermal conductivity at the system temperature T , $\lambda_L(293\text{K})$ is the solvent thermal conductivity at 293 K, $C_{L,\text{ca}}$ is the molar concentration of the apparent electrolyte ca , and a_c and a_a are the cationic and anionic Riedel parameters.

The solvent thermal conductivity is determined from the component thermal conductivities $\lambda_{L,j}$ of H_2O and any molecular species present in the liquid phase via the Vredeveld mixing rule (Reid et al., 1977):

$$\lambda_{L,\text{solvent}} = \left(\sum_j \text{wf}_j \cdot \lambda_{L,j}^{-2} \right)^{-0.5} \quad (\text{B.2.53})$$

where wf_j is the component weight fraction and NC is the number of molecular species present in the liquid phase. The values of $\lambda_{L,j}$ are calculated from the DIPPR equation (Rowley et al., 1998) with the coefficients given in Table B.2.14:

$$\lambda_{L,j} = A_j + B_j \cdot T + C_j \cdot T^2 + D_j \cdot T^3 + E_j \cdot T^4 \quad (\text{B.2.54})$$

where $\lambda_{L,j}$ is in $\text{W/m}\cdot\text{K}$ and T is in K .

Using the Aspen Properties® databank values for the parameters a_c and a_a , equations (B.2.52) to (B.2.54) were applied to potassium carbonate-bicarbonate solutions. The resulting liquid phase thermal conductivity values were found to be inconsistent with the literature data in Table B.2.15. The a_c and a_a values were re-regressed from the literature data using the Aspen Properties® DRS, but this did not improve the performance of equations (B.2.52) to (B.2.54). Consequently, it was decided to extrapolate the literature data to develop an empirical liquid phase thermal conductivity correlation of the form:

$$\lambda_L = \left(A_0 + A_1 \cdot \text{wf}_{\text{K}_2\text{CO}_3} + A_2 \cdot F_{\text{CO}_2} + A_3 \cdot T + A_4 \cdot T^2 \right) \cdot \left(B_0 + B_1 \cdot T + B_2 \cdot T^2 + B_3 \cdot P \right) \quad (\text{B.2.55})$$

where λ_L is in $\text{W/m}\cdot\text{K}$, T is the temperature in $^\circ\text{C}$, P is the pressure in bar, $\text{wf}_{\text{K}_2\text{CO}_3}$ is the equivalent K_2CO_3 weight fraction, and F_{CO_2} is the CO_2 loading. The correlation coefficients were determined via the simple unweighted least squares method in a Microsoft® Excel spreadsheet, and the resulting values are given in Table B.2.16. The dependence of λ_L on pressure was assumed to be the same as

that for the thermal conductivity of water, which increases linearly with pressure within the pressure range of interest (Haar et al., 1984). The correlation is valid for temperatures between 20° and 130°C, pressures between 1 and 75 bar, equivalent K₂CO₃ concentrations of 20 to 40 wt% and CO₂ loadings between 0 and 1.

Figure B.2.4 compares the solution thermal conductivity values predicted by equation (B.2.56) against the literature values. The average absolute deviation is 0.5%, compared to 10.6% for the values predicted by the Riedel and DIPPR equations. As a result, the empirical correlation was used in this work.

Table B.2.14: Coefficients for the DIPPR liquid thermal conductivity equation (Rowley et al., 1998).

Component	A×10 ¹	B×10 ⁴	C×10 ⁷	D×10 ⁹	E
CO ₂	4.4060	-12.1750	0	0	0
H ₂ S	4.8420	-11.8400	0	0	0
H ₂ O	-4.3200	57.2550	-80.7800	1.8610	0
N ₂	2.6540	-16.7700	0	0	0
CH ₄	4.1768	-24.5280	35.5880	0	0
C ₂ H ₆	3.5758	-11.4580	6.1866	0	0
C ₃ H ₈	2.6755	-6.6457	2.7740	0	0
n-C ₄ H ₁₀	2.7349	-7.1267	5.1555	0	0
i-C ₄ H ₁₀	2.0455	-3.6589	0	0	0
n-C ₅ H ₁₂	2.5370	-5.7600	3.4400	0	0
i-C ₅ H ₁₂	2.1246	-3.3581	0	0	0
n-C ₆ H ₁₄	2.2492	-3.5330	0	0	0
n-C ₇ H ₁₆	2.1500	-3.0300	0	0	0

Table B.2.15: Atmospheric solution thermal conductivity data.

Solution	Concentration	CO ₂ Loading	Temperature Range
K ₂ CO ₃ ^a	20 – 40 wt% K ₂ CO ₃	-	20 – 90°C
K ₂ CO ₃ –KHCO ₃ ^b	27 – 30 wt% K ₂ CO ₃ ^c	0 – 0.75	70 – 130°C

^a Chernen'kaya and Revenko (1973) ^b UOP Gas Processing (1998) ^c These concentrations are in terms of equivalent K₂CO₃ weight percent.

Table B.2.16: Liquid phase thermal conductivity correlation coefficients.

Coefficient	Value
A ₀	6.2933×10 ⁻¹
A ₁	-1.8732×10 ⁻¹
A ₂	-2.3768×10 ⁻²
A ₂	1.2144×10 ⁻³
A ₄	-4.9031×10 ⁻⁶
B ₀	9.9983×10 ⁻¹
B ₁	1.1860×10 ⁻⁵
B ₂	1.0952×10 ⁻⁷
B ₃	8.0807×10 ⁻⁵

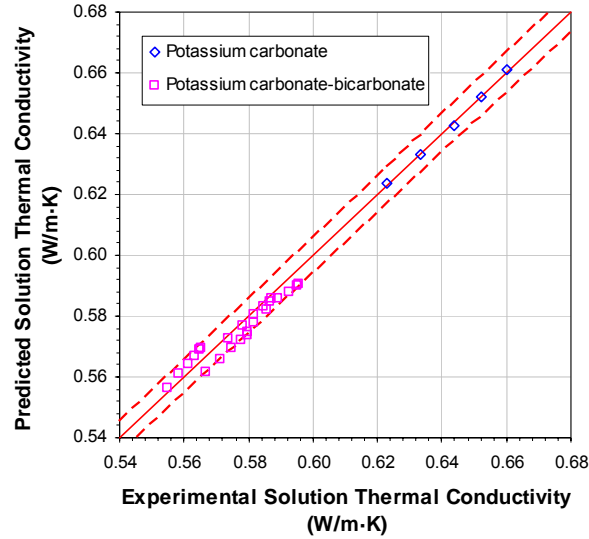


Figure B.2.4: Comparison between the predicted and experimental solution thermal conductivities. The dashed lines (---) represent the $\pm 1\%$ lines.

B.2.7 Diffusivities

B.2.7.1 Vapour Phase Diffusivities

In this work, the vapour phase component diffusivities $D_{c,j}$ were calculated using Blanc's Law (Reid et al., 1977):

$$D_{G,j} = \sum_{\substack{k=1 \\ k \neq j}}^{NC} y_k \cdot \left(\sum_{\substack{k=1 \\ k \neq j}}^{NC} \frac{D_{G,jk}}{y_k} \right) \quad (\text{B.2.56})$$

where y_j and y_k are the component vapour phase mole fractions, NC is the number of vapour phase components, and $D_{g,jk}$ is the vapour phase binary diffusivity for the component pair j-k, which was determined from the corresponding binary diffusivity $D_{G,jk}^{LP}$ at atmospheric pressure using the Dawson-Khoury-Kobayashi expression (Reid et al., 1977):

$$\frac{D_{G,jk} \cdot C_G}{D_{G,jk}^{LP} \cdot C_G^{LP}} = 1 + 0.053432 \cdot C_R - 0.030182 \cdot C_R^2 - 0.029725 \cdot C_R^3 \quad (\text{B.2.57})$$

C_G and C_G^{LP} are the vapour phase molar densities at the system pressure P and at atmospheric pressure, respectively. C_R is the reduced molar density, which was determined from the relation:

$$C_R = C_G \cdot V_{c,jk} = C_G \cdot \left(\frac{y_j \cdot V_{c,j} + y_k \cdot V_{c,k}}{y_j + y_k} \right) \quad (\text{B.2.58})$$

where $V_{c,j}$ and $V_{c,k}$ are the component critical volumes.

The atmospheric vapour phase binary diffusivities $D_{G,jk}^{LP}$ were obtained from the Chapman-Enskog-Brokaw model (Poling et al., 2001):

$$D_{G,jk}^{LP} = \frac{0.00266 \cdot T^{3/2}}{P \cdot MW_{jk}^{1/2} \cdot \sigma_{jk}^2 \cdot \Omega_{D,jk}} \quad (B.2.59)$$

$$MW_{jk} = 2 \cdot \left(\frac{1}{MW_j} + \frac{1}{MW_k} \right)^{-1} \quad (B.2.60)$$

where $D_{G,jk}^{LP}$ is in cm^2/s , T is the system temperature in K, P is the system pressure in bar, MW_j and MW_k are the component molecular weights in kg/kmol , σ_{jk} is the characteristic length in Å, and $\Omega_{D,jk}$ is the diffusion collision integral.

The characteristic length σ_{jk} was obtained from the following relations:

$$\sigma_{jk} = (\sigma_j \cdot \sigma_k)^{1/2} \quad (B.2.61)$$

$$\sigma_j = \left(\frac{1.585 \cdot V_{b,j}}{1 + 1.3 \cdot \delta_{p,j}^2} \right)^{1/3} \quad (B.2.62)$$

$$\delta_{p,jk} = (\delta_{p,j} \cdot \delta_{p,k})^{1/2} \quad (B.2.63)$$

$$\delta_{p,j} = \frac{1.94 \times 10^3 \cdot \delta_j^2}{V_{b,j} \cdot T_{b,j}} \quad (B.2.64)$$

where $T_{b,j}$ is the normal boiling point in K, $V_{b,j}$ is the component liquid molar volume at $T_{b,j}$ in cm^3/mol , and $\delta_{p,j}$ is the component polar parameter, δ_j is the component dipole moment in Debye. Values of $V_{b,j}$ and $T_{b,j}$ are given in Table B.2.17.

The diffusion collision integral $\Omega_{D,jk}$ was determined from the correlation:

$$\Omega_{D,jk} = \frac{A}{T^{*B}} + \frac{C}{e^{D \cdot T^*}} + \frac{E}{e^{F \cdot T^*}} + \frac{G}{e^{H \cdot T^*}} + \frac{0.19 \cdot \delta_{p,jk}^2}{T^*} \quad (B.2.65)$$

where A is 1.06036, B is 0.15610, C is 0.19300, D is 0.47635, E is 1.03587, F is 1.52996, G is 1.76474 and H is 3.89411. The dimensionless temperature T^* was calculated from:

$$T^* = \frac{k \cdot T}{\varepsilon_{jk}} \quad (B.2.66)$$

$$\frac{\varepsilon_{jk}}{k} = \left(\frac{\varepsilon_j}{k} \cdot \frac{\varepsilon_k}{k} \right)^{1/2} \quad (B.2.67)$$

$$\frac{\varepsilon_j}{k} = 1.18 \cdot (1 + 1.3 \cdot \delta_{p,j}^2) \cdot T_{b,j} \quad (B.2.68)$$

where ε_j and ε_k are the component characteristic energies and k is the Boltzmann constant.

Table B.2.17: Normal boiling points and the corresponding liquid molar volumes (Poling et al., 2001).

Component	T_b (K)	V_b^a (cm ³ /mol)
CO ₂	194.70	35.64
H ₂ S	212.80	34.27
H ₂ O	373.20	19.64
N ₂	77.40	34.71
CH ₄	111.70	37.75
C ₂ H ₆	184.50	55.06
C ₃ H ₈	231.10	75.78
n-C ₄ H ₁₀	272.70	96.58
i-C ₄ H ₁₀	261.30	97.82
n-C ₅ H ₁₂	309.20	118.40
i-C ₅ H ₁₂	301.00	117.96
n-C ₆ H ₁₄	341.90	140.90
n-C ₇ H ₁₆	371.60	163.73

^a Calculated from the Rackett equation (B.2.8).

B.2.7.2 Liquid Phase Diffusivities

For ionic and electrolyte species, the liquid phase species diffusivities $D_{L,j}$ were determined in this work using the Stokes-Einstein relation (Poling et al., 2001):

$$\frac{D_{L,j} \cdot \mu_L}{T} = \frac{D_{w,j}^{\infty} \cdot \mu_{L,H_2O}^{25}}{298.15K} \quad (B.2.69)$$

where T is the system temperature in K, μ_L is the liquid phase viscosity, $D_{w,j}^{\infty}$ is the species diffusivity at infinite dilution in water at 25°C, and μ_{L,H_2O}^{25} is the viscosity of water at 25°C. μ_{L,H_2O}^{25} was calculated from (Bingham, 1922):

$$\frac{1}{\mu_{L,H_2O}} = 0.021482 \cdot \left[(T - 8.435) + \sqrt{8078.4 + (T - 8.435)^2} \right] - 1.2 \quad (B.2.70)$$

where μ_{L,H_2O} is in cP and T is in °C. The Nernst equation (Horvath, 1985) was used to obtain the values of $D_{w,j}^{\infty}$:

$$D_{w,j}^{\infty} = \frac{\lambda_j^{\infty} \cdot R \cdot T}{z_j \cdot F^2} \quad \text{for } j = \text{ionic species} \quad (B.2.71)$$

$$D_{w,j}^{\infty} = \frac{(z_c + z_a) \cdot \lambda_c^{\infty} \cdot \lambda_a^{\infty} \cdot R \cdot T}{z_c \cdot z_a \cdot (\lambda_c^{\infty} + \lambda_a^{\infty}) \cdot F^2} \quad \text{for } j = \text{electrolyte species ca} \quad (B.2.72)$$

where λ_j^∞ is the ionic conductivity at infinite dilution, z_j is the charge number (or the absolute value of the species ionic charge), R is the gas constant, T is 298.15 K, and F is Faraday's constant. The subscripts a and c refer to the anions and cations comprising the electrolyte species ca. Values of λ_j^∞ are listed in Table B.2.18.

For molecular species, the liquid phase species diffusivities $D_{L,j}$ were determined using the correlation suggested by Ratcliff and Holdcroft (1963):

$$\log\left(\frac{D_{w,j}}{D_{L,j}}\right) = 0.637 \cdot \log\left(\frac{\mu_L}{\mu_{L,H_2O}}\right) \quad (\text{B.2.73})$$

where μ_L is the liquid phase viscosity, $D_{w,j}$ is the species diffusivity in water, and μ_{L,H_2O} is the viscosity of water.

The values of $D_{w,j}$ for CO_2 and H_2S were calculated from the following correlations, which were derived from the data presented by Versteeg and van Swaaij (1988) and Tamimi and co-workers (1994):

$$D_{w,\text{CO}_2} = 2.9294 \times 10^{-2} \cdot e^{-2184.8/T} \quad (\text{B.2.74})$$

$$D_{w,\text{H}_2\text{S}} = 8.7161 \times 10^{-3} \cdot e^{-1839.7/T} \quad (\text{B.2.75})$$

where D_{w,CO_2} and $D_{w,\text{H}_2\text{S}}$ are in cm^2/s and T is the temperature in K. For the other molecular species present in the liquid phase, $D_{w,j}$ was determined using the Stokes-Einstein relation:

$$\frac{D_{w,j} \cdot \mu_{L,H_2O}}{T} = \frac{D_{w,j}^{25} \cdot \mu_{L,H_2O}^{25}}{298.15\text{K}} \quad (\text{B.2.76})$$

where $D_{w,j}^{25}$ is the species diffusivity in water at 25°C, values of which are given in Table B.2.19, and μ_{L,H_2O}^{25} is the viscosity of water at 25°C.

Table B.2.18: Ionic conductivities at infinite dilution.

Ionic Species	λ^∞ (m ² /Ω·kmol)
H ₃ O ⁺	35.010 ^a
K ⁺	7.352 ^a
OH ⁻	19.830 ^a
HCO ₃ ⁻	4.450 ^a
CO ₃ ²⁻	6.930 ^a
HS ⁻	6.500 ^b
S ²⁻	9.990 ^b

^a Robinson and Stokes (1965) ^b Onda and co-workers (1971)

Table B.2.19: Diffusivities in water at 25°C.

Component	$D_{w,j}^{25} \times 10^5$ (cm ² /s)
H ₂ O	2.57 ^a
N ₂	2.01 ^b
CH ₄	1.88 ^c
C ₂ H ₆	1.52 ^c
C ₃ H ₈	1.21 ^c
n-C ₄ H ₁₀	1.05 ^d
i-C ₄ H ₁₀	1.04 ^d
n-C ₅ H ₁₂	0.93 ^d
i-C ₅ H ₁₂	0.93 ^d
n-C ₆ H ₁₄	0.84 ^d
n-C ₇ H ₁₆	0.77 ^d

^a Wang (1965) ^b Ferrell and Himmelblau (1967) ^c Witherspoon and Saraf (1965) ^d Determined from the equation proposed by Hayduk and Laudie (1974).

APPENDIX C

ELECTROLYTE NRTL ADJUSTABLE PARAMETERS

This appendix outlines the procedure followed for the regression of the model parameters for the Electrolyte NRTL model. The results of the data regression are analysed and the complete set of model parameters is included within.

C.1 Parameter Values

The Electrolyte NRTL adjustable parameters for determining the energy parameter τ from equation (3.2.4) are presented in Tables C.1.1 and C.1.2. The listed values were taken from the Aspen Properties® databanks, unless indicated otherwise. The default values for τ and the non-randomness factor α were set as 0 and 0.2, respectively.

Table C.1.1: The Electrolyte NRTL adjustable parameters used in this work.

Component i	Component j	A	B	C	α
CO ₂	(H ₃ O ⁺ ,OH ⁻)	15.000	0	0	0.1
(H ₃ O ⁺ ,OH ⁻)	CO ₂	-8.000	0	0	0.1
CO ₂	(H ₃ O ⁺ ,CO ₃ ²⁻)	15.000	0	0	0.1
(H ₃ O ⁺ ,CO ₃ ²⁻)	CO ₂	-8.000	0	0	0.1
CO ₂	(H ₃ O ⁺ ,HCO ₃ ⁻)	15.000	0	0	0.1
(H ₃ O ⁺ ,HCO ₃ ⁻)	CO ₂	-8.000	0	0	0.1
CO ₂	(H ₃ O ⁺ ,HS ⁻)	15.000	0	0	0.1
(H ₃ O ⁺ ,HS ⁻)	CO ₂	-8.000	0	0	0.1
CO ₂	(H ₃ O ⁺ ,S ²⁻)	15.000	0	0	0.1
(H ₃ O ⁺ ,S ²⁻)	CO ₂	-8.000	0	0	0.1
CO ₂	(K ⁺ ,OH ⁻)	10.000	0	0	0.2
(K ⁺ ,OH ⁻)	CO ₂	-2.000	0	0	0.2
CO ₂	(K ⁺ ,CO ₃ ²⁻)	10.000	0	0	0.2
(K ⁺ ,CO ₃ ²⁻)	CO ₂	-2.000	0	0	0.2
CO ₂	(K ⁺ ,HCO ₃ ⁻)	10.000	0	0	0.2
(K ⁺ ,HCO ₃ ⁻)	CO ₂	-2.000	0	0	0.2
CO ₂	(K ⁺ ,HS ⁻)	10.000	0	0	0.2
(K ⁺ ,HS ⁻)	CO ₂	-2.000	0	0	0.2
CO ₂	(K ⁺ ,S ²⁻)	10.000	0	0	0.2
(K ⁺ ,S ²⁻)	CO ₂	-2.000	0	0	0.2
H ₂ S	(H ₃ O ⁺ ,OH ⁻)	15.000	0	0	0.1
(H ₃ O ⁺ ,OH ⁻)	H ₂ S	-8.000	0	0	0.1
H ₂ S	(H ₃ O ⁺ ,CO ₃ ²⁻)	15.000	0	0	0.1
(H ₃ O ⁺ ,CO ₃ ²⁻)	H ₂ S	-8.000	0	0	0.1
H ₂ S	(H ₃ O ⁺ ,HCO ₃ ⁻)	15.000	0	0	0.1
(H ₃ O ⁺ ,HCO ₃ ⁻)	H ₂ S	-8.000	0	0	0.1
H ₂ S	(H ₃ O ⁺ ,HS ⁻)	15.000	0	0	0.1
(H ₃ O ⁺ ,HS ⁻)	H ₂ S	-8.000	0	0	0.1
H ₂ S	(H ₃ O ⁺ ,S ²⁻)	15.000	0	0	0.1
(H ₃ O ⁺ ,S ²⁻)	H ₂ S	-8.000	0	0	0.1
H ₂ S	(K ⁺ ,OH ⁻)	10.000	0	0	0.2
(K ⁺ ,OH ⁻)	H ₂ S	-2.000	0	0	0.2
H ₂ S	(K ⁺ ,CO ₃ ²⁻)	10.000	0	0	0.2
(K ⁺ ,CO ₃ ²⁻)	H ₂ S	-2.000	0	0	0.2
H ₂ S	(K ⁺ ,HCO ₃ ⁻)	10.000	0	0	0.2
(K ⁺ ,HCO ₃ ⁻)	H ₂ S	-2.000	0	0	0.2
H ₂ S	(K ⁺ ,HS ⁻)	10.000	0	0	0.2
(K ⁺ ,HS ⁻)	H ₂ S	-2.000	0	0	0.2
H ₂ S	(K ⁺ ,S ²⁻)	10.000	0	0	0.2
(K ⁺ ,S ²⁻)	H ₂ S	-2.000	0	0	0.2

Table C.1.2: The Electrolyte NRTL adjustable parameters used in this work.

Component i	Component j	A	B	C	α
H ₂ O	(H ₃ O ⁺ ,OH ⁻)	8.045	0	0	0.2
(H ₃ O ⁺ ,OH ⁻)	H ₂ O	-4.072	0	0	0.2
H ₂ O	(H ₃ O ⁺ ,CO ₃ ²⁻)	8.045	0	0	0.2
(H ₃ O ⁺ ,CO ₃ ²⁻)	H ₂ O	-4.072	0	0	0.2
H ₂ O	(H ₃ O ⁺ ,HCO ₃ ⁻)	8.045	0	0	0.2
(H ₃ O ⁺ ,HCO ₃ ⁻)	H ₂ O	-4.072	0	0	0.2
H ₂ O	(H ₃ O ⁺ ,HS ⁻)	8.045	0	0	0.2
(H ₃ O ⁺ ,HS ⁻)	H ₂ O	-4.072	0	0	0.2
H ₂ O	(H ₃ O ⁺ ,S ²⁻)	8.045	0	0	0.2
(H ₃ O ⁺ ,S ²⁻)	H ₂ O	-4.072	0	0	0.2
H ₂ O	(K ⁺ ,OH ⁻)	7.841	773.360	0	0.2
(K ⁺ ,OH ⁻)	H ₂ O	-4.259	-305.651	0	0.2
H ₂ O	(K ⁺ ,CO ₃ ²⁻)	-5.020 ^a	-250.640 ^a	0 ^a	0.2
(K ⁺ ,CO ₃ ²⁻)	H ₂ O	-0.176 ^a	-864.400 ^a	0 ^a	0.2
H ₂ O	(K ⁺ ,HCO ₃ ⁻)	6.250 ^a	0 ^a	0 ^a	0.2
(K ⁺ ,HCO ₃ ⁻)	H ₂ O	-3.728 ^a	0 ^a	0 ^a	0.2
H ₂ O	(K ⁺ ,HS ⁻)	3.076 ^a	0 ^a	0 ^a	0.2
(K ⁺ ,HS ⁻)	H ₂ O	-3.253 ^a	-226.148 ^a	0 ^a	0.2
H ₂ O	(K ⁺ ,S ²⁻)	3.438 ^a	4206.772 ^a	0 ^a	0.2
(K ⁺ ,S ²⁻)	H ₂ O	-6.305 ^a	-267.739 ^a	0 ^a	0.2
CO ₂	H ₂ O	10.064	-3268.135	0	0.2
H ₂ O	CO ₂	10.064	-3268.135	0	0.2
H ₂ S	H ₂ O	-3.674	1155.9	0	0.2
H ₂ O	H ₂ S	-3.674	1155.9	0	0.2

^a These values were regressed from literature data.

C.2 Data Regression Procedure

The Electrolyte NRTL adjustable parameter values not taken from the Aspen Properties® databanks were determined using the Aspen Properties® Data Regression System (DRS). The adjustable parameter values for the $\text{H}_2\text{O}-(\text{K}^+, \text{HCO}_3^-)$ and $\text{H}_2\text{O}-(\text{K}^+, \text{CO}_3^{2-})$ binary interaction pairs were first determined from Tosh and co-workers' (1959) data for CO_2 solubility in aqueous potassium carbonate solutions. Adjustable parameter values for the $\text{H}_2\text{O}-(\text{K}^+, \text{HS}^-)$ and $\text{H}_2\text{O}-(\text{K}^+, \text{S}^{2-})$ binary interaction pairs were then determined using Tosh and co-workers' (1960) H_2S solubility data in aqueous potassium carbonate solutions. Both sets of data regressions were performed using the general procedure outlined below.

1. Where available, the Aspen Properties® databank values were set as the initial values for the adjustable parameters to be regressed from the data. Otherwise, the following default values were applied:

Binary Interaction Pair	A	B	C
Water-Electrolyte	8	0	0
Electrolyte-Water	-4	0	0

2. The full set of twelve adjustable parameters was regressed from the data. The resulting set of parameter values was labelled "Full".
3. One of the four C parameters (designated as C1) was excluded from regression (i.e. it was fixed at its initial value) and the remaining adjustable parameters were regressed from the data. The resulting set of parameter values was labelled "C1". Another C parameter (C2) was then excluded instead of C1 to give the parameter value set "C2". This step was repeated with the remaining C parameters (C3 and C4) to give the parameter values sets "C3" and "C4".
4. C1 and C2 were excluded from regression and the remaining adjustable parameters were regressed from the data. The resulting set of parameter values was labelled "C12". C3 was then excluded instead of C2 to give the parameter value set "C13". C4 was then excluded instead of C3 to give the parameter value set "C14".
5. C2 and C3 were excluded from regression and the remaining adjustable parameters were regressed from the data. The resulting set of parameter values was labelled "C23". C4 was then excluded instead of C3 to give the parameter value set "C24".
6. C3 and C4 were excluded from regression and the remaining adjustable parameters were regressed from the data. The resulting set of parameter values was labelled "C34".

7. C1, C2 and C3 were excluded from regression and the remaining adjustable parameters were regressed from the data. The resulting set of parameter values was labelled "C123". C4 was then excluded instead of C3 to give the parameter value set "C124". C3 was then excluded instead of C2 to give the parameter value set "C134".
8. C2, C3 and C3 were excluded from regression and the remaining adjustable parameters were regressed from the data. The resulting set of parameter values was labelled "C234".
9. All four C parameters were excluded from regression and the remaining adjustable parameters were regressed from the data. The resulting set of parameter values was labelled "C".
10. Excluding all four C parameters from regression, steps 3 to 9 were repeated with the four B parameters (B1, B2, B3 and B4) to give the parameter value sets "B1C", "B2C", "B3C", "B4C", "B12C", "B13C", "B14C", "B123C", "B124C", "B134C", "B234C" and "BC".
11. Excluding all C and B parameters from regression, steps 3 to 9 were repeated with the four A parameters (A1, A2, A3 and A4) to give the parameter value sets "A1BC", "A2BC", "A3BC", "A4BC", "A12BC", "A13BC", "A14BC", "A123BC", "A124BC", "A134BC", "A234BC" and "ABC".
12. Each simplified set of parameter values obtained from steps 3 to 11 was compared against the "Full" parameter value set via an F-Test to determine the reliability of the simplified set. The corresponding one-tail p-value was also calculated to determine the probability of observing the F-Test value if the null hypothesis was true.

Null hypothesis: The simplified set fits the data better than the "Full" set.

$$F \approx 1 \text{ or } p > 0.05$$

where

$$F = \frac{\frac{WSSQ_{\text{Simplified}} - WSSQ_{\text{Full}}}{df_{\text{Simplified}} - df_{\text{Full}}}}{\frac{WSSQ_{\text{Full}}}{df_{\text{Full}}}} \quad (\text{C.2.1})$$

$$p = f(F, df_{\text{Simplified}} - df_{\text{Full}}, df_{\text{Full}}) \quad (\text{C.2.2})$$

$$df = N_{\text{Data}} - N_{\text{Parameters}} \quad (\text{C.2.3})$$

$WSSQ_{\text{Full}}$ and $WSSQ_{\text{Simplified}}$ are the weighted sum of squares for the full and simplified parameter value sets, respectively, df_{Full} and $df_{\text{Simplified}}$ are the corresponding degrees of freedom, N_{Data} is the number of data points used in the regression, and $N_{\text{Parameters}}$ is the number of parameters regressed.

13. The simplified parameter value sets which passed the above F-Test were sorted according to their weighted sum of squares. A logic test was then performed on each parameter set to tabulate the number of parameters with a standard error greater than the associated regressed value. The parameter value set with the lowest logic test result and the lowest weighted sum of squares was labelled the optimal set.

C.3 Data Regression Results

The statistical results for the data regression runs for the $\text{CO}_2\text{-K}_2\text{CO}_3\text{-KHCO}_3\text{-H}_2\text{O}$ system are given in Table C.3.1. The weighted sum of squares (WSSQ), residual root mean square error (RRMSQE), degrees of freedom (df), F-value and p-value are listed for each parameter set. The data set used in the regression runs consisted of 120 data points, and the number of parameters regressed ranged from 0 to 12, depending on the parameter set. Using the F-Test, 25 simplified parameter sets were identified as being more suitable than the “Full” set. These are sorted in ascending order according to their WSSQ in Table C.3.1. The corresponding logic test results are also presented.

Of the 25 simplified parameter sets in Table C.3.1, set “B34C” was the only set to have all its regressed parameter values greater than the associated standard error. Consequently, it was selected as the optimal parameter value set and was used in the next series of data regression runs for the $\text{CO}_2\text{-H}_2\text{S-K}_2\text{CO}_3\text{-KHCO}_3\text{-KHS-K}_2\text{S-H}_2\text{O}$ system. The regressed parameter values and standard errors associated with this optimal set are given in Table 3.2.2.

Table C.3.3 presents the statistical results for the data regression runs for the $\text{CO}_2\text{-H}_2\text{S-K}_2\text{CO}_3\text{-KHCO}_3\text{-KHS-K}_2\text{S-H}_2\text{O}$ system. The data set used in this series of regression runs consisted of 127 data points, and the number of parameters regressed ranged from 0 to 12, depending on the parameter set. Only 6 simplified parameter sets were determined to be more suitable than the “Full” set via the F-Test, and these are sorted in ascending order according to their WSSQ in Table C.3.4. The corresponding logic test results are also presented.

Of the 6 simplified parameter sets in Table C.3.4, set “B1C” was the only set to have all its regressed parameter values greater than the associated standard error. It was therefore selected as the optimal parameter value set for the $\text{CO}_2\text{-H}_2\text{S-K}_2\text{CO}_3\text{-KHCO}_3\text{-KHS-K}_2\text{S-H}_2\text{O}$ system. The regressed parameter values and standard errors associated with this optimal set are given in Table 3.2.3.

Table C.3.1: Statistical results for the CO₂-K₂CO₃-KHCO₃-H₂O system data regression runs.

Parameter Set	WSSQ	RRMSQE	df	F	p	Null Hypothesis
Full	1143.4	3.254	108	-	-	-
C1	1378.6	3.573	109	22.21	7.3×10^{-6}	False
C2	1223.8	3.366	109	7.59	6.9×10^{-3}	False
C3	1129.1	3.233	109	-1.36	n/a ^a	True
C4	1160.7	3.278	109	1.63	2.0×10^{-1}	True
C12	1230.6	3.376	110	4.12	1.9×10^{-2}	False
C13	1279.8	3.442	110	6.44	2.3×10^{-3}	False
C14	1230.8	3.376	110	4.12	1.9×10^{-2}	False
C23	1199.3	3.332	110	2.64	7.6×10^{-2}	True
C24	1100.3	3.192	110	-2.03	n/a ^a	True
C34	1198.3	3.331	110	2.59	8.0×10^{-2}	True
C123	1178.2	3.303	111	1.10	3.5×10^{-1}	True
C124	1214.5	3.353	111	2.24	8.8×10^{-2}	True
C134	1192.0	3.322	111	1.53	2.1×10^{-1}	True
C234	1191.1	3.321	111	1.50	2.2×10^{-1}	True
C	1188.6	3.317	112	1.07	3.8×10^{-1}	True
B1C	1105.0	3.199	113	-0.73	n/a ^a	True
B2C	1178.2	3.303	113	0.66	6.6×10^{-1}	True
B3C	1178.4	3.303	113	0.66	6.5×10^{-1}	True
B4C	1206.7	3.343	113	1.19	3.2×10^{-1}	True
B12C	1142.6	3.253	114	-0.01	n/a ^a	True
B13C	1180.1	3.306	114	0.58	7.5×10^{-1}	True
B14C	1198.3	3.331	114	0.86	5.2×10^{-1}	True
B23C	1194.0	3.325	114	0.80	5.7×10^{-1}	True
B24C	1207.2	3.343	114	1.00	4.3×10^{-1}	True
B34C	1201.7	3.336	114	1.04	4.0×10^{-1}	True
B123C	1194.9	3.326	115	0.69	6.8×10^{-1}	True
B124C	1198.1	3.331	115	0.74	6.4×10^{-1}	True
B134C	1204.7	3.340	115	0.83	5.7×10^{-1}	True
B234C	1195.4	3.327	115	0.70	6.7×10^{-1}	True
BC	1195.8	3.328	116	0.62	7.6×10^{-1}	True
A1BC	1471.3	3.691	117	3.44	9.2×10^{-4}	False
A2BC	1467.2	3.686	117	3.40	1.0×10^{-3}	False
A3BC	7246.8	8.191	117	64.05	3.2×10^{-39}	False
A4BC	3356.2	5.575	117	23.22	1.5×10^{-21}	False
A12BC	1889.7	4.183	118	7.05	1.9×10^{-8}	False
A13BC	8143.4	8.683	118	66.12	2.1×10^{-41}	False
A14BC	4755.4	6.636	118	34.12	5.4×10^{-29}	False
A23BC	1577.1	3.821	118	4.10	8.5×10^{-5}	False
A24BC	6965.0	8.031	118	54.99	8.9×10^{-38}	False
A34BC	8706.5	8.979	118	71.44	6.0×10^{-43}	False
A123BC	9897.8	9.573	119	75.17	2.1×10^{-45}	False
A124BC	10029.4	9.637	119	76.30	1.0×10^{-45}	False
A134BC	9693.6	9.474	119	73.42	6.4×10^{-45}	False
A234BC	9920.5	9.584	119	75.37	1.9×10^{-45}	False
ABC	10032.7	9.638	120	69.97	3.2×10^{-45}	False

^a No p-value was calculated as the F-value was negative due to the WSSQ being smaller than that of the "Full" parameter set, indicating the null hypothesis is true.

Table C.3.2: Suitable parameter value sets for the CO₂-K₂CO₃-KHCO₃-H₂O system.

Parameter Set	WSSQ	Logic Test
C24	1100.3	7
B1C	1105.0	3
C3	1129.1	9
B12C	1142.6	2
FULL	1143.4	8
C4	1160.7	8
C123	1178.2	6
B2C	1178.2	5
B3C	1178.4	5
B13C	1180.1	4
C	1188.6	5
C234	1191.1	6
C134	1192.0	6
B23C	1194.0	3
B123C	1194.9	2
B234C	1195.4	2
BC	1195.8	1
B124C	1198.1	3
C34	1198.3	7
B14C	1198.3	3
C23	1199.3	7
B34C	1201.7	0
B134C	1204.7	2
B4C	1206.7	4
B24C	1207.2	4
C124	1214.5	6

Table C.3.3: Statistical results for the CO₂-H₂S-K₂CO₃-KHCO₃-KHS-K₂S-H₂O system data regression runs.

Parameter Set	WSSQ	RRMSQE	df	F	p	Null Hypothesis
Full	2006.6	4.177	115	-	-	-
C1	3221.7	5.293	116	69.63	1.8×10 ⁻¹³	False
C2	1962.6	4.131	116	-2.53	n/a ^a	True
C3	3225.1	5.296	116	69.83	1.7×10 ⁻¹³	False
C4	3850.9	5.787	116	105.69	5.6×10 ⁻¹⁸	False
C12	1985.1	4.155	117	-0.62	n/a ^a	True
C13	3860.6	5.794	117	53.12	4.6×10 ⁻¹⁷	False
C14	3860.6	5.794	117	53.12	4.6×10 ⁻¹⁷	False
C23	1981.6	4.151	117	-0.72	n/a ^a	True
C24	3224.0	5.295	117	34.88	1.4×10 ⁻¹²	False
C34	3851.0	5.787	117	52.85	5.3×10 ⁻¹⁷	False
C123	1995.6	4.166	118	-0.21	n/a ^a	True
C124	1991.8	4.162	118	-0.28	n/a ^a	True
C134	3860.6	5.794	118	35.42	2.8×10 ⁻¹⁶	False
C234	3227.9	5.298	118	23.33	7.2×10 ⁻¹²	False
C	3259.7	5.324	119	17.95	1.8×10 ⁻¹¹	False
B1C	2014.7	4.186	120	0.09	9.9×10 ⁻¹	True
B2C	3314.8	5.369	120	14.99	2.6×10 ⁻¹¹	False
B3C	3892.1	5.818	120	21.61	3.4×10 ⁻¹⁵	False
B4C	3892.1	5.818	120	21.61	3.4×10 ⁻¹⁵	False
B12C	3363.3	5.408	121	12.96	3.8×10 ⁻¹¹	False
B13C	3980.0	5.883	121	18.85	3.5×10 ⁻¹⁵	False
B14C	3980.0	5.883	121	18.85	3.5×10 ⁻¹⁵	False
B23C	3319.9	5.373	121	12.54	7.7×10 ⁻¹¹	False
B24C	3317.9	5.371	121	12.52	7.9×10 ⁻¹¹	False
B34C	3892.1	5.818	121	18.01	1.2×10 ⁻¹⁴	False
B123C	4035.0	5.923	122	16.61	5.5×10 ⁻¹⁵	False
B124C	3366.4	5.410	122	11.13	1.1×10 ⁻¹⁰	False
B134C	3980.0	5.883	122	16.16	1.2×10 ⁻¹⁴	False
B234C	3689.0	5.664	122	13.77	7.5×10 ⁻¹³	False
BC	3718.5	5.686	123	12.26	1.4×10 ⁻¹²	False
A1BC	3898.5	5.822	124	12.05	3.1×10 ⁻¹³	False
A2BC	4906.3	6.532	124	18.46	1.1×10 ⁻¹⁸	False
A3BC	4027.1	5.918	124	12.87	5.4×10 ⁻¹⁴	False
A4BC	4031.1	5.921	124	12.89	5.1×10 ⁻¹⁴	False
A12BC	255230.6	47.110	125	1451.21	5.2×10 ⁻¹¹⁶	False
A13BC	4445.9	6.218	125	13.98	7.1×10 ⁻¹⁶	False
A14BC	4466.3	6.232	125	14.10	5.5×10 ⁻¹⁶	False
A23BC	5648.7	7.009	125	20.87	1.4×10 ⁻²¹	False
A24BC	5730.4	7.059	125	21.34	6.2×10 ⁻²²	False
A34BC	22110.0	13.866	125	115.21	4.4×10 ⁻⁵⁵	False
A123BC	255249.6	47.112	126	1319.39	1.8×10 ⁻¹¹⁵	False
A124BC	255255.3	47.113	126	1319.41	1.8×10 ⁻¹¹⁵	False
A134BC	24056.8	14.463	126	114.88	1.2×10 ⁻⁵⁶	False
A234BC	23051.6	14.158	126	109.64	1.4×10 ⁻⁵⁵	False
ABC	268481.8	48.318	127	1272.63	3.5×10 ⁻¹¹⁶	False

^a No p-value was calculated as the F-value was negative due to the WSSQ being smaller than that of the "Full" parameter set, indicating the null hypothesis is true.

Table C.3.4: Suitable parameter value sets for the CO₂-H₂S-K₂CO₃-KHCO₃-KHS-K₂S-H₂O system.

Parameter Set	WSSQ	Logic Test
C2	1962.6	4
C23	1981.6	7
C12	1985.1	5
C124	1991.8	6
C123	1995.6	7
FULL	2006.6	12
B1C	2014.7	0

APPENDIX D

ASPEN CUSTOM MODELER® SIMULATION RESULTS

This appendix presents the results for the Aspen Custom Modeler® simulations. The column profiles generated from the preliminary column simulations are provided; along with the column profiles produced by the Aspen Custom Modeler® CO₂ train process models. Also included is a table of alternative correlations for estimating the mass transfer coefficients and effective interfacial area.

D.1 The Different Modelling Approaches

The absorber CO₂ and H₂S vapour phase profiles and the regenerator liquid phase CO₂ and H₂S loading profiles for CO₂ trains #2 to #6 are presented below for the three different modelling approaches.

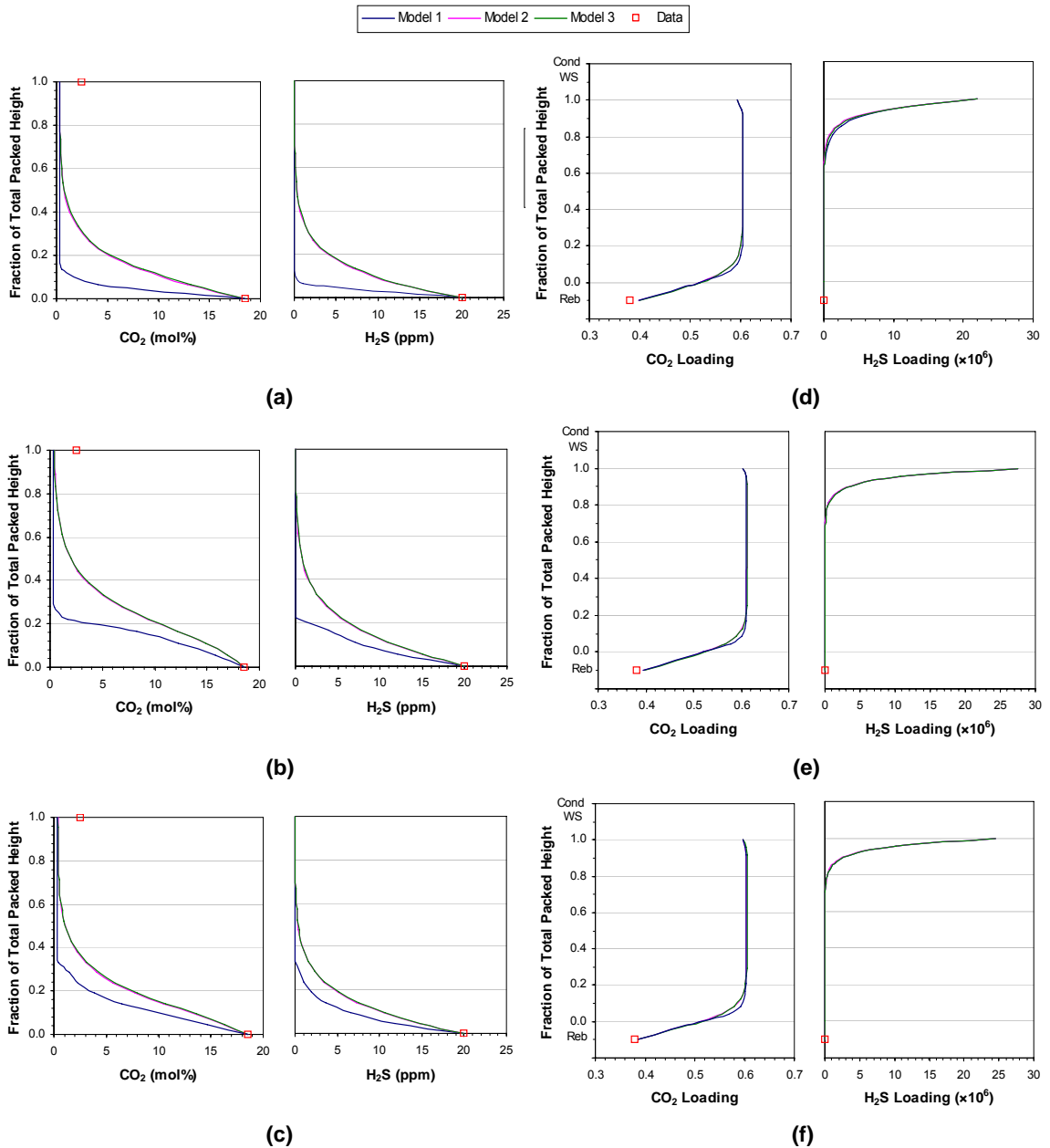
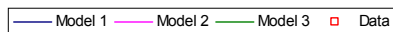


Figure D.1.1: Results of the different modelling approaches for CO₂ trains #2 to #4. Absorber CO₂ and H₂S vapour phase profiles for (a) train #2, (b) train #3 and (c) train #4. Regenerator liquid phase CO₂ and H₂S loading profiles for (d) train #2, (e) train #3 and (f) train #4 (Cond = condenser, WS = wash section, Reb = reboiler).



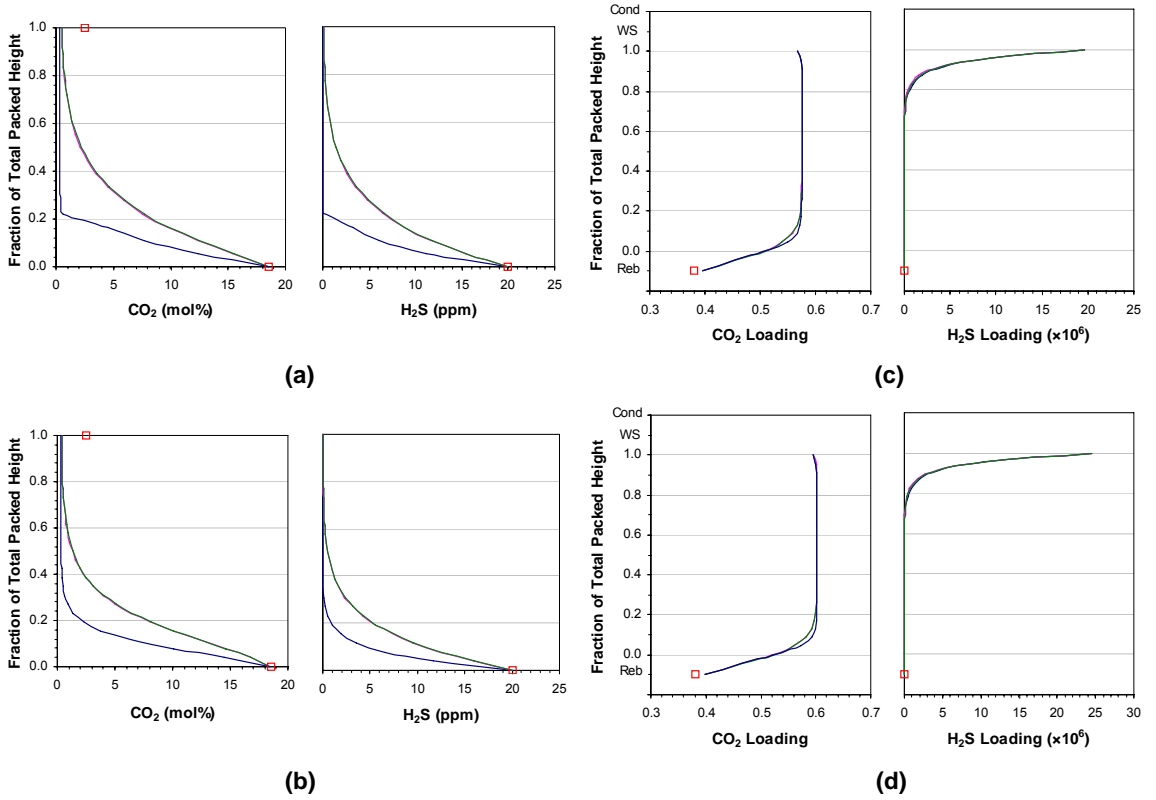


Figure D.1.2: Results of the different modelling approaches for CO₂ trains #5 and #6. Absorber CO₂ and H₂S vapour phase profiles for (a) train #5 and (b) train #6. Regenerator liquid phase CO₂ and H₂S loading profiles for (c) train #5 and (d) train #6 (Cond = condenser, WS = wash section, Reb = reboiler).

D.2 Model Adjustments

D.2.1 Liquid Phase Enthalpy Correction

The temperature profiles predicted by Model 2 for the absorber and regenerator columns in CO₂ trains #2 to #6 are presented below. The effect of the liquid phase enthalpy correction on the absorber temperature profiles is also included.

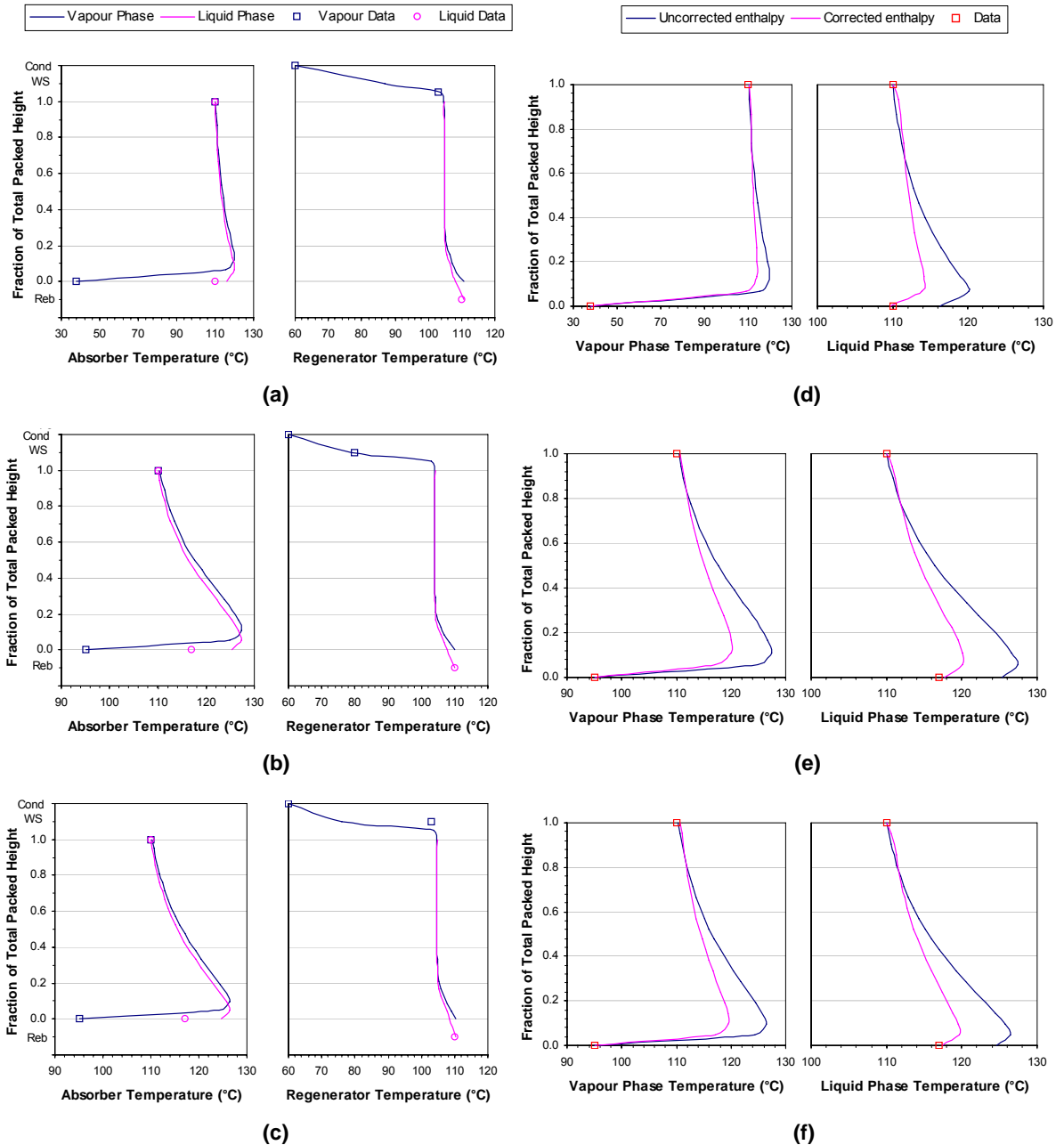


Figure D.2.1: Temperature profiles for CO₂ trains #2 to #4. Temperature profiles predicted by Model 2 for (a) train #2, (b) train #3 and (c) train #4 (Cond = condenser, WS = wash section, Reb = reboiler). Effect of the liquid phase enthalpy correction on the absorber temperatures for (d) train #2, (e) train #3 and (f) train #4.

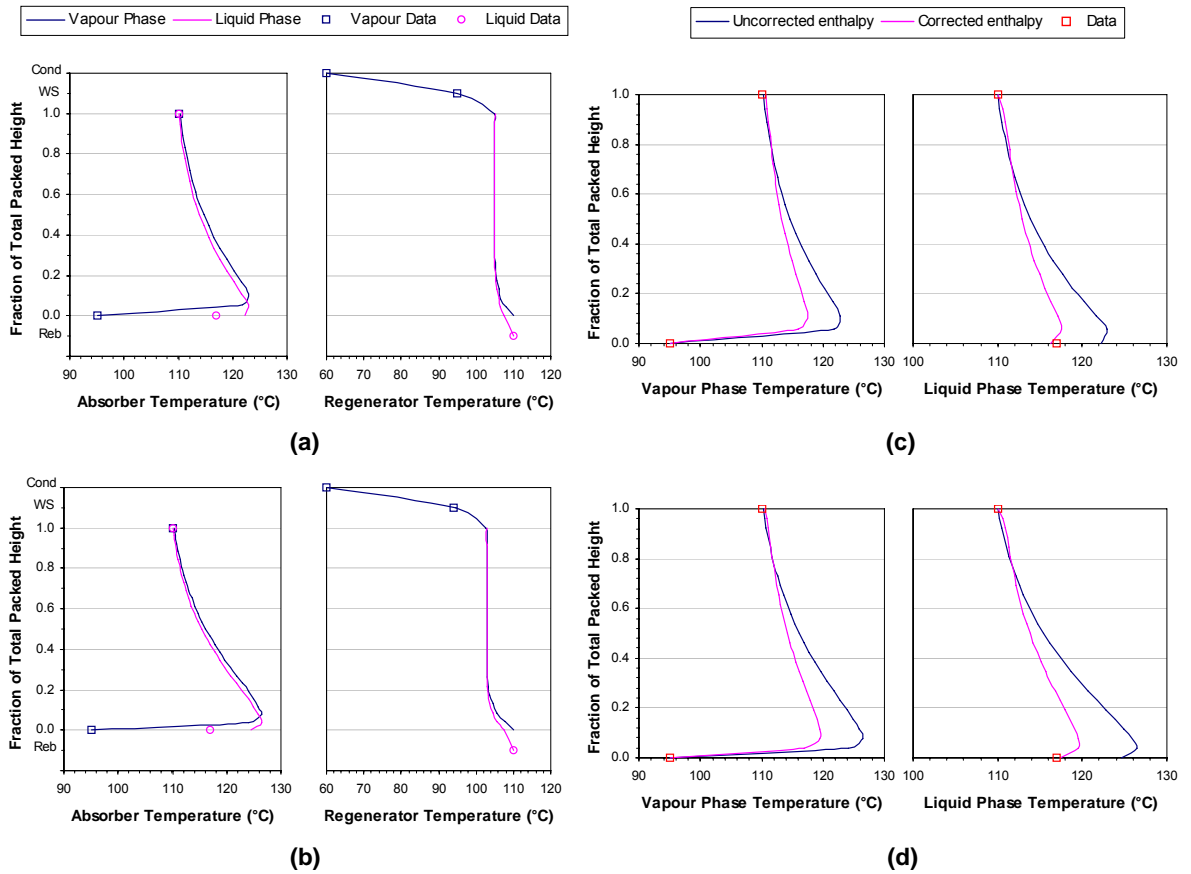


Figure D.2.2: Temperature profiles for CO₂ trains #5 and #6. Temperature profiles predicted by Model 2 for (a) train #5 and (b) train #6 (Cond = condenser, WS = wash section, Reb = reboiler). Effect of the liquid phase enthalpy correction on the absorber temperatures for (c) train #5 and (d) train #6.

D.2.2 Sensitivity to Model Parameters

Table D.2.1 lists some alternative correlations for estimating the mass transfer coefficients and the effective interfacial area.

Table D.2.1: Alternative mass transfer coefficient and effective interfacial area correlations.

Mass Transfer Coefficient Correlations	
Van Krevelen and Hoftijzer (1948)	$k_{Gj} = 0.2 \cdot \frac{D_{Gj}}{d_N} \cdot \left(\frac{\rho_G \cdot v_G}{a \cdot \mu_G} \right)^{0.8} \cdot \left(\frac{\mu_G}{\rho_G \cdot D_{Gj}} \right)^{1/3}$ $k_{Lj} = 0.015 \cdot D_{Lj} \cdot \left(\frac{\rho_L^2 \cdot g}{\mu_L^2} \right)^{1/3} \cdot \left(\frac{\rho_L \cdot v_L}{a_i \cdot \mu_L} \right)^{2/3} \cdot \left(\frac{\mu_L}{\rho_L \cdot D_{Lj}} \right)^{1/3}$
Shulman and co-workers (1955)	$k_{Gj} = 1.195 \cdot v_G \cdot \left(\frac{d_p \cdot \rho_G \cdot v_G}{\mu_G \cdot (1 - \phi)} \right)^{0.8} \cdot \left(\frac{\rho_G \cdot D_{Gj}}{\mu_G} \right)^{2/3}$ $k_{Lj} = 25.1 \cdot \frac{D_{Lj}}{d_p} \cdot \left(\frac{d_p \cdot \rho_L \cdot v_L}{a_i \cdot \mu_L} \right)^{0.45} \cdot \left(\frac{\mu_L}{\rho_L \cdot D_{Lj}} \right)^{0.5}$
Billet and Schultes (1999)	$k_{Gj} = \beta_G \cdot D_{Gj} \cdot \left(\frac{a}{d_h \cdot (\phi - \phi_L)} \right)^{0.5} \cdot \left(\frac{\rho_G \cdot v_G}{a \cdot \mu_G} \right)^{0.75} \cdot \left(\frac{\mu_G}{\rho_G \cdot D_{Gj}} \right)^{1/3}$ $k_{Lj} = \beta_L \cdot \left(\frac{\rho_L \cdot g}{\mu_L} \right)^{1/6} \cdot \left(\frac{D_{Lj}}{d_h} \right)^{0.5} \cdot \left(\frac{v_L}{a} \right)^{1/3}$
Effective Interfacial Area Correlations	
Puranik and Vogelwohl (1974)	$\frac{a_i}{a} = 1.045 \cdot \left(\frac{\rho_L \cdot v_L}{a \cdot \mu_L} \right)^{0.041} \cdot \left(\frac{\rho_L \cdot v_L^2}{a \cdot \sigma_L} \right)^{0.133} \cdot \left(\frac{\sigma_c}{\sigma_L} \right)^{0.182}$
Kolev (1976)	$\frac{a_i}{a} = 0.583 \cdot \left(\frac{\rho_L \cdot g}{a^2 \cdot \sigma_L} \right)^{0.49} \cdot \left(\frac{v_L^2 \cdot a}{g} \right)^{0.196} \cdot (a \cdot d_p)^{0.42}$
Bravo and Fair (1982)	$\frac{a_i}{a} = 19.76 \cdot \left(\frac{v_L \cdot \mu_L}{\sigma_L} \cdot \frac{\rho_G \cdot v_G}{a \cdot \mu_G} \right)^{0.392} \cdot \frac{\sigma_L^{0.5}}{H_c^{0.4}}$
Billet and Schultes (1999)	$\frac{a_i}{a} = \frac{1.5}{(a \cdot d_h)^{0.5}} \cdot \left(\frac{\rho_L \cdot v_L \cdot d_h}{\mu_L} \right)^{-0.2} \cdot \left(\frac{\rho_L \cdot v_L^2 \cdot d_h}{\sigma_L} \right)^{0.75} \cdot \left(\frac{v_L^2}{g \cdot d_h} \right)^{-0.45}$

Note: All variables are in SI units. Notation: D_j is the component diffusivity; ρ is the mass density; μ is the viscosity; a is the packing specific surface area; v is the phase flow velocity; g is the gravitational constant; d_N is the nominal packing size; d_p is the packing particle diameter; d_h is the packing hydraulic diameter; ϕ is the voidage; ϕ_L is the liquid phase volumetric holdup; β is a packing-specific constant; σ_L is the surface tension; σ_c is the critical surface tension parameter; H_c is the column height; D_c is the column diameter; G and L are the vapour and liquid phase molar flow rates; C_i is the molar density; and the subscripts G and L denote the vapour and liquid phases.

D.2.3 Effective Interfacial Area Adjustment Factor

The effect of the effective interfacial area adjustment factor on the absorber CO₂ and H₂S vapour phase profiles for CO₂ trains #2 to #6 are presented below.

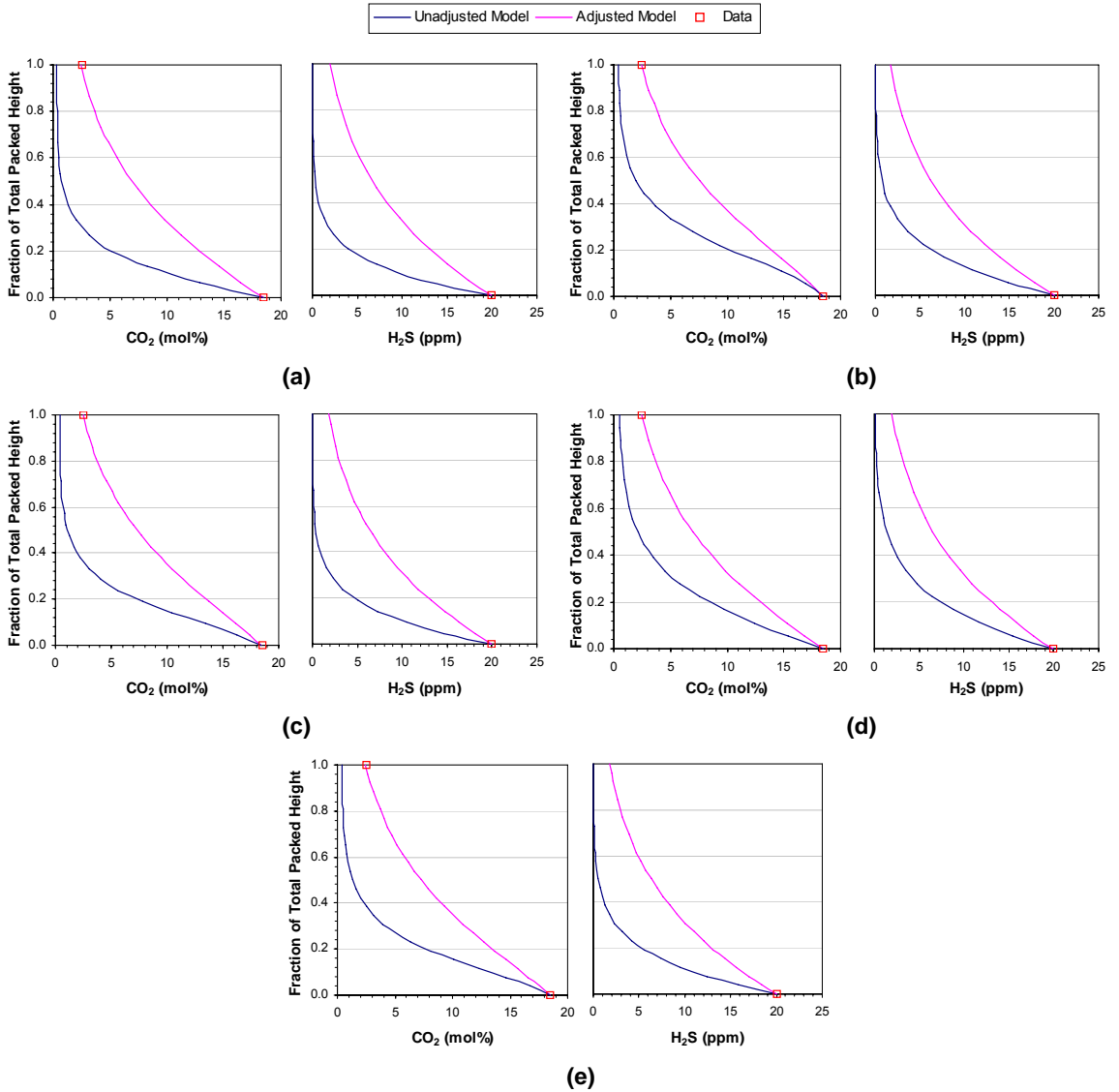


Figure D.2.3: Effect of the effective interfacial area adjustment factor on the absorber CO₂ and H₂S vapour phase profiles. (a) CO₂ train #2. (b) CO₂ train #3. (c) CO₂ train #4. (d) CO₂ train #5. (e) CO₂ train #6.

D.3 CO₂ Train Model Validation

The vapour and liquid phase composition profiles and the temperature profiles for the absorber and regenerator columns in the Aspen Custom Modeler® models for CO₂ trains #2 to #6 are presented below.

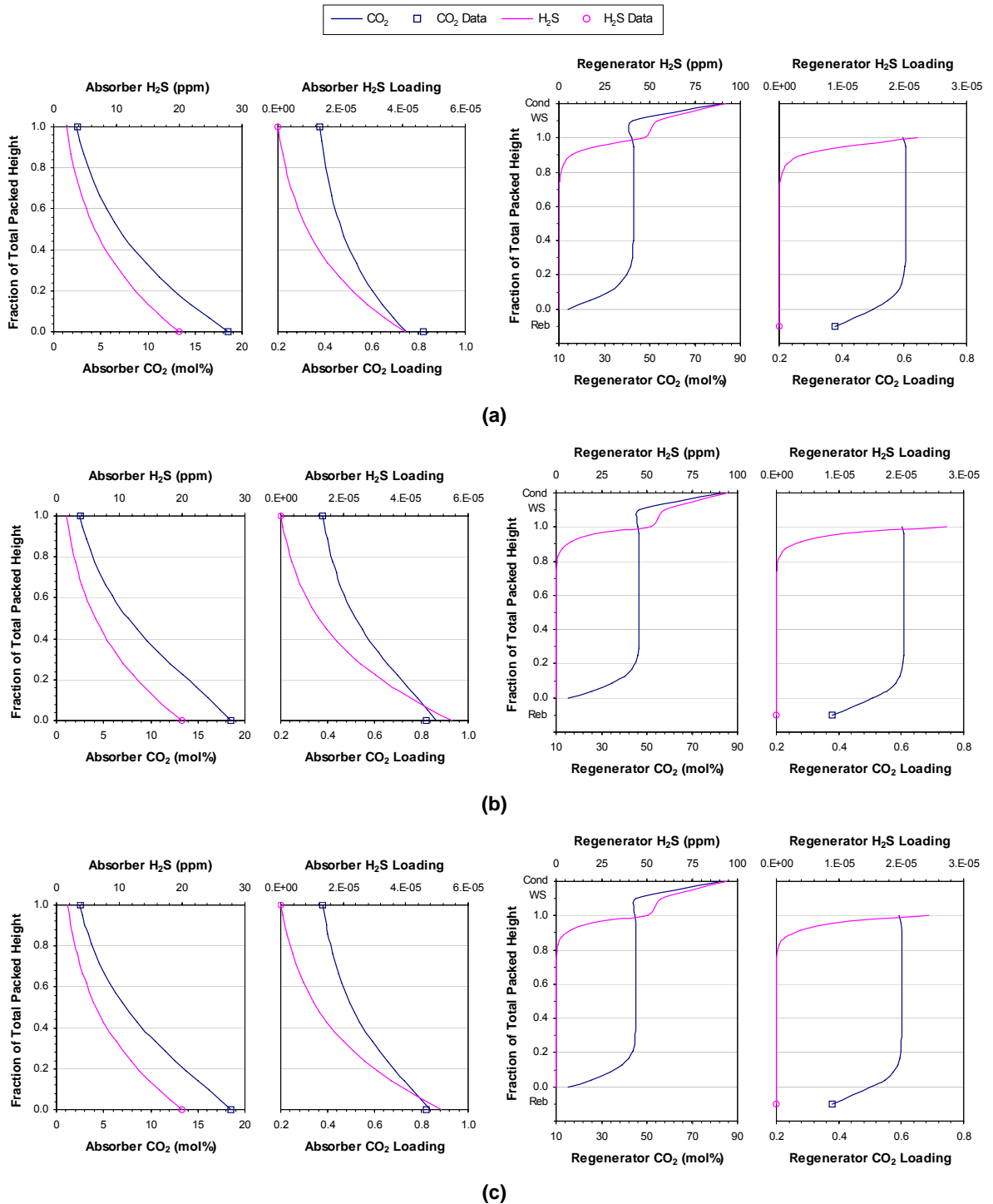


Figure D.3.1: CO₂ and H₂S vapour and liquid phase column profiles for the first set of plant data. (a) CO₂ train #2. (b) CO₂ train #3. (c) CO₂ train #4. (Cond = condenser, WS = wash section, Reb = reboiler)

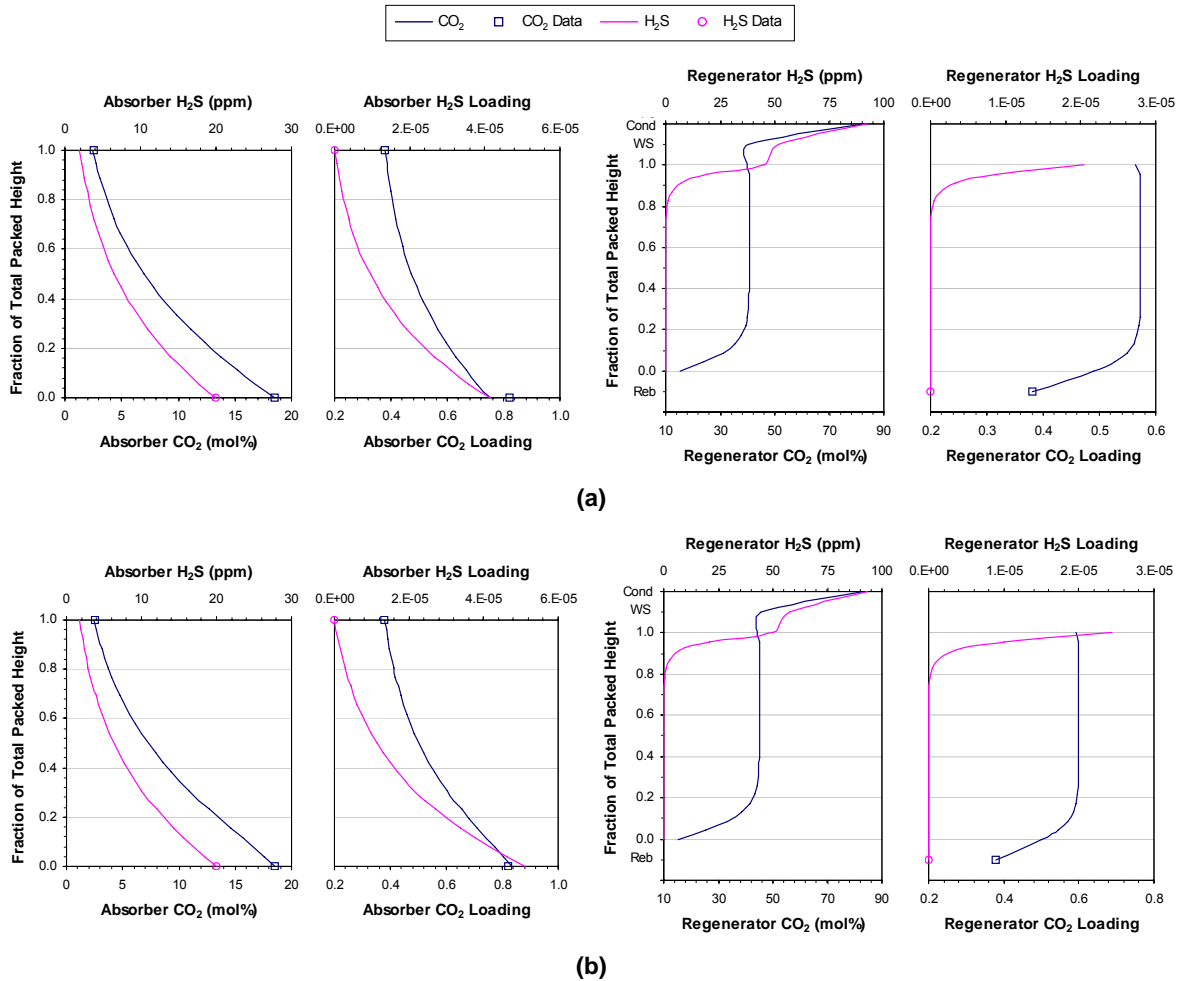


Figure D.3.2: CO₂ and H₂S vapour and liquid phase column profiles for the first set of plant data. (a) CO₂ train #5. (b) CO₂ train #6. (Cond = condenser, WS = wash section, Reb = reboiler)

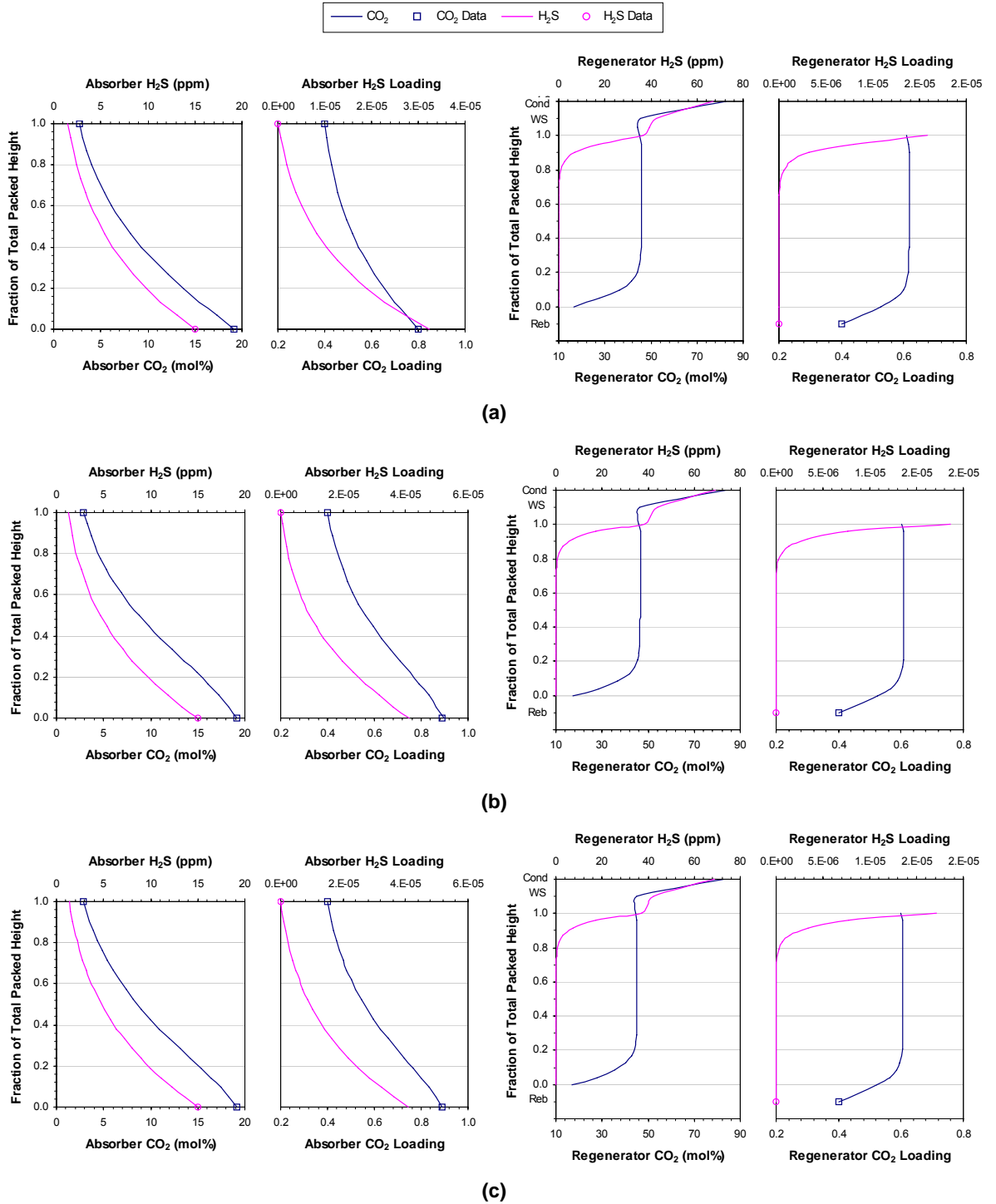


Figure D.3.3: CO₂ and H₂S vapour and liquid phase column profiles for the second set of plant data. (a) CO₂ train #2. (b) CO₂ train #3. (c) CO₂ train #4. (Cond = condenser, WS = wash section, Reb = reboiler)

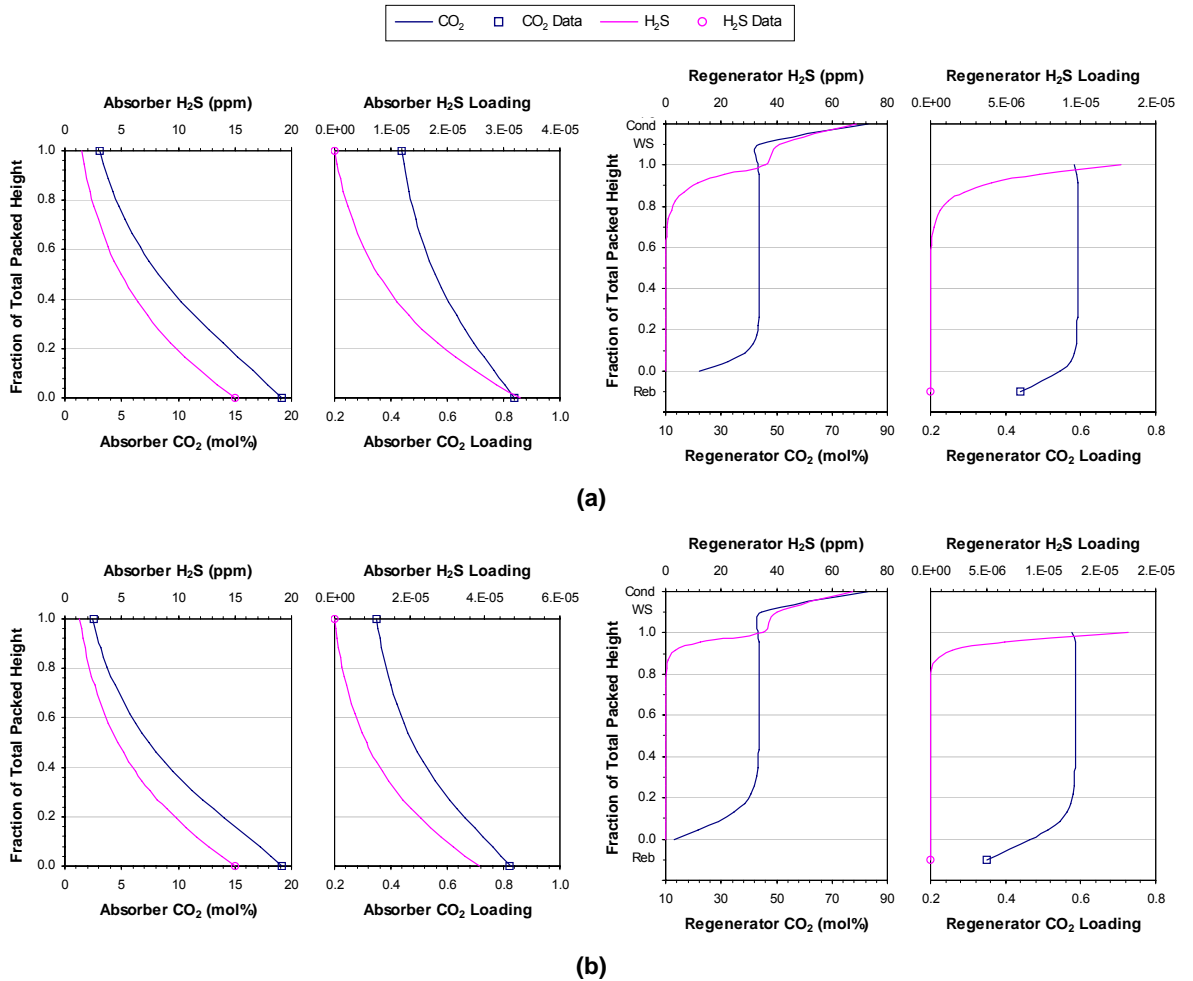


Figure D.3.4: CO₂ and H₂S vapour and liquid phase column profiles for the second set of plant data. (a) CO₂ train #5. (b) CO₂ train #6. (Cond = condenser, WS = wash section, Reb = reboiler)

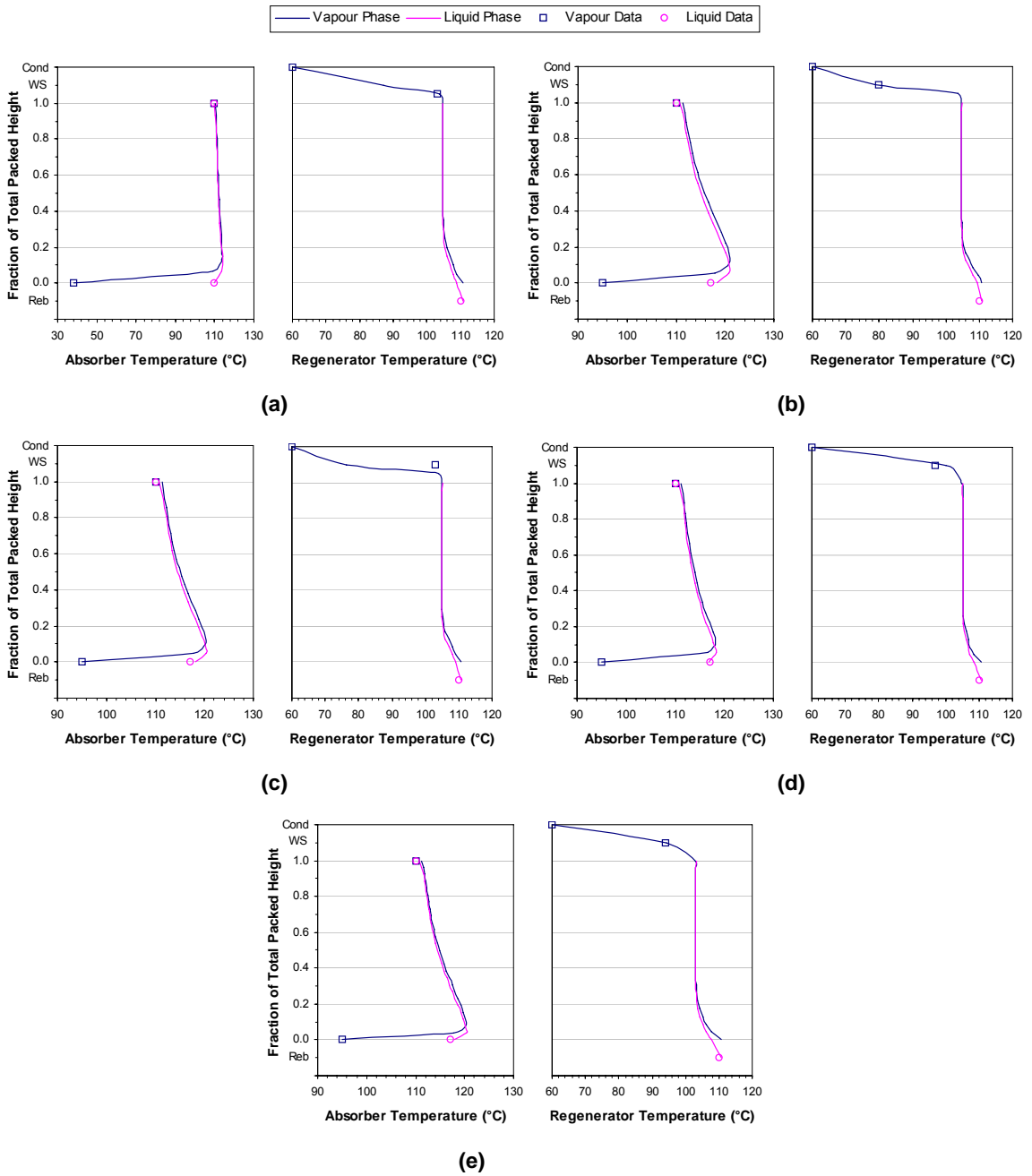


Figure D.3.5: Column temperature profiles for the first set of plant data. (a) CO₂ train #2. (b) CO₂ train #3. (c) CO₂ train #4. (d) CO₂ train #5. (e) CO₂ train #6. (Cond = condenser, WS = wash section, Reb = reboiler)

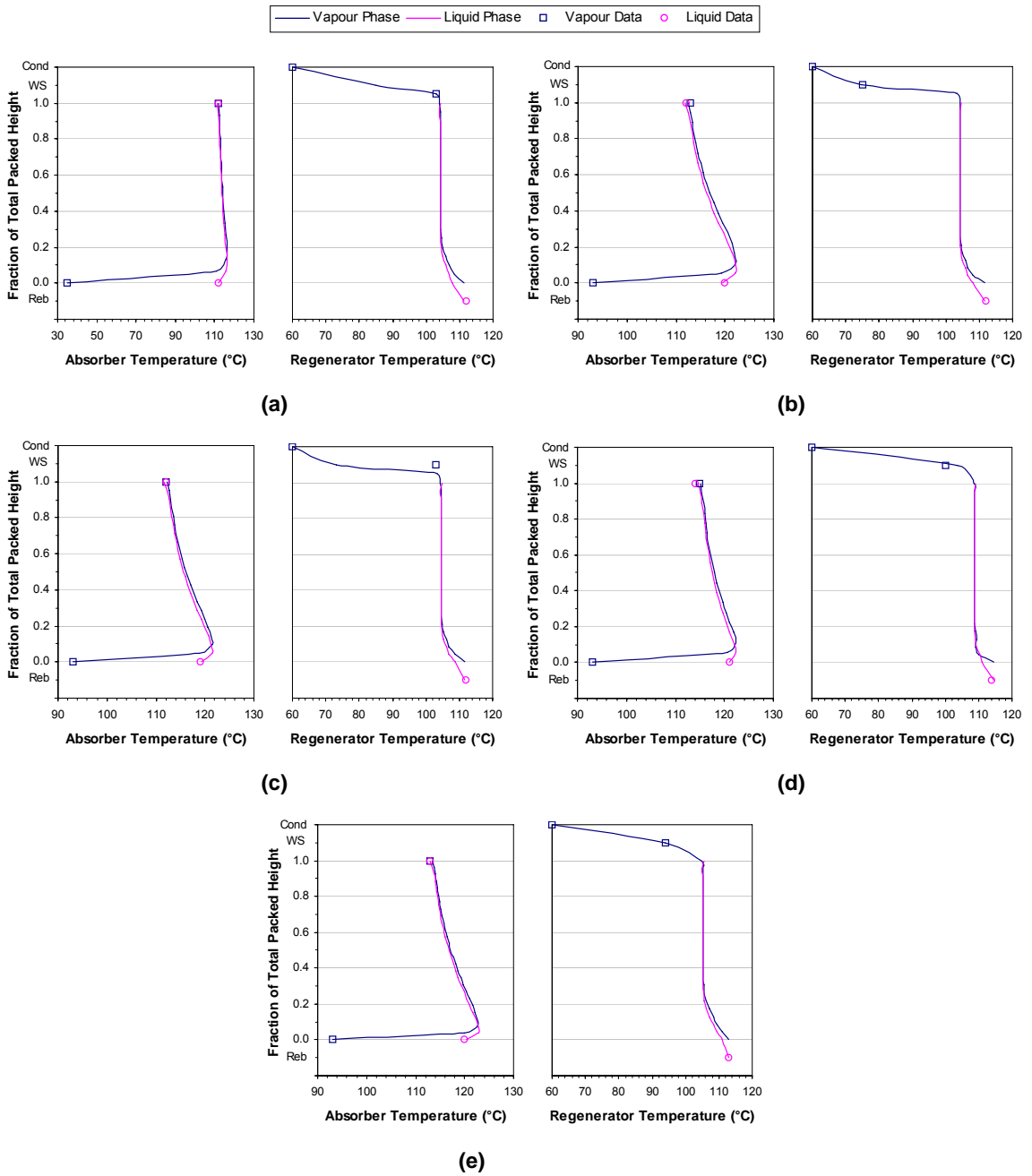


Figure D.3.6: Column temperature profiles for the second set of plant data. (a) CO₂ train #2. (b) CO₂ train #3. (c) CO₂ train #4. (d) CO₂ train #5. (e) CO₂ train #6. (Cond = condenser, WS = wash section, Reb = reboiler)

APPENDIX E

HYPOTHETICAL K₂CO₃* HYSYS® COMPONENT PROPERTIES

This appendix presents the various physical and thermodynamic properties required for the creation of the hypothetical K₂CO₃* HYSYS® component.

E.1 Base Properties

E.1.1 Normal Boiling Point

When the normal boiling point is unknown for a hypothetical component, HYSYS® uses a proprietary method to estimate this property (Hyprotech Ltd, 2001a). In the case of the hypothetical $K_2CO_3^*$ component, the potassium carbonate melting point of 900.85°C (Chase, 1998) was used as the hypothetical component's normal boiling point since potassium carbonate does not boil, but instead begins to decompose at temperatures close to its melting point.

E.1.2 Molecular Weight

HYSYS® has two default methods for estimating the molecular weight of hypothetical components: the Bergman method (Bergman et al., 1975) and the Lee-Kesler model (Kesler and Lee, 1976). The former method is applied only to components with boiling points less than 155°F (68.3°C) and is based on tabulated molecular weights of gas condensate carbon number fractions from C_5 to C_{45} that were obtained from a study of US gas condensate mixtures by Bergman and co-workers (1975). The latter estimation method is used for all other hypothetical components and gives the molecular weight MW as a function of the boiling point T_b in °R and the specific gravity SG:

$$\begin{aligned} MW = & -12272.6 + 9486.4 \cdot SG + (4.6523 - 3.3287 \cdot SG) \cdot T_b \\ & + \left(1 - 0.77084 \cdot SG - 0.02058 \cdot SG^2\right) \cdot \left(1.3437 - \frac{720.79}{T_b}\right) \cdot \frac{10^7}{T_b} \\ & + \left(1 - 0.80882 \cdot SG + 0.02226 \cdot SG^2\right) \cdot \left(1.8828 - \frac{181.9}{T_b}\right) \cdot \frac{10^{12}}{T_b^3} \end{aligned} \quad (E.1.1)$$

It should be noted that SG refers to 60°F/60°F specific gravity, i.e. the mass ratio of equal volumes of the component of interest and water at 60°F.

For the hypothetical $K_2CO_3^*$ component, neither estimation method was used since the molecular weight was taken to be that of potassium carbonate: 138.2058 kg/kmol (Chase, 1998).

E.1.3 Ideal Liquid Density

The default estimation method for determining the ideal liquid density of a hypothetical component in HYSYS® is the following correlation proposed by Yen and Woods (1966):

$$\frac{V_c}{V_L^s} = 1 + \sum_{j=1}^4 K_j \cdot \left(1 - \frac{T}{T_c}\right)^j \quad (E.1.2)$$

$$K_1 = 17.4425 - 214.578 \cdot Z_c + 989.625 \cdot Z_c^2 - 1522.06 \cdot Z_c^3 \quad (E.1.3)$$

$$K_2 = -3.28257 + 13.6377 \cdot Z_c + 107.4844 \cdot Z_c^2 - 384.211 \cdot Z_c^3 \quad \text{if } Z_c \leq 0.26 \quad (E.1.4)$$

$$K_2 = 60.2091 - 402.063 \cdot Z_c + 501.0 \cdot Z_c^2 + 641.0 \cdot Z_c^3 \quad \text{if } Z_c > 0.26 \quad (E.1.5)$$

$$K_3 = 0 \quad (E.1.6)$$

$$K_4 = 0.93 - K_2 \quad (E.1.7)$$

where V_c is the critical molar volume, V_L^s is the saturated liquid molar volume, T is the temperature, T_c is the critical temperature, and Z_c is the critical compressibility.

For the hypothetical $K_2CO_3^*$ component, the ideal liquid density was not estimated by the above method, but was instead taken to be 2423.11 kg/m^3 , the density of solid potassium carbonate (Perry and Green, 1997).

E.1.4 Critical Temperature and Critical Pressure

Three default methods are available in HYSYS® for estimating the critical temperatures and critical pressures of hypothetical components: the Lee-Kesler model (Kesler and Lee, 1976), the Bergman method (Bergman, 1976) and the Cavett relations (Cavett, 1964). The first method is used for components with liquid densities greater than 1067 kg/m^3 or boiling points above 800 K, and consists of the following correlations:

$$T_c = 341.7 + 811 \cdot SG + (0.4244 + 0.1174 \cdot SG) \cdot T_b + (0.4669 - 3.2623 \cdot SG) \cdot \frac{10^5}{T_b} \quad (E.1.8)$$

$$\begin{aligned} \ln P_c = & 8.3634 - \frac{0.0566}{SG} - \left(0.24244 + \frac{2.2898}{SG} + \frac{0.11857}{SG^2} \right) \cdot 10^{-3} \cdot T_b \\ & + \left(1.4685 + \frac{3.648}{SG} + \frac{0.47227}{SG^2} \right) \cdot 10^{-7} \cdot T_b^2 - \left(0.42019 + \frac{1.6977}{SG^2} \right) \cdot 10^{-10} \cdot T_b^3 \end{aligned} \quad (E.1.9)$$

where the critical temperature T_c and the boiling point T_b are in °R, P_c is the critical pressure in psia, and SG is the 60°F/60°F specific gravity. The second method by Bergman (1976) is only applied to components with low densities ($< 850 \text{ kg/m}^3$) and low boiling points ($< 548.316 \text{ K}$), and was therefore not of interest in this work. The last method by Cavett (1964) is used for all other hypothetical components and is of the following form:

$$\begin{aligned} T_c = & 768.071 + 1.7134 \cdot T_b - 0.10834 \times 10^{-2} \cdot T_b^2 + 0.3889 \times 10^{-6} \cdot T_b^3 \\ & - 0.89213 \times 10^{-2} \cdot T_b \cdot \left(\frac{141.5}{SG} - 131.5 \right) + 0.53095 \times 10^{-6} \cdot T_b^2 \cdot \left(\frac{141.5}{SG} - 131.5 \right) \\ & + 0.32712 \times 10^{-7} \cdot T_b^2 \cdot \left(\frac{141.5}{SG} - 131.5 \right)^2 \end{aligned} \quad (E.1.10)$$

$$\begin{aligned} \log P_c = & 2.829 + 0.9412 \times 10^{-3} \cdot T_b - 0.30475 \times 10^{-5} \cdot T_b^2 + 0.15141 \times 10^{-8} \cdot T_b^3 \\ & - 0.20876 \times 10^{-4} \cdot T_b \cdot \left(\frac{141.5}{SG} - 131.5 \right) + 0.11048 \times 10^{-7} \cdot T_b^2 \cdot \left(\frac{141.5}{SG} - 131.5 \right) \\ & + 0.1395 \times 10^{-9} \cdot T_b^2 \cdot \left(\frac{141.5}{SG} - 131.5 \right)^2 - 0.4827 \times 10^{-7} \cdot T_b \cdot \left(\frac{141.5}{SG} - 131.5 \right)^2 \end{aligned} \quad (E.1.11)$$

where T_c and T_b are in °F, P_c is in psia, and SG is the 60°F/60°F specific gravity.

Since the critical temperature and critical pressure of potassium carbonate were not available in literature, the Lee-Kesler model was used to estimate these two critical properties for the hypothetical $K_2CO_3^*$ component. The critical temperature was estimated to be 1645.10°C while the critical pressure was estimated to be 4507.57 kPa.

E.1.5 Critical Volume and Acentricity

In HYSYS®, the correlations proposed by Pitzer and co-workers (1955) are the default estimation method for determining the critical volume and acentricity of hypothetical components belonging to the Miscellaneous class of components. These correlations take the following form:

$$Z_c = \frac{P_c \cdot V_c}{R \cdot T_c} = Z^{(0)}\left(\frac{T}{T_c}, \frac{P}{P_c}\right) + \omega \cdot Z^{(1)}\left(\frac{T}{T_c}, \frac{P}{P_c}\right) \quad \text{at } \frac{T}{T_c} = 1 \text{ and } \frac{P}{P_c} = 1 \quad (\text{E.1.12})$$

$$\omega = -\log\left(\frac{P^s}{P_c}\right) - 1.000 \quad \text{at } \frac{T}{T_c} = 0.7 \quad (\text{E.1.13})$$

where Z_c is the critical compressibility, P_c is the critical pressure, V_c is the critical molar volume, T_c is the critical temperature, P is the pressure, T is the temperature, ω is the acentricity, and P^s is the vapour pressure. $Z^{(0)}$ and $Z^{(1)}$ are functions of T , P , T_c and P_c .

As literature values for the critical volume and acentricity of potassium carbonate were unavailable, the Pitzer model was used to estimate these two properties for the hypothetical $K_2CO_3^*$ component. The critical volume was estimated to be 0.997346 m³/kmol while the acentricity was estimated to be 0.107562.

E.2 Additional Point Properties

E.2.1 Heat of Formation

Two default methods are available for the estimation of the heat (or enthalpy) of formation at 25°C for hypothetical HYSYS® components. If the component's structure can be defined in terms of UNIFAC groups, the method proposed by Joback (1984) is applied; otherwise, a simple ratio with respect to octane (Hyprotech Ltd, 2001a) is used instead. The Joback method is a group contribution method that takes the form:

$$\Delta h_{25^\circ\text{C}}^f = 68.29 + \sum_k N_k \cdot \Delta h_{fk} \quad (\text{E.2.1})$$

where $\Delta h_{25^\circ\text{C}}^f$ is the heat of formation at 25°C in kJ/mol, N_k is the number of UNIFAC groups of type k and Δh_{fk} is the contribution for group k to the heat of formation in kJ/mol. The alternative HYSYS® default method takes the form:

$$\Delta h_{25^\circ\text{C}}^f = \frac{\Delta h_{25^\circ\text{C}, \text{octane}}^f \cdot \text{MW}}{\text{MW}_{\text{octane}}} \quad (\text{E.2.2})$$

where MW is the molecular weight.

For the hypothetical $K_2CO_3^*$ component, the heat of formation was not estimated by either of the above two methods, but was instead taken to be that for potassium carbonate: -1144610 kJ/kmol (Chase, 1998).

E.2.2 Dipole Moment

No default estimation method for the dipole moment of a hypothetical component is currently available in HYSYS®. Instead, the dipole moments for such components are set equal to zero (Hyprotech Ltd, 2001a). Consequently, the dipole moment for the hypothetical $K_2CO_3^*$ component was set as 0.00 Debye.

E.2.3 Radius of Gyration

To estimate the radius of gyration for a hypothetical component, HYSYS® uses a proprietary method (Hyprotech Ltd, 2001a). For the hypothetical $K_2CO_3^*$ component, the radius of gyration estimated by this method was 2.64138 Å.

E.3 Temperature Dependent Properties

E.3.1 Ideal Gas Enthalpy

In HYSYS®, the ideal gas enthalpy h_{IG} of a component is calculated from the following temperature dependent relation:

$$h_{IG} = a + b \cdot T + c \cdot T^2 + d \cdot T^3 + e \cdot T^4 + f \cdot T^5 \quad (E.3.1)$$

where h_{IG} is in kJ/kg, T is in K, and the reference point is an ideal gas at 0 K. If not provided, the coefficients a to f are estimated from the ideal gas heat capacity correlation proposed by Cavett (1964):

$$\begin{aligned} C_{pIG} = & \left(0.036863384 \cdot \left(\frac{T_b^{1/3}}{SG} \right) - 0.4673722 \right) \cdot MW \\ & + \left(3.1865 \times 10^{-5} \cdot \left(\frac{T_b^{1/3}}{SG} \right) + 0.001045186 \right) \cdot MW \cdot T \\ & + \left(-4.9572 \times 10^{-7} \cdot MW \right) \cdot T^2 \end{aligned} \quad (E.3.2)$$

where C_{pIG} is the ideal gas heat capacity in Btu/lbmol·°R, T_b is the boiling point in °R, SG is the 60°F/60°F specific gravity, MW is the molecular weight, and T is the temperature in °R.

No thermochemical data were available for potassium carbonate in the ideal gas state. Consequently, heat capacity and enthalpy data from the NIST-JANAF Thermochemical Tables (Chase, 1998) for crystalline potassium carbonate were instead used to derive the coefficients for equation (E.3.1) for the hypothetical $K_2CO_3^*$ component. After the data had been corrected to account for the different reference temperatures (0 K for equation (E.3.1) and 25°C for the NIST-JANAF tables), the following relationship between heat capacity C_p and enthalpy h was used to regress the coefficient values given in Table E.3.1:

$$C_p = \left(\frac{\partial h}{\partial T} \right)_p = b + 2 \cdot c \cdot T + 3 \cdot d \cdot T^2 + 4 \cdot e \cdot T^3 + 5 \cdot f \cdot T^4 \quad (E.3.3)$$

where C_p is in kJ/kg·K, h is in kJ/kg, and T is in K.

Table E.3.1: Temperature dependent property correlation coefficients.

Coefficient	Ideal Gas Enthalpy	Ideal Gas Gibbs Free Energy	Vapour Pressure
a	-19.8419	-1142180	22.0529
b	0.365850	246.572	-27345.9
c	9.80515×10^{-4}	4.51346×10^{-2}	0.00
d	-5.86603×10^{-7}	0.00	-0.515316
e	2.49532×10^{-10}	0.00	2.08489
f	-3.99650×10^{-14}	–	0.00

E.3.2 Ideal Gas Gibbs Free Energy

The ideal gas Gibbs free energy G_{IG} of a component in HYSYS® is calculated from the following temperature dependent relation:

$$G_{IG} = a + b \cdot T + c \cdot T^2 + d \cdot T^3 + e \cdot T^4 \quad (E.3.4)$$

where G_{IG} is in kJ/kmol, T is in K, and the reference point is an ideal gas at 25°C. If not provided, the coefficients a to e are estimated from a HYSYS® proprietary method (Hyprotech Ltd, 2001a).

As mentioned above, no thermochemical data were available for potassium carbonate in the ideal gas state. Consequently, Gibbs free energy data from the NIST-JANAF Thermochemical Tables (Chase, 1998) for crystalline potassium carbonate were instead used to regress the coefficients for equation (E.3.4) for the hypothetical $K_2CO_3^*$ component. The resulting coefficient values are given in Table E.3.1.

E.3.3 Vapour Pressure

In HYSYS®, the vapour pressure of a component is calculated from the Modified Antoine equation:

$$\ln P^s = a + \frac{b}{T + c} + d \cdot \ln T + e \cdot T^f \quad (E.3.5)$$

where P^s is the vapour pressure in kPa and T is the temperature in K. If the coefficients a to f are not provided, HYSYS® estimates these based on the vapour pressures calculated from the correlation proposed by Riedel (1954):

$$\ln\left(\frac{P^s}{P_c}\right) = -2.933 \cdot (3.758 - \alpha_c) - 3.0168 \cdot (3.758 - \alpha_c) \cdot \left(\frac{T_c}{T}\right) + (3.5196 \cdot (3.758 - \alpha_c) + \alpha_c) \cdot \ln\left(\frac{T}{T_c}\right) - 0.0838 \cdot (3.758 - \alpha_c) \cdot \left(\frac{T}{T_c}\right)^6 \quad (E.3.6)$$

$$\alpha_c = \frac{0.315 \cdot \psi_b + \ln P_c}{0.0838 \cdot \psi_b - \ln\left(\frac{T_b}{T_c}\right)} \quad (E.2.7)$$

$$\psi_b = -35 + 36 \cdot \left(\frac{T_c}{T_b}\right) + 42 \cdot \ln\left(\frac{T_b}{T_c}\right) - \left(\frac{T_b}{T_c}\right)^6 \quad (E.3.8)$$

where P^s and the critical pressure P_c are in atm, and T, the critical temperature T_c and the boiling point T_b are in K.

Since vapour pressure data for potassium carbonate was unavailable in literature, data for an inorganic compound with a melting point similar to that for potassium carbonate was used instead to derive the coefficients for equation (E.3.5). The compound selected was lead oxide PbO which has a

melting point of 890°C (c.f. 900.85°C for potassium carbonate) and the coefficient values in Table E.3.1 were regressed from its vapour pressure data provided by Perry and Green (1997).

APPENDIX F

PROPERTY MODELS FOR HYSYS®

This appendix presents the various thermodynamic and physical property models utilised in the HYSYS® process models for the CO₂ trains. Where necessary, model parameters are regressed from literature data.

F.1 Thermodynamic Property Models

F.1.1 Enthalpy

For the HYSYS® simulations, the vapour and liquid phase enthalpies h were calculated from the rigorous thermodynamic relation:

$$\frac{h - h_{IG}}{R \cdot T} = Z - 1 + \frac{1}{R \cdot T} \cdot \int_{\infty}^V \left[T \cdot \left(\frac{\partial P}{\partial T} \right)_V - P \right] \cdot dV \quad (F.1.1)$$

which in terms of the enhanced PR equation of state is:

$$\frac{h - h_{IG}}{R \cdot T} = Z - 1 - \frac{1}{2^{1.5} \cdot b \cdot R \cdot T} \cdot \left(a - T \cdot \frac{da}{dT} \right) \cdot \ln \left(\frac{V + (\sqrt{2} + 1) \cdot b}{V + (\sqrt{2} - 1) \cdot b} \right) \quad (F.1.2)$$

h_{IG} is the ideal gas enthalpy (the ideal gas enthalpy of formation at 25°C), R is the gas constant, T is the absolute temperature, Z is the compressibility, V is the molar volume, P is the pressure, and a and b are the PR parameters.

F.1.2 Heat Capacity

The heat capacity C_p was calculated from the rigorous relation:

$$C_p = C_v - T \cdot \left(\frac{dP}{dV} \right)_T \cdot \left(\frac{dV}{dT} \right)_P^2 = \left(\frac{dU}{dT} \right)_V - T \cdot \left(\frac{dP}{dV} \right)_T \cdot \left(\frac{dV}{dT} \right)_P^2 \quad (F.1.3)$$

where U is the total internal energy. If a solution could not be obtained for this equation, the ideal gas method was applied instead:

$$\frac{C_p}{C_v} = \frac{C_p}{C_p - R} \quad (F.1.4)$$

F.2 Physical and Transport Property Models

F.2.1 Molecular Weight

For the HYSYS® simulations, the molecular weight MW of a phase was determined from the mole-fraction-weighted sums of the individual component molecular weights:

$$MW = \sum_{j=1}^{NC} x_j \cdot MW_j \quad (F.2.1)$$

where x is the mole fraction and NC is the number of components.

F.2.2 Density

F.2.2.1 Vapour Phase Density

The vapour phase mass density ρ_G was determined from:

$$\rho_G = \frac{P \cdot MW_G}{Z \cdot R \cdot T} \quad (F.2.2)$$

where P is the pressure, MW_G is the vapour phase molecular weight, Z is the vapour phase compressibility factor calculated from the enhanced PR equation of state, R is the gas constant, and T is the absolute pressure.

F.2.2.2 Liquid Phase Density

F.2.2.2.1 Sour PR Property Package

For the Sour PR property package, the liquid phase mass density ρ_L was determined from the corresponding states liquid density (COSTALD) equation by Hankinson and Thomson (1979):

$$\rho_L = \frac{1}{\sum_{j=1}^{NC} \frac{x_j}{\rho_{L,j}}} = \frac{1}{\sum_{j=1}^{NC} \frac{x_j \cdot V_{L,j}}{MW_j}} \quad (F.2.3)$$

$$V_{L,j} = v_j^* \cdot V_R^o \cdot (1 - \omega_j \cdot V_R^\delta) \quad (F.2.4)$$

$$V_R^o = 1 - 1.52816 \cdot \left(1 - \frac{T}{T_{c,j}}\right)^{1/3} + 1.43907 \cdot \left(1 - \frac{T}{T_{c,j}}\right)^{2/3} - 0.81446 \cdot \left(1 - \frac{T}{T_{c,j}}\right) + 0.190454 \cdot \left(1 - \frac{T}{T_{c,j}}\right)^{4/3} \quad (F.2.5)$$

$$V_R^\delta = \frac{-0.296123 + 0.386914 \cdot \left(\frac{T}{T_{c,j}}\right) - 0.0427258 \cdot \left(\frac{T}{T_{c,j}}\right)^2 - 0.0480645 \cdot \left(\frac{T}{T_{c,j}}\right)^2}{\frac{T}{T_{c,j}} - 1.00001} \quad (F.2.6)$$

where x is the liquid phase mole fraction, V_L is the liquid phase molar volume, MW is the molecular weight, v^* is the characteristic volume, ω is the acentricity, T is the absolute temperature, T_c is the critical temperature, and NC is the number of components.

F.2.2.2.2 PR Property Package

In the PR property package, the HYSYS® tabular model was used instead of the default COSTALD equation to facilitate the more accurate prediction of the liquid phase density. The temperature dependence of the pure component liquid mass densities $\rho_{L,j}$ was described by polynomials of the form:

$$\rho_{L,j} = A + B \cdot T + C \cdot T^2 + D \cdot T^3 + E \cdot T^4 \quad (F.2.7)$$

where $\rho_{L,j}$ is in kg/m^3 and T is the absolute temperature in K, and the overall liquid phase density was calculated from equation (F.2.3).

The default HYSYS® coefficient values for H_2O were used for H_2O and the hypothetical water component H_2O^* . The effect of H_2S and other gases (such as N_2 , CH_4 and other hydrocarbons) on the liquid phase density was disregarded due to their negligible liquid phase concentrations compared to that of CO_2 , and these gases were assigned the same coefficient values as H_2O . The coefficient values for the hypothetical potassium carbonate component K_2CO_3^* were regressed from the literature data in Table B.2.3 for pure potassium carbonate solutions while the coefficient values for CO_2 were regressed from the data for pure potassium bicarbonate and potassium carbonate-bicarbonate solutions. The K_2CO_3^* and CO_2 coefficients were determined via the simple unweighted least squares method in a Microsoft® Excel spreadsheet, and the resulting values are listed in Table F.2.1.

Figure F.2.1 compares the liquid phase mass density values predicted by the tabular model against the literature values. The average absolute deviation between the predicted and literature values is 0.8%, compared to 4.3% for the values predicted by the COSTALD equation.

Table F.2.1: Coefficient values for the HYSYS® liquid density tabular model.

Coefficient	K_2CO_3^*	CO_2	H_2O and other components
A	3.4050×10^1	-7.5735×10^2	5.8305×10^1
B	-2.1173×10^{-2}	7.2698	-5.3842×10^{-3}
C	0	-2.1830×10^{-2}	-2.4881×10^{-5}
D	0	2.1418×10^{-5}	4.7481×10^{-8}
E	0	0	-6.5125×10^{-11}

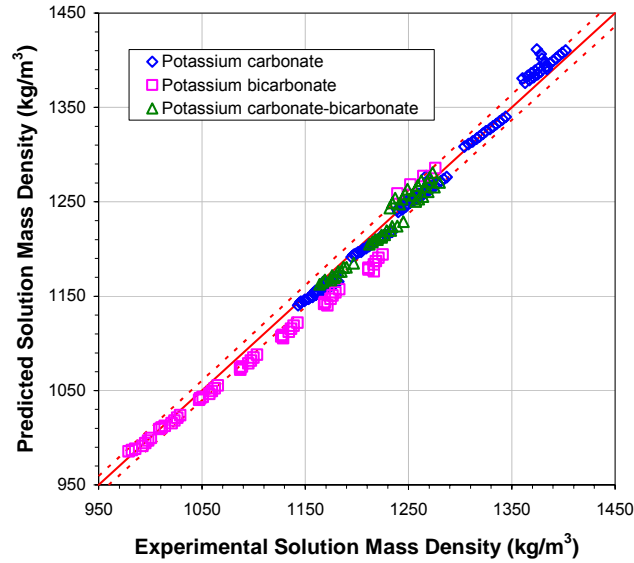


Figure F.2.1: Comparison between the predicted and experimental solution mass densities. The dashed lines (---) represent the $\pm 1\%$ lines.

F.2.3 Viscosity

F.2.3.1 Vapour Phase Viscosity

The vapour phase dynamic viscosity was determined from a proprietary modification of the model proposed by Ely and Hanley (1981). In the original model, the viscosity μ of a mixture at density ρ , temperature T and composition x is equated to the viscosity μ_x of a hypothetical pure fluid:

$$\mu(\rho, T) = \mu_x(\rho, T) \quad (\text{F.2.8})$$

This enables the use of the following corresponding states argument to determine μ from the viscosity μ_0 of a reference fluid:

$$\mu_x(\rho, T) = \mu_0(\rho_0, T_0) \cdot \sqrt{\frac{MW_x}{MW_0}} \cdot \frac{\sqrt{f_{x,0}}}{h_{x,0}^{2/3}} \quad (\text{F.2.9})$$

$$T_0 = \frac{T}{f_{x,0}} \quad (\text{F.2.10})$$

$$\rho_0 = \rho \cdot h_{x,0} \quad (\text{F.2.11})$$

MW is the molecular weight. The subscript x refers to the fluid of interest while the subscript 0 refers to the reference fluid. $f_{x,0}$ and $h_{x,0}$ are functions of the critical parameters and the acentricities of the reference fluid and the fluid of interest.

F.2.3.2 Liquid Phase Viscosity

F.2.3.2.1 Sour PR Property Package

In the Sour PR property package, the liquid phase viscosity was determined in one of three ways: via the proprietary modified Ely-Hanley model for light hydrocarbons; via the Twu model (Twu, 1985) for heavy hydrocarbons; or via the proprietary modified Letsou-Stiel model (Letsou and Stiel, 1973) for all other chemicals.

In the original model proposed by Letsou and Stiel (1973), the liquid phase dynamic viscosity μ_L is determined from the following equations:

$$\mu_L = \left(\sum_{j=1}^{NC} x_j \cdot \mu_{L,j}^{1/3} \right)^3 \quad (\text{F.2.12})$$

$$\begin{aligned} \mu_{L,j} \cdot \frac{T_{c,j}^{1/6}}{P_{c,j}^{2/3} \cdot \sqrt{MW_j}} = & 0.015174 - 0.02135 \cdot \frac{T}{T_{c,j}} + 0.0075 \cdot \left(\frac{T}{T_{c,j}} \right)^2 \\ & + \omega_j \cdot \left(0.042552 - 0.07674 \cdot \frac{T}{T_{c,j}} + 0.0340 \cdot \left(\frac{T}{T_{c,j}} \right)^2 \right) \end{aligned} \quad (\text{F.2.13})$$

where μ_L is in cP, x is the mole fraction, NC is the number of components, T_c is the critical temperature in K, P_c is the critical pressure in atm, MW is the molecular weight, and ω is the acentricity.

The Twu model is more complex, first requiring the calculation of the component kinematic viscosities at 100°F and 210°F from their boiling points T_b and specific gravities SG :

$$\ln \left(\nu_{L,j,T} + \frac{450}{T_{b,j}} \right) = \ln \left(\nu_{L,j,T}^o + \frac{450}{T_{b,j}} \right) \cdot \left(\frac{1 + 2 \cdot f_{T,j}}{1 - 2 \cdot f_{T,j}} \right)^2 \quad \text{for } T = 100^\circ\text{F}, 210^\circ\text{F} \quad (\text{F.2.14})$$

$$f_{100^\circ\text{F},j} = 1.33932 \cdot \left| 1.99873 - \frac{56.7394}{\sqrt{T_{b,j}}} \right| \cdot \Delta SG_j - \frac{21.1141 \cdot \Delta SG_j^2}{\sqrt{T_{b,j}}} \quad (\text{F.2.15})$$

$$f_{210^\circ\text{F},j} = \left| 1.99873 - \frac{56.7394}{\sqrt{T_{b,j}}} \right| \cdot \Delta SG_j - \frac{21.1141 \cdot \Delta SG_j^2}{\sqrt{T_{b,j}}} \quad (\text{F.2.16})$$

$$\Delta SG_j = (SG_j - SG_j^o) \cdot (1.49546 - SG_j) \cdot \left(\frac{1 + 2 \cdot h_j}{1 - 2 \cdot h_j} \right)^2 \quad (\text{F.2.17})$$

$$\begin{aligned} h_j = & \left(-21.6364 + \frac{844.687}{\sqrt{T_{b,j}}} \right) \cdot (SG_j - SG_j^o) \cdot (1.49546 - SG_j) \\ & - \left(458.199 - \frac{7543.00}{\sqrt{T_{b,j}}} \right) \cdot \left[(SG_j - SG_j^o) \cdot (1.49546 - SG_j) \right]^2 \end{aligned} \quad (\text{F.2.18})$$

where ν_L is the kinematic viscosity in cSt, T is the temperature in °F, and T_b is in °R. The reference variables, denoted by the superscript o, are obtained from:

$$\ln(\nu_{L,210^\circ\text{F},j}^o + 1.5) = 4.73227 - 27.0975 \cdot \left(1 - \frac{T_{b,j}^o}{T_{c,j}^o}\right) + 49.4491 \cdot \left(1 - \frac{T_{b,j}^o}{T_{c,j}^o}\right)^2 - 50.4706 \cdot \left(1 - \frac{T_{b,j}^o}{T_{c,j}^o}\right)^4 \quad (\text{F.2.19})$$

$$\ln(\nu_{L,100^\circ\text{F},j}^o) = 0.801621 + 1.37179 \cdot \ln(\nu_{L,210^\circ\text{F},j}^o) \quad (\text{F.2.20})$$

$$\text{SG}_j^o = 0.843593 - 0.128624 \cdot \left(1 - \frac{T_{b,j}^o}{T_{c,j}^o}\right) - 3.36129 \cdot \left(1 - \frac{T_{b,j}^o}{T_{c,j}^o}\right)^3 - 13749.5 \cdot \left(1 - \frac{T_{b,j}^o}{T_{c,j}^o}\right)^{12} \quad (\text{F.2.21})$$

$$T_{c,j}^o = \frac{T_{b,j}^o}{\left(\begin{array}{l} 0.533272 + 0.191017 \times 10^{-3} \cdot T_{b,j}^o + 0.779681 \times 10^{-7} \cdot T_{b,j}^o{}^2 \\ - 0.284376 \times 10^{-10} \cdot T_{b,j}^o{}^3 + 0.959468 \times 10^{-28} \cdot T_{b,j}^o{}^{-13} \end{array} \right)} \quad (\text{F.2.22})$$

The two calculated kinematic viscosities are then substituted into the following equations to determine the component dynamic viscosities $\mu_{L,j}$ at temperature T , which are then used to calculate the liquid phase dynamic viscosity from equation (F.2.12):

$$Z_{T,j} = \nu_{L,T,j} + 0.7 + e^{-1.47 - 1.84 \cdot \nu_{L,T,j} - 0.51 \cdot \nu_{L,T,j}^2} \quad \text{for } T = 100^\circ\text{F}, 210^\circ\text{F} \quad (\text{F.2.23})$$

$$\ln(\ln Z_j) = \ln(\ln Z_{100^\circ\text{F},j}) + \frac{\ln(\ln Z_{100^\circ\text{F},j}) - \ln(\ln Z_{210^\circ\text{F},j})}{\ln 100^\circ\text{F} - \ln 210^\circ\text{F}} \cdot (\ln T - \ln 100^\circ\text{F}) \quad (\text{F.2.24})$$

$$\nu_{L,j} = Z_j - 0.7 - e^{-0.7487 - 3.295 \cdot (Z_j - 0.7) + 6.119 \cdot (Z_j - 0.7)^2 - 0.3193 \cdot (Z_j - 0.7)^3} \quad (\text{F.2.25})$$

$$\mu_{L,j} = \rho_{L,j} \cdot \nu_{L,j} \quad (\text{F.2.26})$$

It should be noted that in equation (F.2.26), $\mu_{L,j}$ is in kg/m·s, $\nu_{L,j}$ is in m²/s and the density $\rho_{L,j}$ is in kg/m³.

F.2.3.2.2 PR Property Package

In the PR property package, the HYSYS® tabular model was used, instead of the above-mentioned default HYSYS® models, to facilitate the more accurate prediction of the liquid phase viscosity. The temperature dependence of the pure component liquid dynamic viscosities $\mu_{L,j}$ was described by polynomials of the form:

$$\ln \mu_{L,j} = A + \frac{B}{T} + C \cdot \ln T + D \cdot T^E \quad (\text{F.2.27})$$

where $\mu_{L,j}$ is in cP and T is the absolute temperature in K, and the overall liquid phase viscosity μ_L was calculated from equation (F.2.12).

As for the liquid density tabular model, the default HYSYS® coefficient values for H₂O were used for H₂O, the hypothetical water component H₂O* and H₂S and other gases (such as N₂, CH₄ and other hydrocarbons). The coefficient values for the hypothetical potassium carbonate component K₂CO₃* were regressed from the literature data in Table B.2.8 for pure potassium carbonate solutions while the coefficient values for CO₂ were regressed from the data for pure potassium bicarbonate and potassium carbonate-bicarbonate solutions. The K₂CO₃* and CO₂ coefficients were determined via the simple unweighted least squares method in a Microsoft® Excel spreadsheet, and the resulting values are listed in Table F.2.2.

Figure F.2.2 compares the liquid phase dynamic viscosity values predicted by the tabular model against the literature values. The average absolute deviation between the predicted and literature values is 4.6%, compared to 7.5% for the values predicted by the default HYSYS® models.

Table F.2.2: Coefficient values for the HYSYS® liquid viscosity tabular model.

Coefficient	K ₂ CO ₃ *	CO ₂	H ₂ O and other components
A	-2.3878×10 ²	-2.7937E+03	-1.1213×10 ⁻¹
B	9.7635E×10 ³	8.0287E+04	-2.4004×10 ⁻⁴
C	3.8379E×10 ¹	4.8288E+02	-3.1123
D	-4.2743×10 ⁻²	-7.3978E-01	0
E	1.0000	1.0000	0

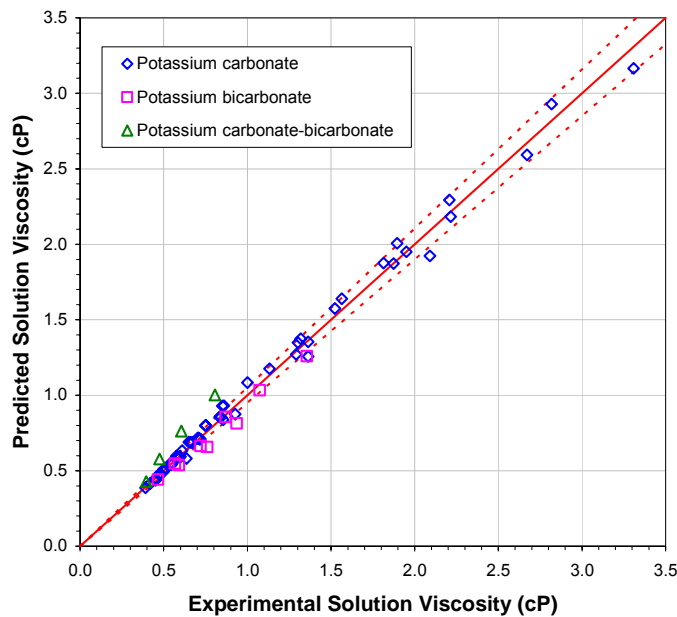


Figure F.2.2: Comparison between the predicted and experimental solution viscosities. The dashed lines (---) represent the ± 5% lines.

F.2.4 Surface Tension

F.2.4.1 Sour PR Property Package

In the Sour PR property package, the liquid phase surface tension σ_L was determined in one of two ways: via a proprietary modification of the correlation proposed by Brock and Bird (1955) for hydrocarbon systems or via a proprietary polynomial for aqueous systems. The original form of the Brock-Bird model is as follows:

$$\sigma_L = \frac{1}{\sum_{j=1}^{NC} \frac{x_j}{\sigma_{L,j}}} \quad (\text{F.2.28})$$

$$\sigma_{L,j} = P_{c,j}^{2/3} \cdot T_{c,j}^{1/3} \cdot \left(0.1207 \cdot \left(1 + \frac{T_{b,j} \cdot \ln P_{c,j}}{T_{c,j}} \right) - 0.281 \right) \cdot \left(1 - \frac{T}{T_{c,j}} \right)^{11/9} \quad (\text{F.2.29})$$

where σ_L is in dyne/cm, x is the mole fraction, NC is the number of components, P_c is the critical pressure in atm, T_c is the critical temperature in K, and T_b is the boiling point in K.

F.2.4.2 PR Property Package

In the PR property package, the HYSYS® tabular model was used, instead of the above-mentioned default HYSYS® models, to facilitate the more accurate prediction of the liquid phase surface tension. The temperature dependence of the pure component liquid surface tensions $\sigma_{L,j}$ was described by polynomials of the form:

$$\sigma_{L,j} = A + B \cdot T + C \cdot T^2 + D \cdot T^3 + E \cdot T^4 \quad (\text{F.2.30})$$

where $\sigma_{L,j}$ is in dyne/cm and T is the absolute temperature in K, and the overall liquid phase surface tension σ_L was calculated from equation (F.2.28).

Like the liquid density and liquid viscosity tabular models, the default HYSYS® coefficient values for H₂O were used for H₂O, the hypothetical water component H₂O* and H₂S and other gases (such as N₂, CH₄ and other hydrocarbons). The coefficient values for the hypothetical potassium carbonate component K₂CO₃* and for CO₂ were regressed from a set of values generated using the empirical surface tension correlation (B.2.37). The K₂CO₃* and CO₂ coefficients were determined via the simple unweighted least squares method in a Microsoft® Excel spreadsheet, and the resulting values are listed in Table F.2.3.

Figure F.2.3 compares the liquid phase surface tension values predicted by the tabular model against those generated by the empirical correlation. The average absolute deviation between the two sets of values is 3.8%, compared to 94.4% for the values predicted by the modified Brock-Bird model.

Table F.2.3: Coefficient values for the HYSYS® liquid surface tension tabular model.

Coefficient	K ₂ CO ₃ *	CO ₂	H ₂ O and other components
A	2.5209×10 ²	-3.0588×10 ²	1.8277×10 ⁴
B	-1.4077	1.2235	-9.3402×10 ¹
C	4.4242×10 ⁻³	-1.2345×10 ⁻³	1.1945×10 ⁻¹
D	-6.9349×10 ⁻⁶	0	0
E	3.9069×10 ⁻⁹	0	0

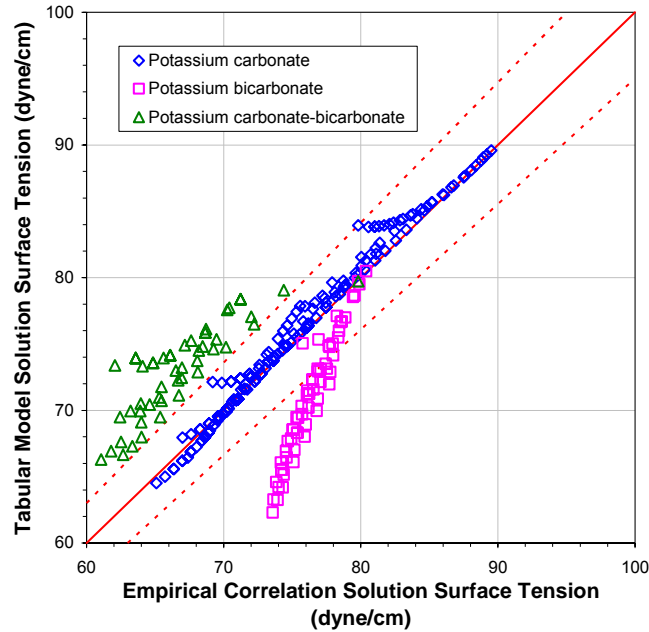


Figure F.2.3: Comparison between the solution surface tensions predicted by the tabular model and the empirical correlation. The dashed lines (---) represent the ± 5% lines.

F.2.5 Thermal Conductivity

F.2.5.1 Vapour Phase Thermal Conductivity

The vapour phase thermal conductivity was determined from a proprietary modification of the model proposed by Ely and Hanley (1983). In the original model, the thermal conductivity λ of the fluid of interest (a pure fluid or a mixture) at density ρ and temperature T is divided into two contributory terms:

$$\lambda(\rho, T) = \lambda'(\rho, T) + \lambda''(T) \quad (F.2.31)$$

The first term λ' represents the transfer of energy from purely collisional or translational effects, while the second term λ'' is due to the transfer of energy via the internal degrees of freedom. The translational contribution λ' for a mixture of composition x is equated to the contribution λ'_x for a hypothetical pure fluid:

$$\lambda'(\rho, T) = \lambda'_x(\rho, T) \quad (F.2.32)$$

Consequently, from the corresponding states argument, λ'_x is obtained from the translational contribution λ'_{0} of a reference fluid:

$$\lambda'_x(\rho, T) = \lambda'_{0}(\rho_0, T_0) \cdot \sqrt{\frac{MW_0}{MW_x}} \cdot \frac{\sqrt{f_{x,0}}}{h_{x,0}^{2/3}} \cdot \left[\left(1 - \frac{T}{f_{x,0}} \cdot \left(\frac{\partial f_{x,0}}{\partial T} \right)_{V_x} \right) \cdot \frac{Z_{c,0}}{Z_{c,x}} \right]^{3/2} \quad (\text{F.2.33})$$

MW is the molecular weight and Z_c is the critical compressibility. The subscript x refers to the fluid of interest while the subscript 0 refers to the reference fluid. T_0 and ρ_0 are given by equations (F.2.10) and (F.2.11). $f_{x,0}$ and $h_{x,0}$ are functions of the critical parameters and the acentricities of the reference fluid and the fluid of interest.

The internal contribution λ'' is given by:

$$\lambda''(T) = 1.32 \cdot \left(C_{pIG} - \frac{5 \cdot R}{2} \right) \cdot \frac{\mu}{MW} \quad (\text{F.2.34})$$

where C_{pIG} is the ideal gas heat capacity, R is the gas constant, and μ is the viscosity from equation (F.2.8).

Two other methods were also used to calculate the vapour phase thermal conductivities in the HYSYS® simulations: the simple set of correlations proposed by Misić and Thodos (1961, 1963) and the more complex model by Chung and co-workers (1988). The Misić-Thodos correlations are based on dimensional analysis and assume that the vapour phase thermal conductivity λ_G is described by a function with the general form:

$$\lambda_G = f(MW^A \cdot T_c^B \cdot T^C \cdot P_c^D \cdot V_c^E \cdot C_p^F \cdot R^G) \\ = \frac{P_c^{2/3}}{T_c^{1/6} \cdot \sqrt{MW}} \cdot f\left(\left(\frac{T}{T_c} \right)^C \cdot \left(\frac{C_p}{R} \right)^F \cdot Z_c^{5/6 - G - F} \cdot R^{5/6} \right) \quad (\text{F.2.35})$$

where λ_G is in cal/cm·s·K, MW is the molecular weight in g/mol, T_c is the critical temperature in K, T is the temperature in K, P_c is the critical pressure in atm, V_c is the critical volume in cm³/mol, Z_c is the critical compressibility, C_p is the heat capacity in cal/mol·K, and R is the gas constant in atm·cm³/mol·K. Several functions, based on the equation (F.2.35), were obtained by Misić and Thodos (1961, 1963) for different types of compounds over various reduced temperature ranges.

While the Misić-Thodos correlations are suitable only for low pressures, the Chung model is applicable to both high and low pressures:

$$\lambda_G = \frac{31.2 \times 10^3 \cdot \mu_G^{LP} \cdot \Psi}{MW} \cdot \left(F_1 + F_2 \cdot \frac{V_c}{6 \cdot V} \right) \\ + 3.586 \times 10^{-3} \cdot \sqrt{\frac{10^3 \cdot T_c}{MW}} \cdot V_c^{-2/3} \cdot F_1 \cdot F_3 \cdot \left(\frac{V_c}{6 \cdot V} \right)^2 \cdot \sqrt{\frac{T}{T_c}} \quad (\text{F.2.36})$$

$$\Psi = f(T, T_c, C_v, \omega) \quad (\text{F.2.37})$$

$$F_1 = f(T_c, V, V_c, \omega, \delta, \kappa) \quad (\text{F.2.38})$$

$$F_2 = f(T_c, V_c, \omega, \delta, \kappa) \quad (\text{F.2.39})$$

$$F_3 = f(T_c, V_c, \omega, \delta, \kappa) \quad (\text{F.2.40})$$

where λ_G is in $\text{W/m}\cdot\text{K}$, μ_G^{LP} is the low pressure vapour phase viscosity in $\text{kg/m}\cdot\text{s}$, MW is the molecular weight in kg/kmol , V_c is the critical volume in cm^3/mol , V is the molar volume in cm^3/mol , T is the temperature in K, T_c is the critical temperature in K, C_v is the heat capacity at constant volume in $\text{J/mol}\cdot\text{K}$, ω is the acentricity, δ is the dipole moment in Debye, and κ is the Chung association factor.

F.2.5.2 Liquid Phase Thermal Conductivity

F.2.5.2.1 Sour PR Property Package

In the Sour PR property package, the liquid phase thermal conductivity was determined in one of five ways: via the proprietary modified Ely-Hanley model; via a proprietary polynomial for selected components including H_2O , CH_4 , C_2H_6 and C_3H_8 ; via a proprietary modification of the Missenard-Riedel equation (Reid et al., 1977) for hydrocarbons with molecular weights greater than 140 kg/kmol at reduced temperatures greater than 0.8; via the Latini method (Baroncini et al., 1980) for alcohols, esters and all other hydrocarbons; or via the Sato-Riedel equation (Reid et al., 1977) for all other compounds.

The liquid phase thermal conductivity λ_L is determined from the original Missenard-Riedel equation as follows:

$$\lambda_L = \left(\sum_{j=1}^{\text{NC}} x_j \cdot \lambda_{L,j}^{1/3} \right)^3 \quad (\text{F.2.41})$$

$$\lambda_{L,j} = \frac{84 \times 10^{-6} \cdot \sqrt{T_{b,j}} \cdot C_{L,0^\circ\text{C},j} \cdot C_{p,0^\circ\text{C},j}}{\sqrt{\text{MW}_j} \cdot N_j^{1/4}} \cdot \frac{3 + 20 \cdot \left(1 - \frac{T}{T_{c,j}}\right)^{2/3}}{3 + 20 \cdot \left(1 - \frac{273}{T_{c,j}}\right)^{2/3}} \quad (\text{F.2.42})$$

where λ_L is in $\text{cal/cm}\cdot\text{s}\cdot\text{K}$, x is the mole fraction, T_b is the normal boiling point in K, $C_{L,0^\circ\text{C}}$ is the liquid phase density at 0°C in mol/cm^3 , $C_{p,0^\circ\text{C}}$ is the liquid heat capacity at 0°C in $\text{cal/mol}\cdot\text{K}$, MW is the molecular weight in g/mol , N is the number of atoms in the molecule, and T_c is the critical temperature in K.

The Sato-Reidel equation takes a similar form to the Missenard-Riedel equation. The liquid phase thermal conductivity is determined from equation (F.2.41) and the component thermal conductivities are obtained from:

$$\lambda_{L,j} = \frac{2.64 \times 10^{-3}}{\sqrt{MW_j}} \cdot \frac{3 + 20 \cdot \left(1 - \frac{T}{T_{c,j}}\right)^{2/3}}{3 + 20 \cdot \left(1 - \frac{T_{b,j}}{T_{c,j}}\right)^{2/3}} \quad (\text{F.2.43})$$

The Latini method also uses equation (F.2.41) to calculate the liquid phase thermal conductivity from component thermal conductivities given by:

$$\lambda_{L,j} = \frac{A^* \cdot T_{b,j}^\alpha}{MW_j^\beta \cdot T_{c,j}^\gamma} \cdot \frac{\left(1 - \frac{T}{T_{c,j}}\right)^{0.38}}{\left(\frac{T}{T_{c,j}}\right)^{1/6}} \quad (\text{F.2.44})$$

where λ_L is in W/m·K, and A^* , α , β and γ are component specific parameters.

F.2.5.2.2 PR Property Package

In the PR property package, the HYSYS® tabular model was used, instead of the above-mentioned default HYSYS® models, to facilitate the more accurate prediction of the liquid phase thermal conductivity. The temperature dependence of the pure component liquid thermal conductivities $\lambda_{L,j}$ was described by polynomials of the form:

$$\lambda_{L,j} = A + B \cdot T + C \cdot T^2 + D \cdot T^3 + E \cdot T^4 \quad (\text{F.2.45})$$

where $\lambda_{L,j}$ is in W/m·K and T is the absolute temperature in K, and the overall liquid phase surface tension λ_L was calculated from:

$$\lambda_L = \frac{1}{\left(\sum_{j=1}^{NC} \frac{y_j}{\lambda_{L,j}^2}\right)^2} \quad (\text{F.2.46})$$

where y is the mass fraction and NC is the number of components.

Like the other liquid property tabular models, the default HYSYS® coefficient values for H₂O were used for H₂O, the hypothetical water component H₂O* and H₂S and other gases (such as N₂, CH₄ and other hydrocarbons). The coefficient values for the hypothetical potassium carbonate component K₂CO₃* and for CO₂ were regressed from a set of values generated using the empirical thermal conductivity correlation (B.2.55). The K₂CO₃* and CO₂ coefficients were determined via the simple unweighted least squares method in a Microsoft® Excel spreadsheet, and the resulting values are listed in Table F.2.4.

Figure F.2.4 compares the liquid phase thermal conductivity values predicted by the tabular model against those generated by the empirical correlation. The average absolute deviation between the two sets of values is 1.2%, compared to 59.1% for the values predicted by the default HYSYS® methods.

Table F.2.4: Coefficient values for the HYSYS® liquid thermal conductivity tabular model.

Coefficient	K ₂ CO ₃ *	CO ₂	H ₂ O and other components
A	-4.3200×10^{-1}	5.1309×10^{-1}	1.7269
B	5.7255×10^{-3}	2.4746×10^{-4}	-3.0912×10^{-3}
C	-8.0780×10^{-6}	0	0
D	1.8610×10^{-9}	0	0
E	0	0	0

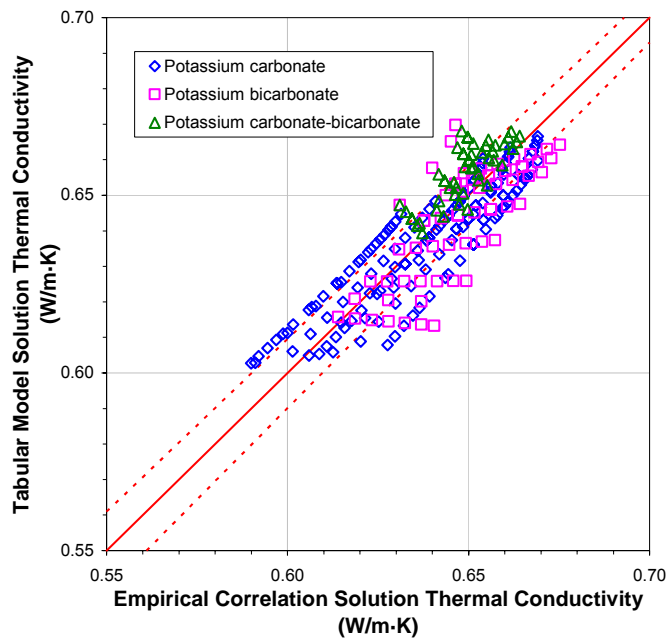


Figure F.2.4: Comparison between the solution thermal conductivities predicted by the tabular model and the empirical correlation. The dashed lines (---) represent the $\pm 1\%$ lines.

APPENDIX G

ENHANCED PR BINARY INTERACTION PARAMETERS

This appendix outlines the procedure followed for the regression of the model parameters for the enhanced PR equation of state. The results for the data regression are analysed and presented within.

G.1 Data Regression Procedure

The enhanced PR equation of state binary interaction parameter values that were not taken from the HYSYS® property library were determined from a series of data regressions. As discussed in Sections 6.2.2.1 and 6.2.2.2, binary interaction parameters for the H₂O*-K₂CO₃*, CO₂-H₂O* and CO₂-K₂CO₃* component pairs were first obtained from the CO₂ solubility data presented by Tosh and co-workers (1959). The interaction parameters for the H₂S-H₂O* and H₂S-K₂CO₃* component pairs were then determined using the H₂S solubility data presented by Tosh and co-workers (1960). Both sets of data regressions were performed using the following general procedure:

1. The initial values for the binary interaction parameters were taken as 0 (the HYSYS® default value), except for the CO₂-H₂O* and H₂S-H₂O* component pairs. These were set equal to the default HYSYS® values for the CO₂-H₂O and H₂S-H₂O component pairs.
2. Parameter bounds were set according to findings from the preliminary simulations discussed in Section 6.1.1. It was determined that negative values were required for the H₂O*-K₂CO₃*, CO₂-H₂O*, CO₂-K₂CO₃* and H₂S-K₂CO₃* component pair parameters in order to ensure sufficient absorption of CO₂ and H₂S in the absorber, while the H₂S-H₂O* component pair parameter had to be positive to ensure sufficient H₂S desorption in the regenerator. Consequently, the upper bounds for the H₂O*-K₂CO₃*, CO₂-H₂O*, CO₂-K₂CO₃* and H₂S-K₂CO₃* component pair parameters were set as 0, while the lower bound for the H₂S-H₂O* component pair parameter was set as 0.
3. The full set of interaction parameters was regressed from the data, and the resulting set of parameter values was labelled "Full".
4. One of the interaction parameters was excluded from regression (i.e. it was fixed at its initial value) and the remaining parameters were regressed from the data. This step was repeated with the remaining parameters.
5. Step 3 was repeated with an additional interaction parameter being excluded from regression until all the parameters were fixed at their initial values.
6. Each simplified set of parameter values obtained from steps 3 and 4 was compared against the "Full" parameter value set via an F-Test to determine the reliability of the simplified set. The corresponding one-tail p-value was also calculated to determine the probability of observing the F-Test value if the null hypothesis was true.

Null hypothesis: The simplified set fits the data better than the "Full" set.

$$F \approx 1 \text{ or } p > 0.05$$

where

$$F = \frac{\frac{SSQ_{\text{Simplified}} - SSQ_{\text{Full}}}{df_{\text{Simplified}} - df_{\text{Full}}}}{\frac{SSQ_{\text{Full}}}{df_{\text{Full}}}} \quad (\text{G.1.1})$$

$$p = f(F, df_{\text{Simplified}} - df_{\text{Full}}, df_{\text{Full}}) \quad (\text{G.1.2})$$

$$df = N_{\text{Data}} - N_{\text{Parameters}} \quad (\text{G.1.3})$$

SSQ_{Full} and $SSQ_{\text{Simplified}}$ are the sum of squares for the full and simplified parameter value sets, respectively, df_{Full} and $df_{\text{Simplified}}$ are the corresponding degrees of freedom, N_{Data} is the number of data points used in the regression, and $N_{\text{Parameters}}$ is the number of parameters regressed.

7. The simplified parameter value sets which passed the above F-Test were sorted according to their sum of squares. A logic test was then performed on each parameter set to tabulate the number of parameters with a standard error greater than the associated regressed value. The parameter value set with the lowest logic test result and the lowest weighted sum of squares was labelled the optimal set.

G.2 Data Regression Results

The statistical results for the data regression runs for the CO₂-K₂CO₃-H₂O system are given in Table G.2.1. The sum of squares (SSQ), residual root mean square error (RRMSQE), degrees of freedom (df), F-value and p-value are listed for each parameter set. The data set used in the regression runs consisted of 120 data points, and the number of parameters regressed ranged from 0 to 3, depending on the parameter set. From the F-Test, none of the simplified parameter sets were identified as being more suitable than the “Full” set. Consequently, the “Full” set was selected as the optimal parameter value set and was used in the next series of data regression runs for the CO₂-H₂S-K₂CO₃-H₂O system. The regressed parameter values and standard errors associated with this optimal set are given in Table 6.2.2.

Table G.2.2 presents the statistical results for the data regression runs for the CO₂-H₂S-K₂CO₃-H₂O system. The data set used in this series of regression runs consisted of 127 data points, and the number of parameters regressed ranged from 0 to 2, depending on the parameter set. As for the previous set of regressions, none of the simplified parameter sets were determined to be more suitable than the “Full” set via the F-Test. Consequently, the “Full” set was selected as the optimal parameter value set for the CO₂-H₂S-K₂CO₃-H₂O system, and its regressed parameter values and standard errors are given in Table 6.2.3.

Table G.2.1: Statistical results for the CO₂-K₂CO₃-H₂O system data regression runs.

Parameter Set	SSQ	RRMSQE	df	F	p	Null Hypothesis
Full	150.9	1.290	117	-	-	-
Fixed $k_{\text{H}_2\text{O}^*-\text{K}_2\text{CO}_3^*}$	185.9	1.255	118	27.18	8.1×10^{-7}	False
Fixed $k_{\text{CO}_2-\text{K}_2\text{CO}_3^*}$	211.5	1.339	118	47.04	3.5×10^{-10}	False
Fixed $k_{\text{CO}_2-\text{H}_2\text{O}^*}$	375.2	1.783	118	173.93	6.8×10^{-25}	False
Fixed $k_{\text{H}_2\text{O}^*-\text{K}_2\text{CO}_3^*}$ and $k_{\text{CO}_2-\text{K}_2\text{CO}_3^*}$	220.9	1.363	119	27.16	2.0×10^{-10}	False
Fixed $k_{\text{H}_2\text{O}^*-\text{K}_2\text{CO}_3^*}$ and $k_{\text{CO}_2-\text{H}_2\text{O}^*}$	385.4	1.800	119	90.93	1.5×10^{-24}	False
Fixed $k_{\text{CO}_2-\text{K}_2\text{CO}_3^*}$ and $k_{\text{CO}_2-\text{H}_2\text{O}^*}$	1160.3	3.123	119	391.37	1.5×10^{-52}	False
All Fixed	2704.5	4.747	120	660.07	4.0×10^{-73}	False

Table G.2.2: Statistical results for the CO₂-H₂S-K₂CO₃-H₂O system data regression runs.

Parameter Set	SSQ	RRMSQE	df	F	p	Null Hypothesis
Full	1611.9	3.591	125	-	-	-
Fixed $k_{\text{H}_2\text{S}-\text{K}_2\text{CO}_3^*}$	2361.1	4.329	126	58.10	5.4×10^{-12}	False
Fixed $k_{\text{H}_2\text{S}-\text{K}_2\text{CO}_3^*}$	2971.0	4.856	126	105.39	2.6×10^{-18}	False
All Fixed	5113.9	6.346	127	135.78	4.6×10^{-32}	False

APPENDIX H

HYSYS® SIMULATION RESULTS

This appendix presents the results of the HYSYS® simulations for CO₂ trains #2 to #6. Included are the column profiles generated by the preliminary column simulations and the column profiles predicted by the full CO₂ trains process models. Also presented are the process flow diagrams for the HYSYS® process models for CO₂ trains #2 to #6.

H.1 Preliminary Column Model Simulations

H.1.1 Equilibrium Stage Model Approach

The composition and temperature profiles predicted by the equilibrium stage models for the absorber and regenerator columns in CO₂ trains #2 to #6 are presented below.

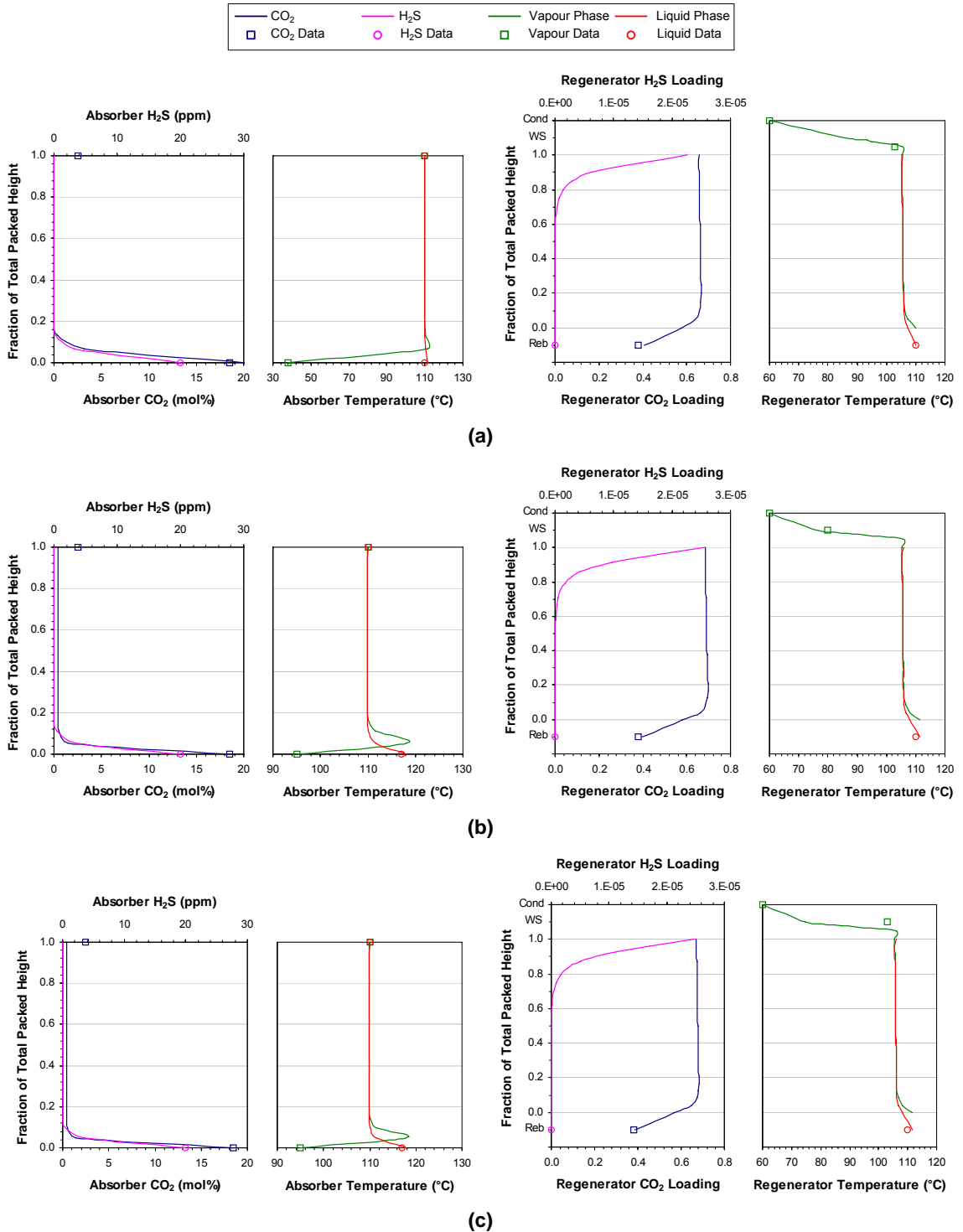


Figure H.1.1: Equilibrium stage simulation results for the absorber and regenerator columns. (a) CO₂ train #2. (b) CO₂ train #3. (c) CO₂ train #4. (Cond = condenser, WS = wash section, Reb = reboiler)

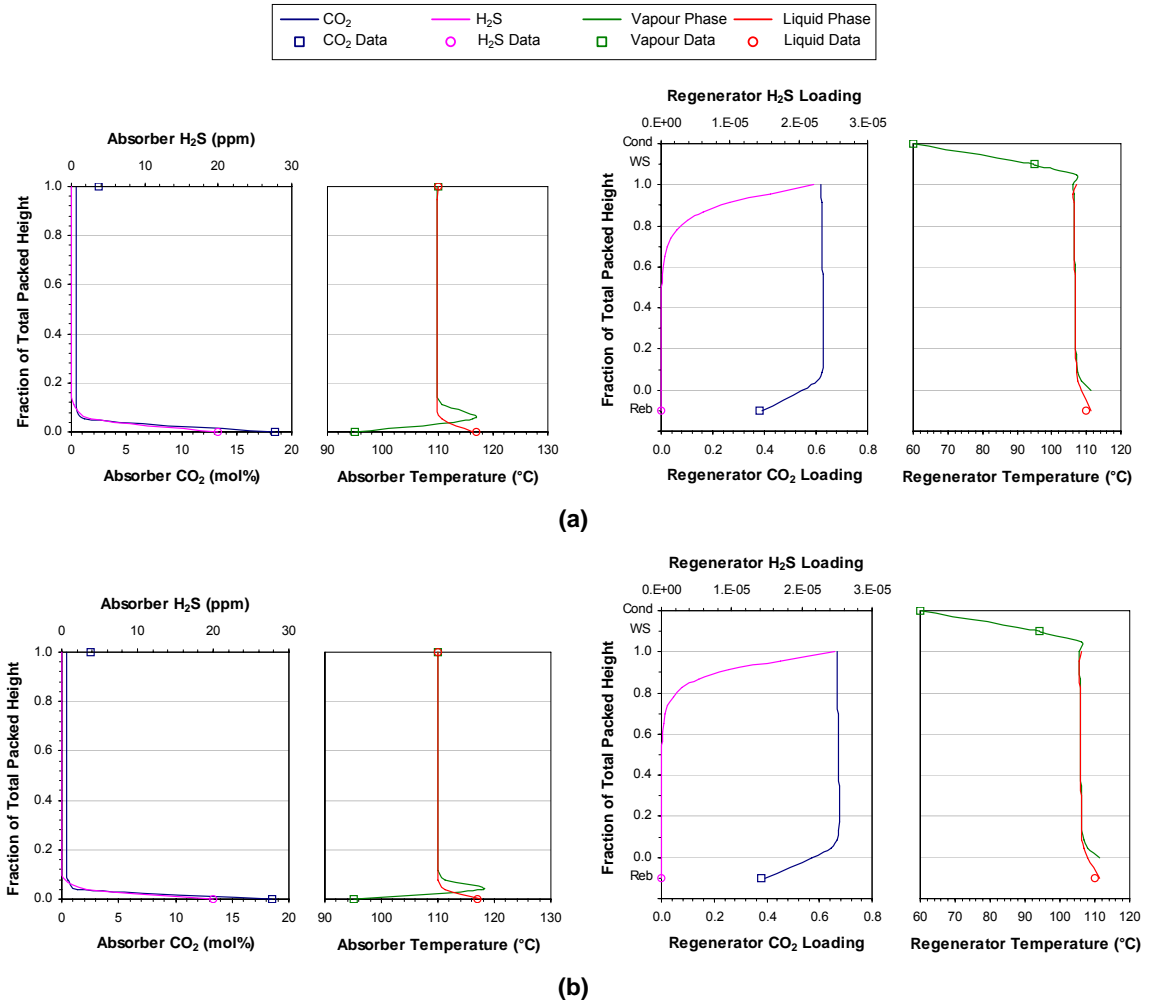


Figure H.1.2: Equilibrium stage simulation results for the absorber and regenerator columns. (a) CO₂ train #5. (b) CO₂ train #6. (Cond = condenser, WS = wash section, Reb = reboiler)

H.1.2 Column Stage Efficiency Correlations

The composition and temperature profiles predicted using the correlated overall stage efficiencies for the steady-state and dynamic absorber columns in CO₂ trains #2 to #6 are presented below.

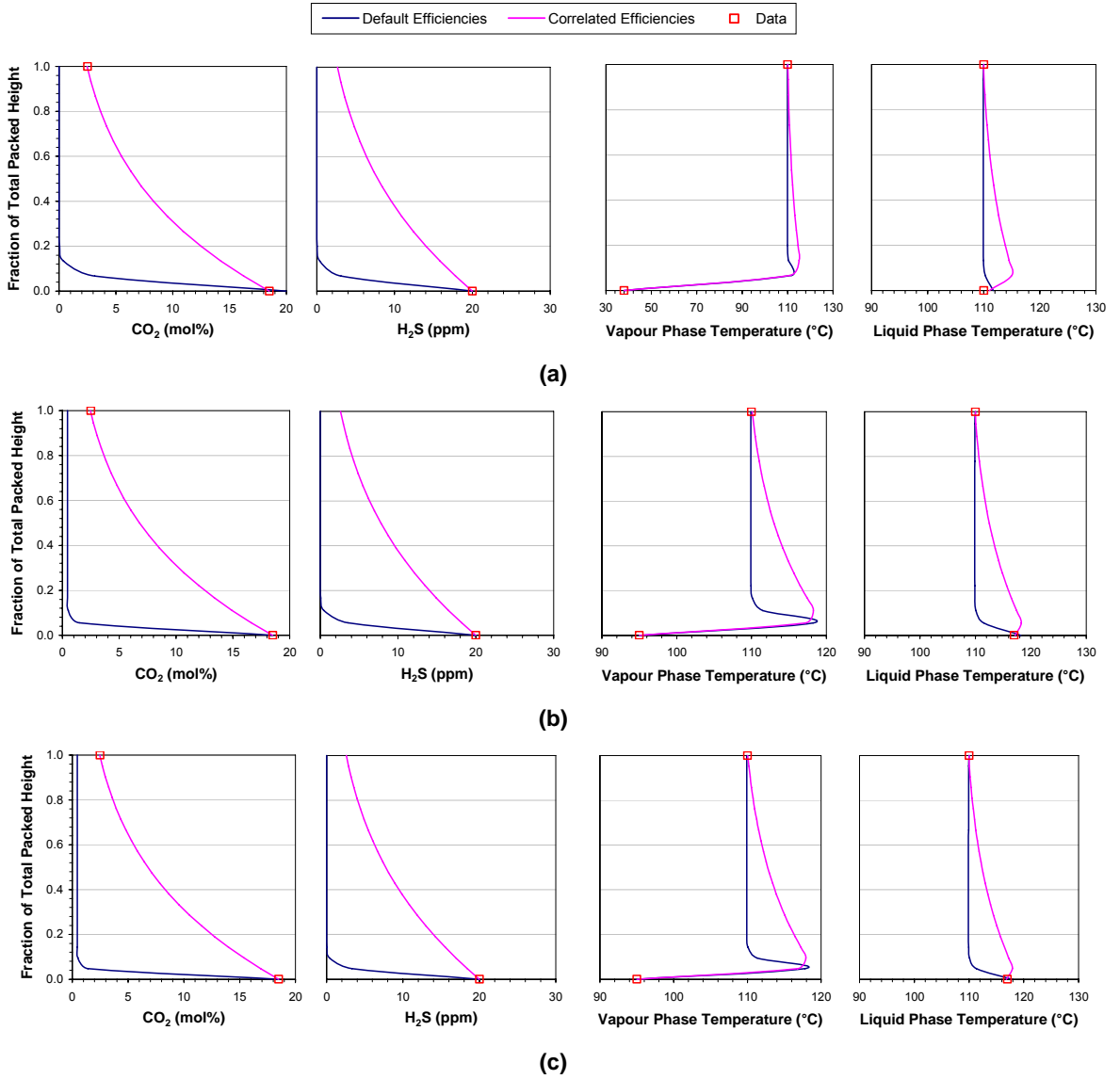


Figure H.1.3: Effect of the correlated overall stage efficiencies on the steady-state absorber columns. (a) CO₂ train #2. (b) CO₂ train #3. (c) CO₂ train #4.

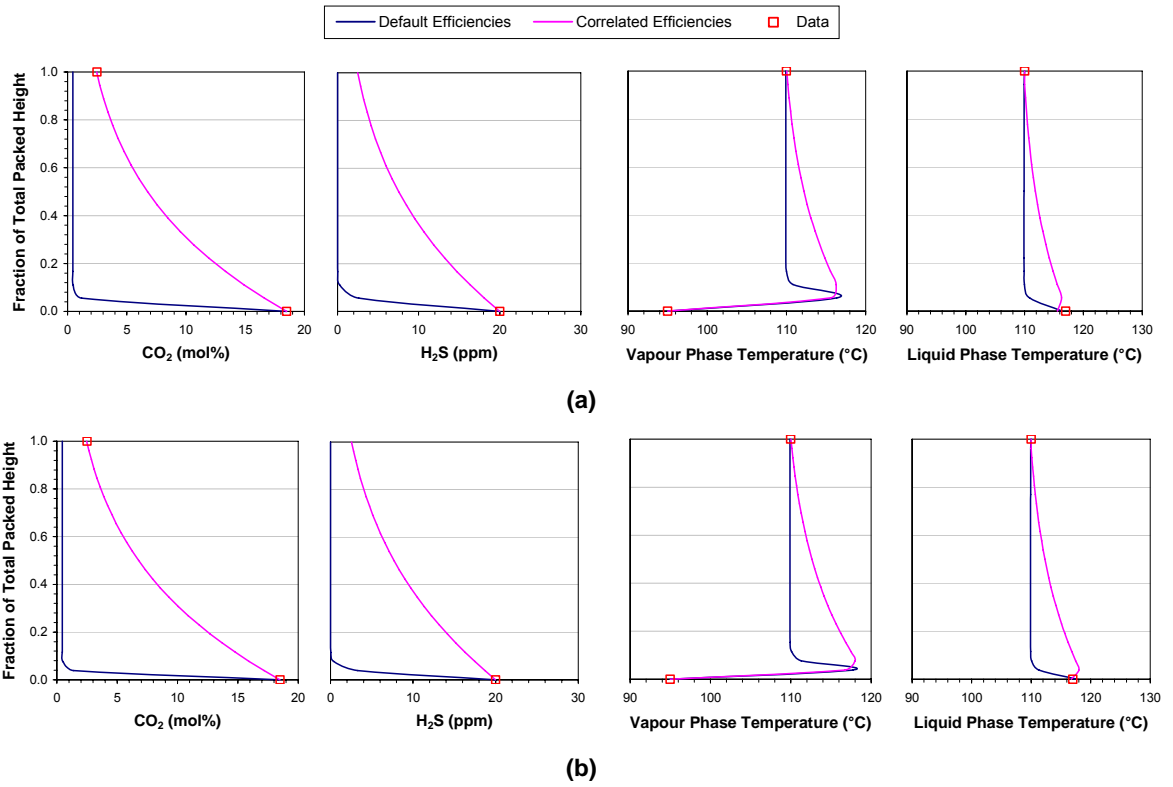


Figure H.1.4: Effect of the correlated overall stage efficiencies on the steady-state absorber columns. (a) CO₂ train #5. (b) CO₂ train #6.

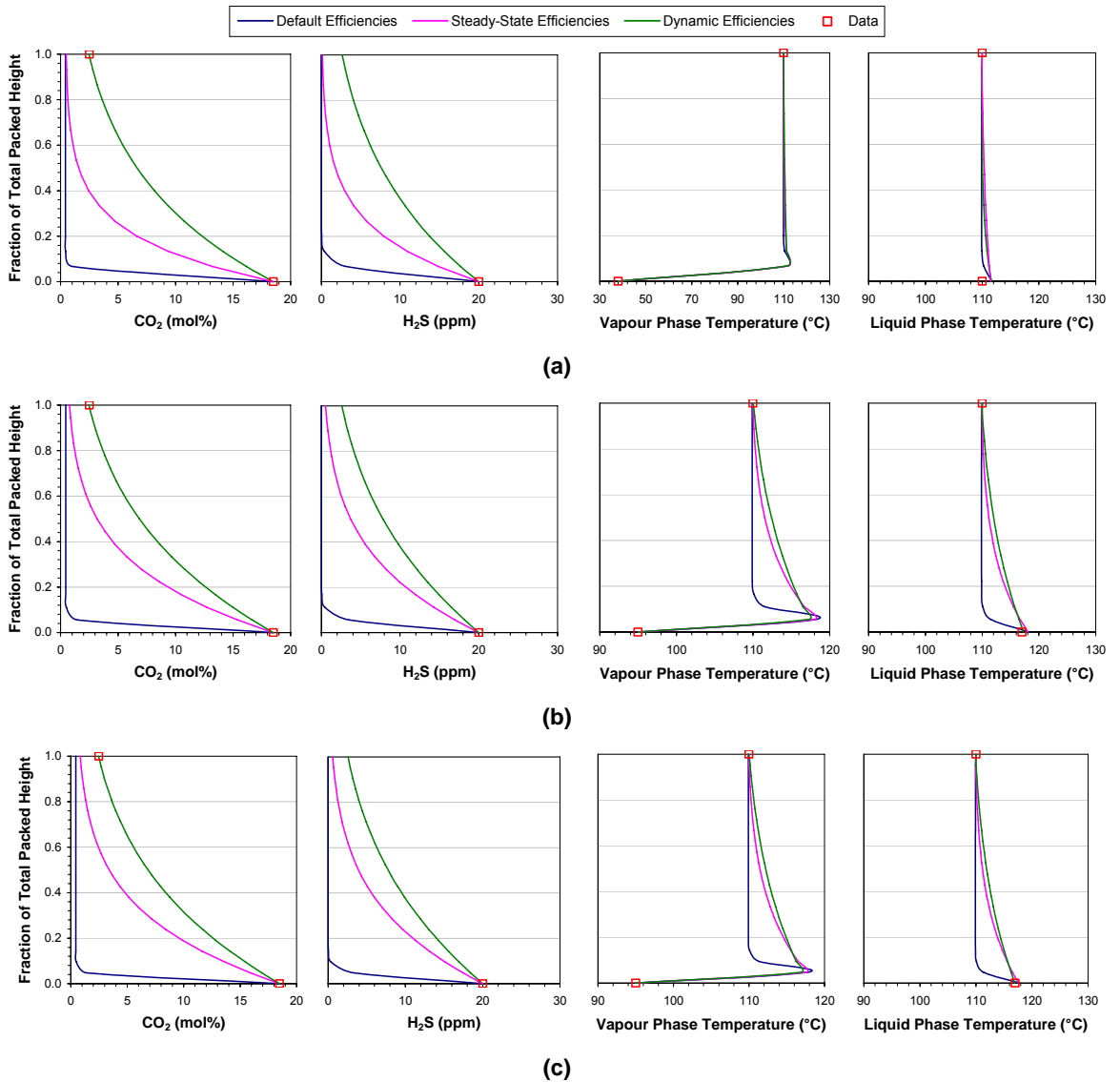


Figure H.1.5: Effect of the correlated overall stage efficiencies on the steady-state behaviour of the dynamic absorber columns. (a) CO₂ train #2. (b) CO₂ train #3. (c) CO₂ train #4.

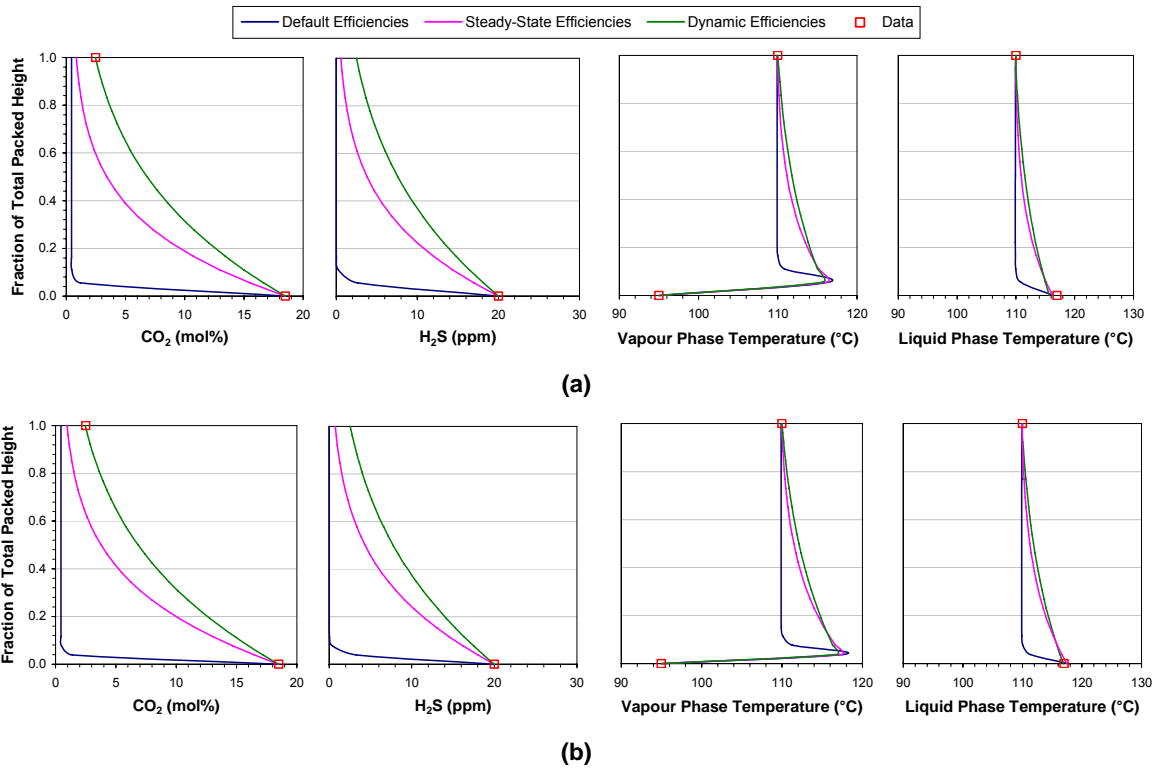


Figure H.1.6: Effect of the correlated overall stage efficiencies on the steady-state behaviour of the dynamic absorber columns. (a) CO₂ train #5. (b) CO₂ train #6.

H.2 Steady-State CO₂ Train Models

The process flow diagrams for the steady-state HYSYS® models of CO₂ trains #2 to #6 are provided on the following pages.

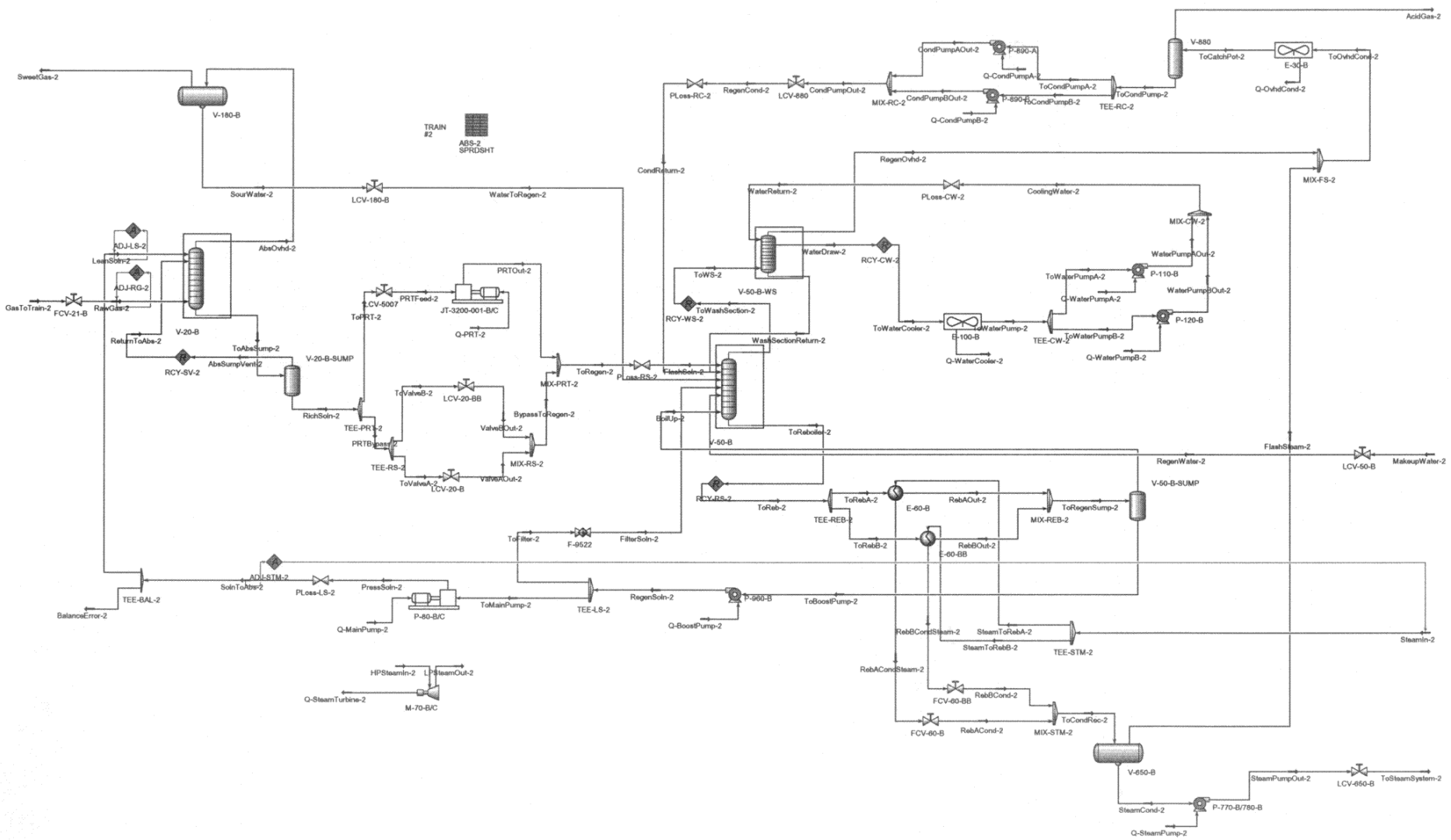
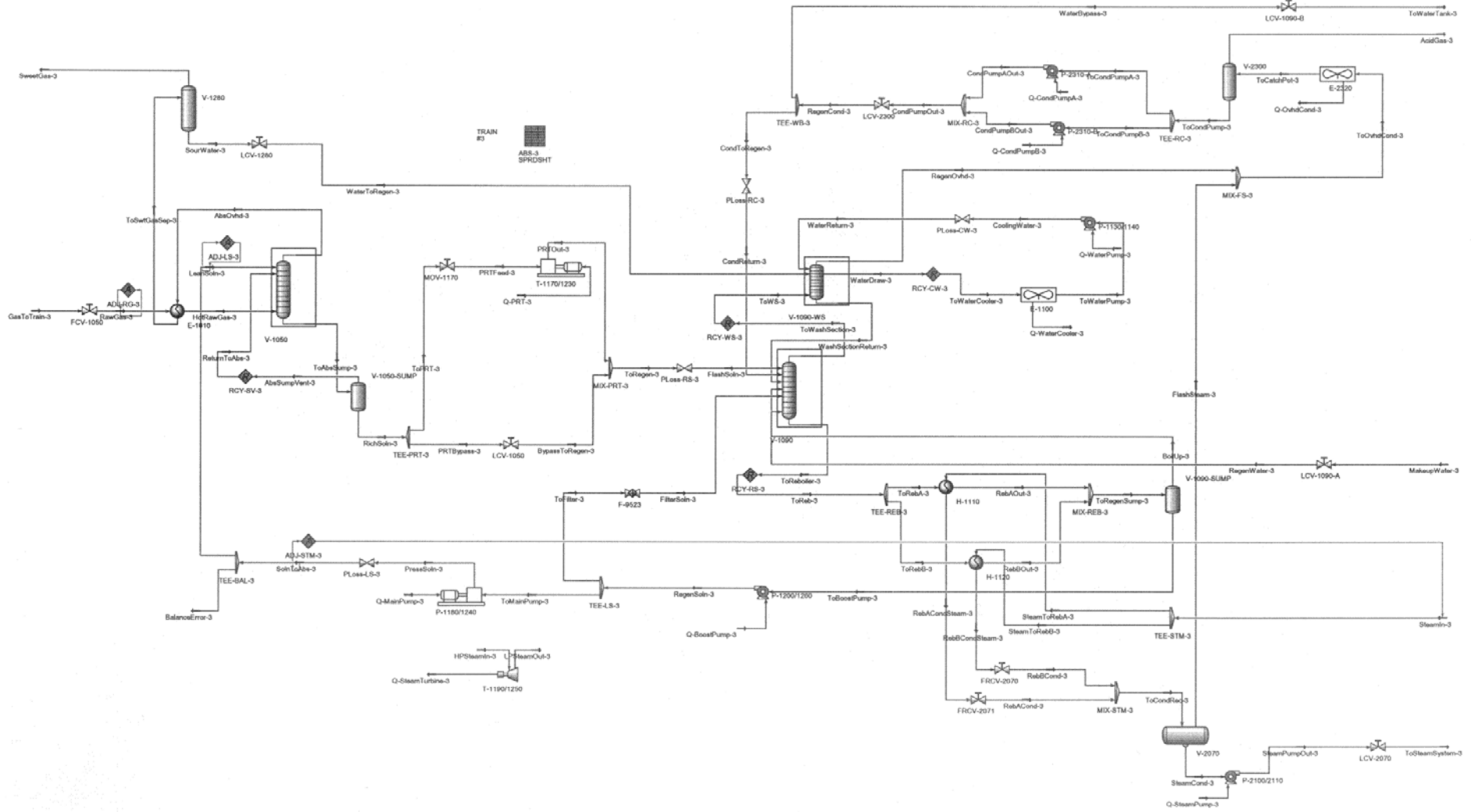


Figure H.2.1: Process flow diagram for the steady-state model of CO₂ train #2.



A-97

Figure H.2.2: Process flow diagram for the steady-state model of CO₂ train #3.

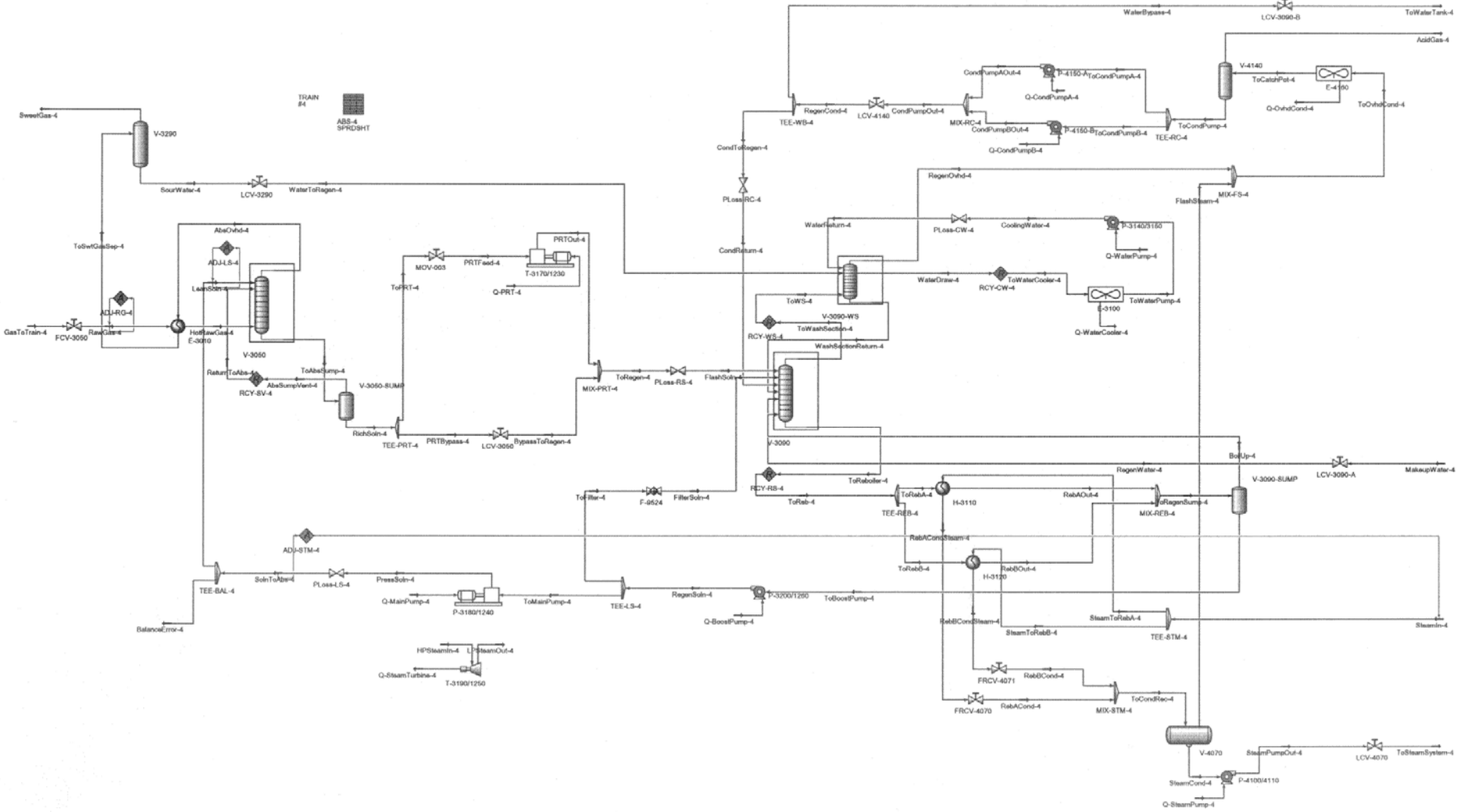


Figure H.2.3: Process flow diagram for the steady-state model of CO₂ train #4.

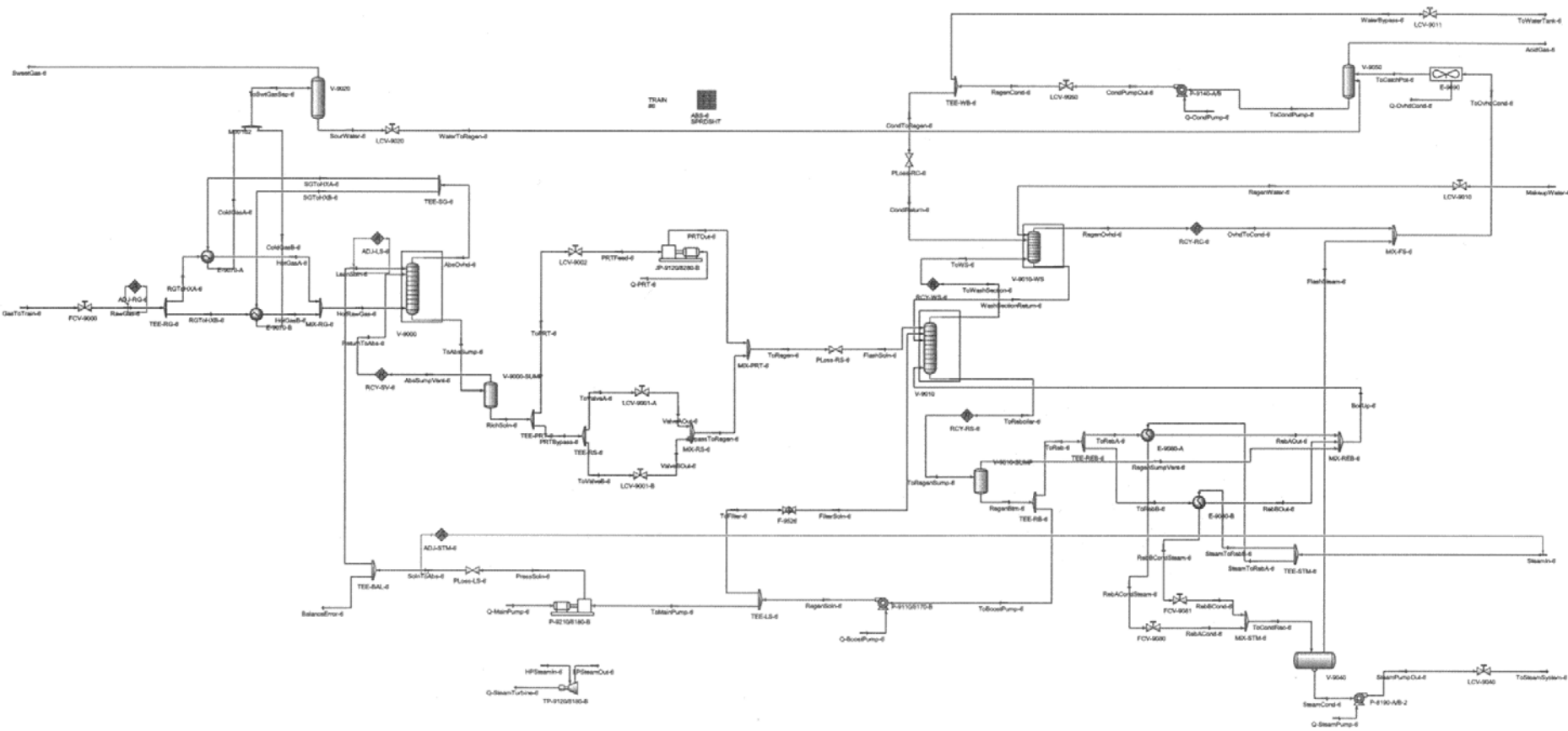


Figure H.2.5: Process flow diagram for the steady-state model of CO2 train #6.

H.3 CO₂ Train Model Validation

The vapour and liquid phase composition profiles and the temperature profiles for the absorber and regenerator columns in the steady-state HYSYS® models for CO₂ trains #2 to #6 are presented below.

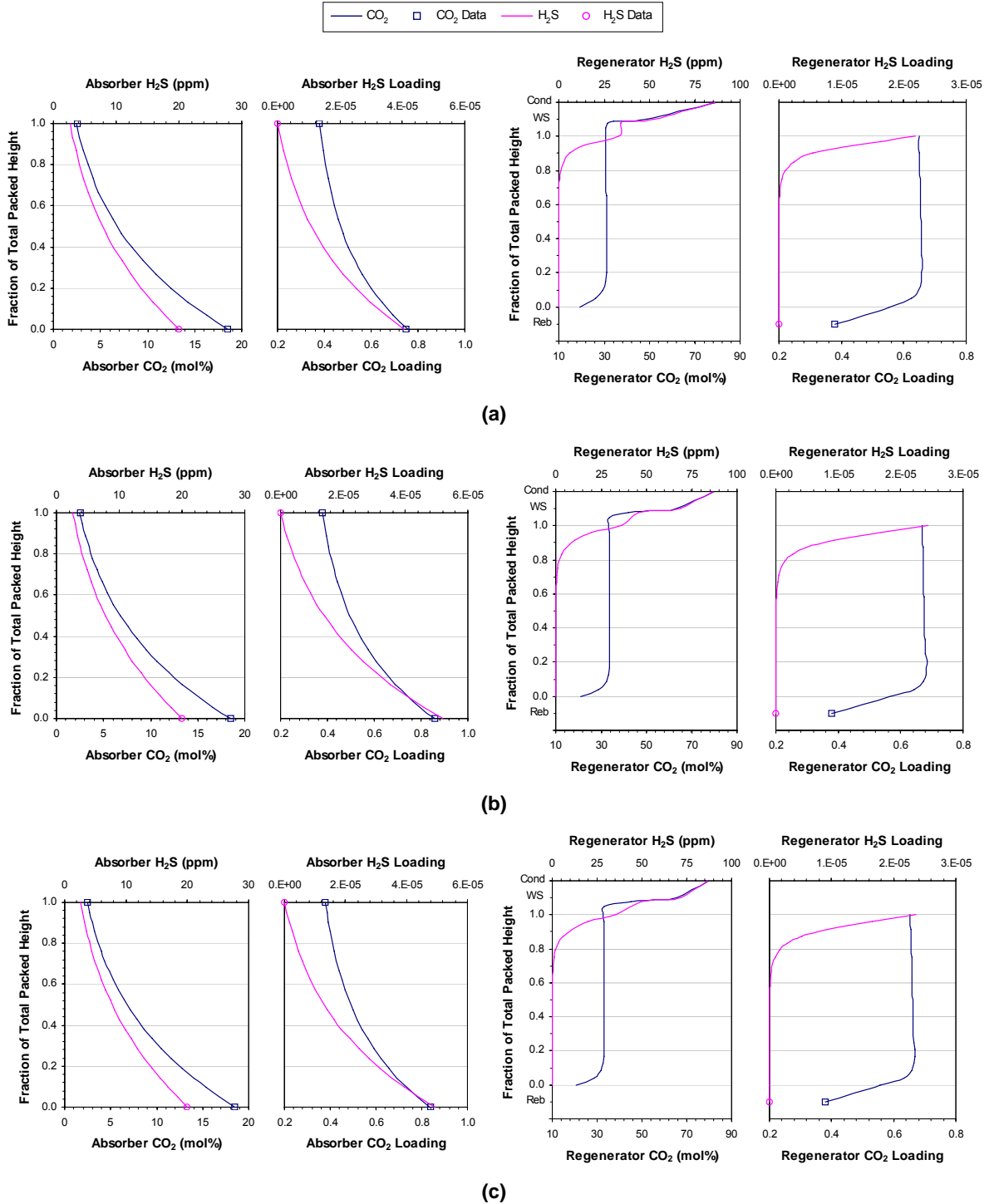


Figure H.3.1: CO₂ and H₂S vapour and liquid phase column profiles for the first set of plant data. (a) CO₂ train #2. (b) CO₂ train #3. (c) CO₂ train #4. (Cond = condenser, WS = wash section, Reb = reboiler)

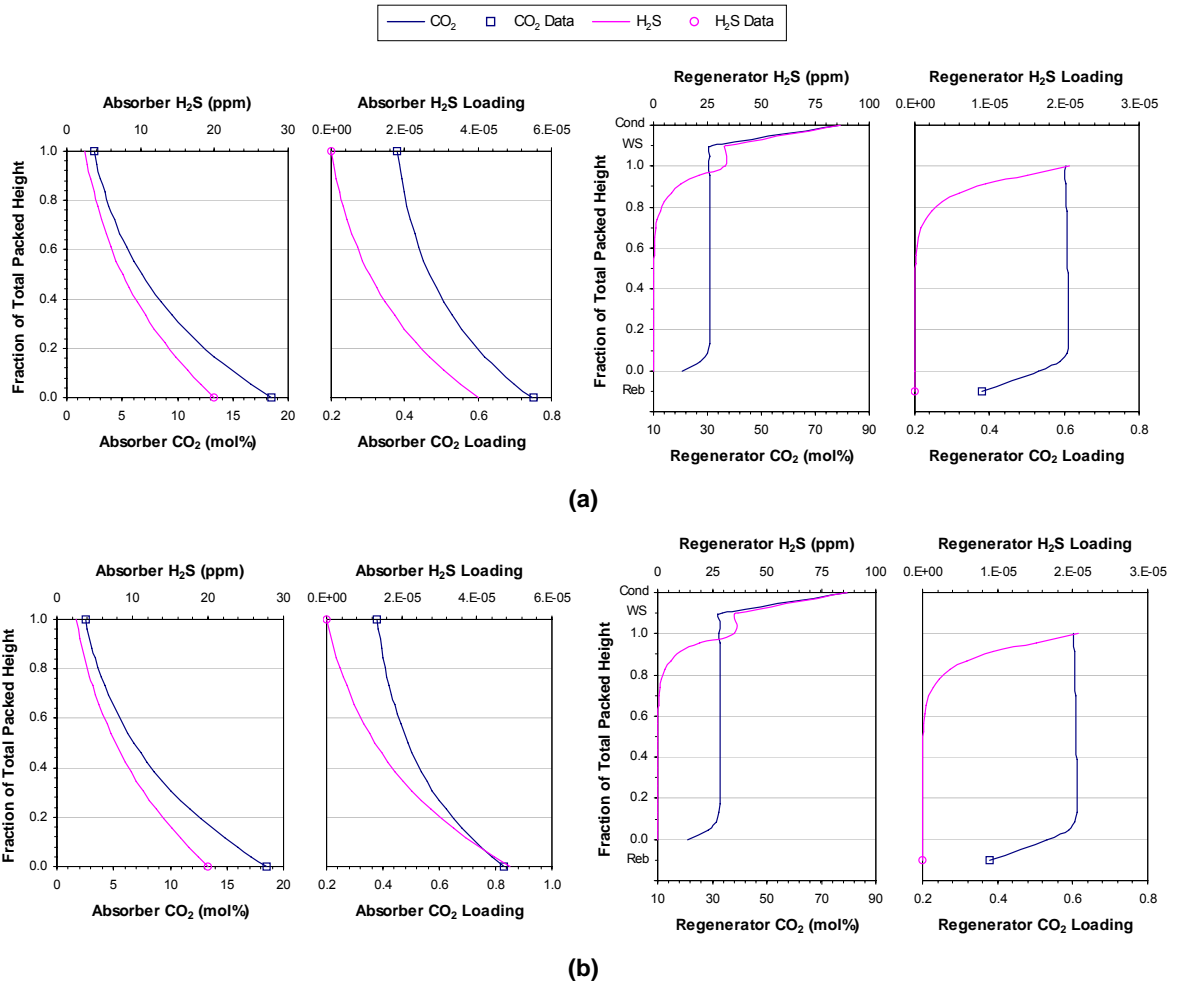


Figure H.3.2: CO₂ and H₂S vapour and liquid phase column profiles for the first set of plant data. (a) CO₂ train #5. (b) CO₂ train #6. (Cond = condenser, WS = wash section, Reb = reboiler)

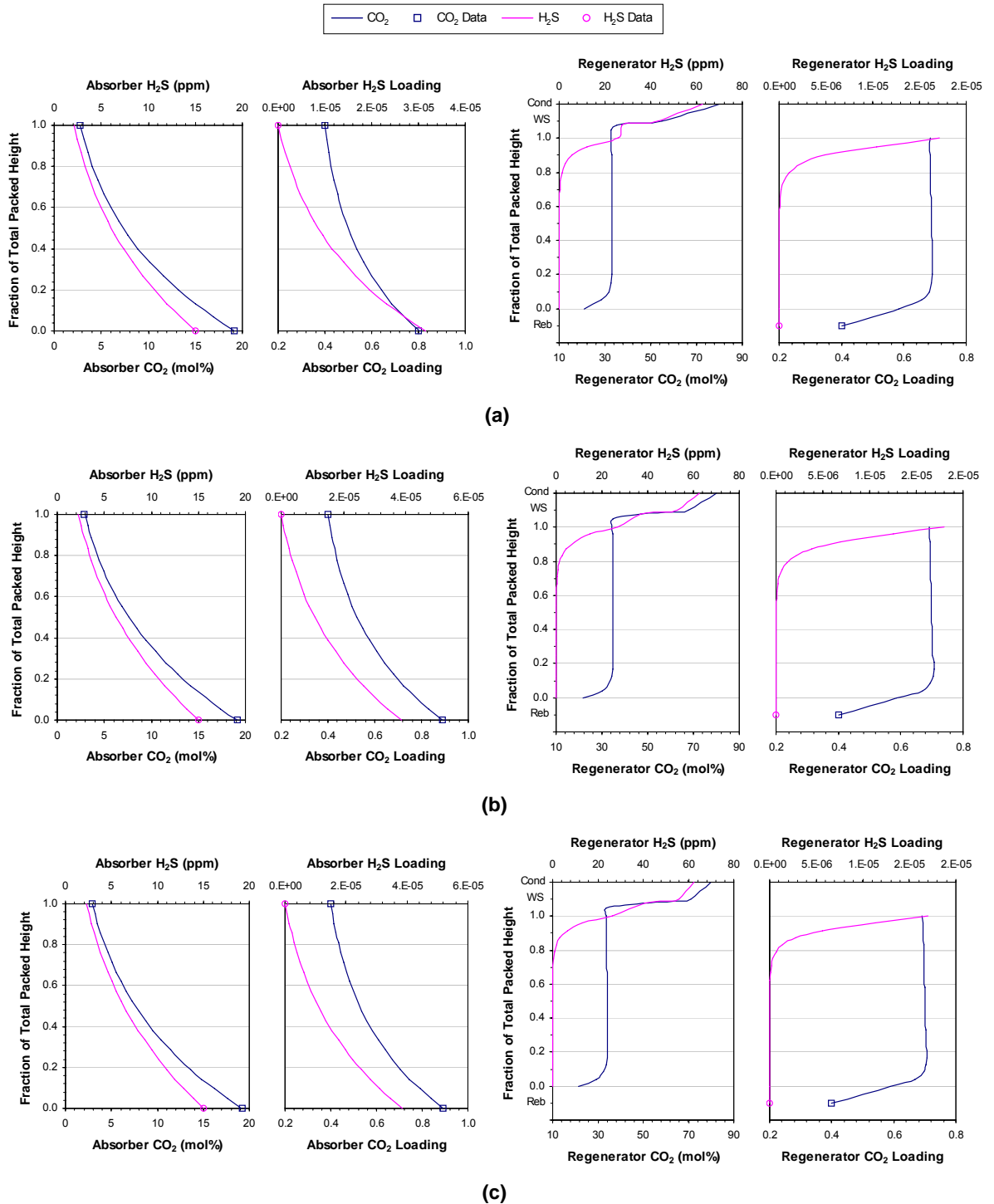


Figure H.3.3: CO₂ and H₂S vapour and liquid phase column profiles for the second set of plant data. (a) CO₂ train #2. (b) CO₂ train #3. (c) CO₂ train #4. (Cond = condenser, WS = wash section, Reb = reboiler)

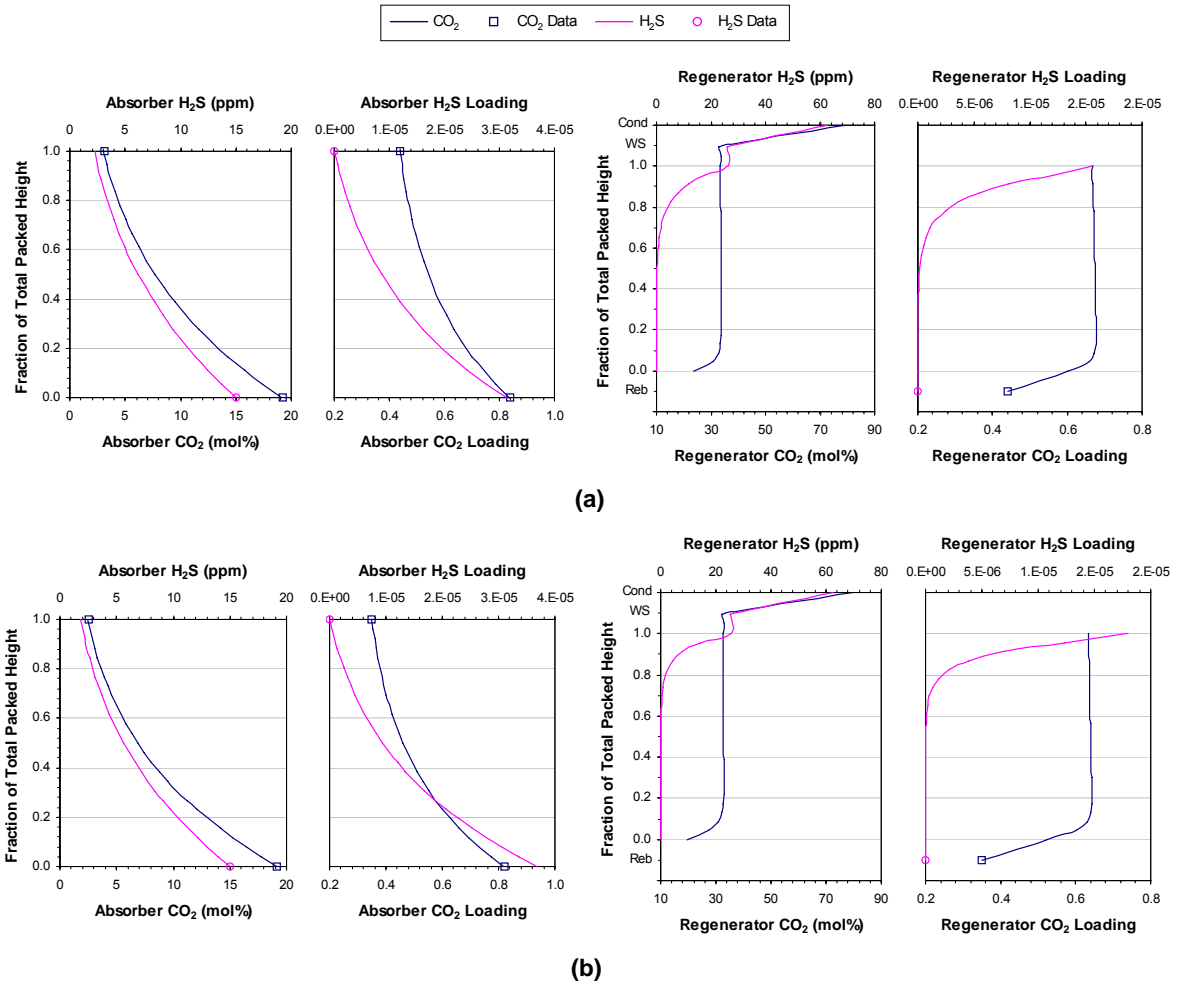


Figure H.3.4: CO₂ and H₂S vapour and liquid phase column profiles for the second set of plant data. (a) CO₂ train #5. (b) CO₂ train #6. (Cond = condenser, WS = wash section, Reb = reboiler)

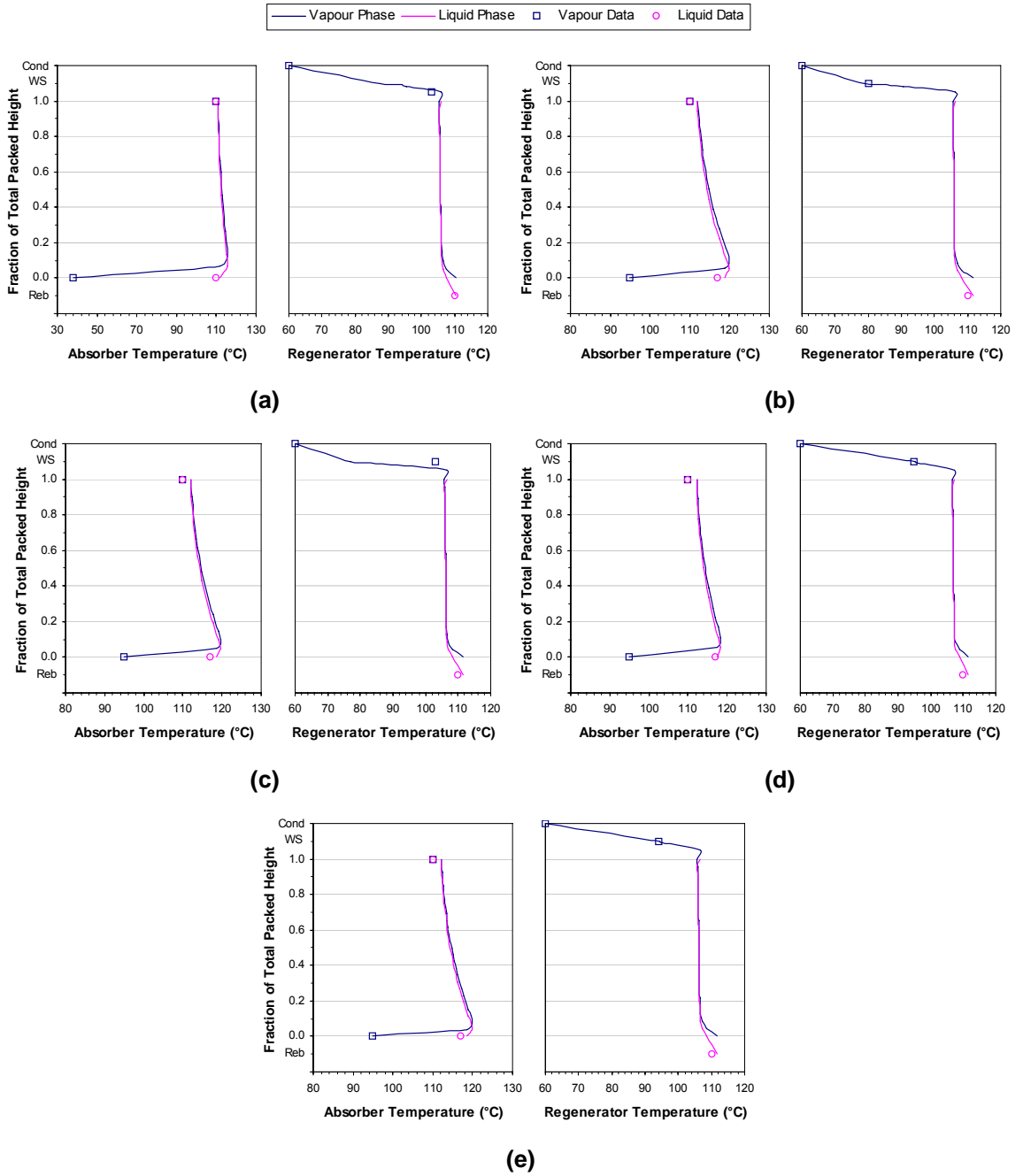


Figure H.3.5: Column temperature profiles for the first set of plant data. (a) CO₂ train #2. (b) CO₂ train #3. (c) CO₂ train #4. (d) CO₂ train #5. (e) CO₂ train #6. (Cond = condenser, WS = wash section, Reb = reboiler)

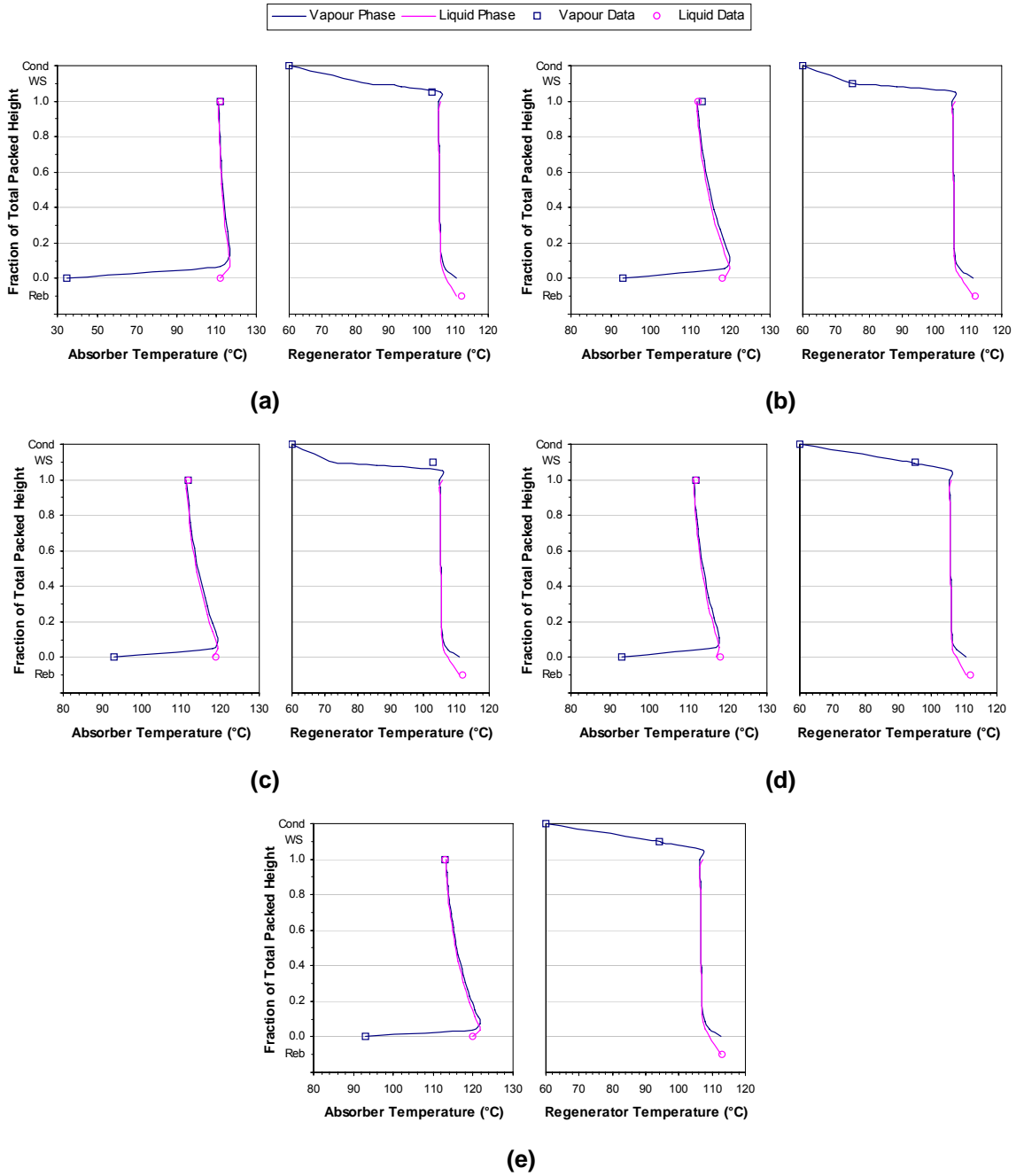


Figure H.3.6: Column temperature profiles for the second set of plant data. (a) CO₂ train #2. (b) CO₂ train #3. (c) CO₂ train #4. (d) CO₂ train #5. (e) CO₂ train #6. (Cond = condenser, WS = wash section, Reb = reboiler)

APPENDIX I

PROCESS CONTROL STUDIES OF THE CO₂ TRAINS

This appendix provides examples of the MATLAB® scripts used in the process control studies for CO₂ trains #1 and #7. Also included are the step response curves generated from the closed-loop testing of the optimal diagonal control structures for the two CO₂ trains.

I.1 Selection of Diagonal Control Structure

An example of the MATLAB® scripts used to calculate the various sensitivity analysis indices is provided below.

```
% Program sensitivity.m
% Compares alternative diagonal control structures for CO2 Train #1
% at high gas throughput
% Calculates CN, MRI, DCN and DC
%
% Notation:
% alt1 = SGC-LSF
% alt2 = SGC-RSF
% alt3 = SGC-RLL
% y1 = Sweet gas CO2 content
% y2 = Sweet gas flow rate
% d1 = Raw gas CO2 content
%
clear
%
% Process gain matrices
KpH1alt1=[1.1695 -0.0635; 1.0881 -0.0026];
KpH1alt2=[1.1695 -0.9885; 1.0881 -0.0262];
KpH1alt3=[1.1695 0.0412; 1.0881 0.0032];
%
% Process time constant matrices
TpH1alt1=[8.2231 2.2825; 1.6168 3.3742];
TpH1alt2=[8.2231 13.1691; 1.6168 16.0241];
TpH1alt3=[8.2231 10.2357; 1.6168 9.4975];
%
% Process dead time matrices
DTH1alt1=[0.1667 0.1667; 0.1667 0.1667];
DTH1alt2=[0.1667 0.6667; 0.1667 0.8333];
DTH1alt3=[0.1667 51.9408; 0.1667 69.1521];
%
% Disturbance gain, time constant and dead time vectors
KdH1=[0.5757; -0.0735];
TpdH1=[6.1206; 3.4381];
DTdH1=[0.1667; 0.1667];

%
% Unit magnitude disturbance in d1 and unit magnitude setpoint changes
% in y1 and y2
Dd1=[1];
Dy=eye(2);
%
for i=1:2
    for j=1:2
        % 3rd order Pade approximations for dead times
        [DTH1alt1num(i,:,j),DTH1alt1den(i,:,j)]=pade(DTH1alt1(i,j),3);
        [DTH1alt2num(i,:,j),DTH1alt2den(i,:,j)]=pade(DTH1alt2(i,j),3);
        [DTH1alt3num(i,:,j),DTH1alt3den(i,:,j)]=pade(DTH1alt3(i,j),3);
        %
        [DTdH1num(i,:),DTdH1den(i,:)]=pade(DTdH1(i),3);
        %
        % Process transfer functions
        GpH1alt1(i,j)=tf(KpH1alt1(i,j)*DTH1alt1num(i,:,j),
            conv([TpH1alt1(i,j) 1],DTH1alt1den(i,:,j)));
        GpH1alt2(i,j)=tf(KpH1alt2(i,j)*DTH1alt2num(i,:,j),
            conv([TpH1alt2(i,j) 1],DTH1alt2den(i,:,j)));
        GpH1alt3(i,j)=tf(KpH1alt3(i,j)*DTH1alt3num(i,:,j),
            conv([TpH1alt3(i,j) 1],DTH1alt3den(i,:,j)));
        %
        % Disturbance transfer functions
        GdH1(i,1)=tf(KdH1(i)*DTdH1num(i,:),conv([TpdH1(i) 1],DTdH1den(i,:)));
```

```

end
end
%
% Steady-state analysis
% Singular value decomposition
SVDH1(:,1)=svd(KpH1alt1);
SVDH1(:,2)=svd(KpH1alt2);
SVDH1(:,3)=svd(KpH1alt3);
%
% MRI values
MRIH1(1)=min(SVDH1(:,1));
MRIH1(2)=min(SVDH1(:,2));
MRIH1(3)=min(SVDH1(:,3));
%
% CN values
CNH1(1)=cond(KpH1alt1);
CNH1(2)=cond(KpH1alt2);
CNH1(3)=cond(KpH1alt3);
%
% DCN and DC values
DCH1(1,1)=norm(inv(KpH1alt1)*KdH1*Dd1);
DCH1(1,2)=norm(inv(KpH1alt2)*KdH1*Dd1);
DCH1(1,3)=norm(inv(KpH1alt3)*KdH1*Dd1);
%
DCNH1(1,1)=DCH1(1,1)/norm(KdH1*Dd1)*max(SVDH1(:,1));
DCNH1(1,2)=DCH1(1,2)/norm(KdH1*Dd1)*max(SVDH1(:,2));
DCNH1(1,3)=DCH1(1,3)/norm(KdH1*Dd1)*max(SVDH1(:,3));
%
for i=1:2
    DCH1(i+1,1)=norm(inv(KpH1alt1)*Dy(:,i));
    DCH1(i+1,2)=norm(inv(KpH1alt2)*Dy(:,i));
    DCH1(i+1,3)=norm(inv(KpH1alt3)*Dy(:,i));
    %
    DCNH1(i+1,1)=DCH1(i+1,1)/norm(Dy(:,i))*max(SVDH1(:,1));
    DCNH1(i+1,2)=DCH1(i+1,2)/norm(Dy(:,i))*max(SVDH1(:,2));
    DCNH1(i+1,3)=DCH1(i+1,3)/norm(Dy(:,i))*max(SVDH1(:,3));
end
DCNH1, DCH1
%
% Frequency analysis
w=logspace(-5,2,100);
%
% Evaluate process and disturbance transfer functions over frequency range
GpH1alt1_w=freqresp(GpH1alt1,w);
GpH1alt2_w=freqresp(GpH1alt2,w);
GpH1alt3_w=freqresp(GpH1alt3,w);
GdH1_w=freqresp(GdH1,w);
%
% Calculate indices over frequency range and print to text file
for i=1:length(w)
    % Singular value decomposition
    SVDH1_w(:,1,i)=svd(GpH1alt1_w(:, :, i));
    SVDH1_w(:,2,i)=svd(GpH1alt2_w(:, :, i));
    SVDH1_w(:,3,i)=svd(GpH1alt3_w(:, :, i));
    %
    % MRI values
    for j=1:3
        MRIH1_w(j,i)=min(SVDH1_w(:, j, i));
    end
    %
    % CN values
    CNH1_w(1,i)=cond(GpH1alt1_w(:, :, i));
    CNH1_w(2,i)=cond(GpH1alt2_w(:, :, i));
    CNH1_w(3,i)=cond(GpH1alt3_w(:, :, i));
    %
    % DCN and DC values
    DCH1alt1_w(1,i)=norm(inv(GpH1alt1_w(:, :, i))*GdH1_w(:, :, i)*Dd1);
    DCH1alt2_w(1,i)=norm(inv(GpH1alt2_w(:, :, i))*GdH1_w(:, :, i)*Dd1);

```

```

DCH1alt3_w(1,i)=norm(inv(GpH1alt3_w(:, :, i))*GdH1_w(:, :, i)*Dd1);
%
DCNH1alt1_w(1,i)=DCH1alt1_w(1,i)/norm(GdH1_w(:, :, i)*Dd1)*max(SVDH1_w(:, 1, i));
DCNH1alt2_w(1,i)=DCH1alt2_w(1,i)/norm(GdH1_w(:, :, i)*Dd1)*max(SVDH1_w(:, 2, i));
DCNH1alt3_w(1,i)=DCH1alt3_w(1,i)/norm(GdH1_w(:, :, i)*Dd1)*max(SVDH1_w(:, 3, i));
%
for j=1:2
    DCH1alt1_w(j+1,i)=norm(inv(GpH1alt1_w(:, :, i))*Dy(:, j));
    DCH1alt2_w(j+1,i)=norm(inv(GpH1alt2_w(:, :, i))*Dy(:, j));
    DCH1alt3_w(j+1,i)=norm(inv(GpH1alt3_w(:, :, i))*Dy(:, j));
    %
    DCNH1alt1_w(j+1,i)=DCH1alt1_w(j+1,i)/norm(Dy(:, j))*max(SVDH1_w(:, 1, i));
    DCNH1alt2_w(j+1,i)=DCH1alt2_w(j+1,i)/norm(Dy(:, j))*max(SVDH1_w(:, 2, i));
    DCNH1alt3_w(j+1,i)=DCH1alt3_w(j+1,i)/norm(Dy(:, j))*max(SVDH1_w(:, 3, i));
end
end
y=[w; MRIH1_w];
fid=fopen('MRIH1_w.txt','w');
fprintf(fid,'%12.8f %12.8f %12.8f %12.8f\n',y);
fclose(fid);
y=[w; CNH1_w];
fid=fopen('CNH1_w.txt','w');
fprintf(fid,'%12.8f %12.8f %12.8f %12.8f\n',y);
fclose(fid);
y=[w; DCNH1alt1_w; DCNH1alt2_w; DCNH1alt3_w];
fid=fopen('DCNH1_w.txt','w');
fprintf(fid,'%12.8f %12.8f %12.8f %12.8f %12.8f %12.8f %12.8f %12.8f %12.8f
%12.8f\n',y);
fclose(fid);
y=[w; DCH1alt1_w; DCH1alt2_w; DCH1alt3_w];
fid=fopen('DCH1_w.txt','w');
fprintf(fid,'%12.8f %12.8f %12.8f %12.8f %12.8f %12.8f %12.8f %12.8f %12.8f
%12.8f\n',y);
fclose(fid);

```

I.2 Selection of Diagonal Control Structure Configuration

I.2.1 MATLAB® Script for Stability Analysis

An example of the MATLAB® scripts used to analyse system stability is provided below. The calculated system poles and zeros are given in Table I.2.1.

```
% Program Stability.m
% Determines the system poles and zeros for CO2 train #1 at high gas throughput
%
clear
%
% Process gain, time constant and dead time matrices
KpH1=[1.1695 -0.9885; 1.0881 -0.0262];
TpH1=[8.2231 13.1691; 1.6168 16.0241];
DTH1=[0.1667 0.6667; 0.1667 0.8333];
%
for i=1:2
    for j=1:2
        % Find 3rd order Pade approximations for dead times
        [DTH1num(i,:,j),DTH1den(i,:,j)]=pade(DTH1(i,j),3);
        %
        % Create system transfer function matrices
        GpH1(i,j)=tf(KpH1(i,j)*DTH1num(i,:,j),conv([TpH1(i,j) 1],DTH1den(i,:,j)));
    end
end
%
% Obtain state-space model coefficient matrices
% and calculate system poles and zeros
[AH1,BH1,CH1,DH1]=ssdata(GpH1);
PH1=eig(AH1)
ZH1=tzero(AH1,BH1,CH1,DH1)
```

Table I.2.1: System poles and zeros for the SGC-RSF control structure.

	CO ₂ Train #1			CO ₂ Train #7		
	High Gas Throughput	Medium Gas Throughput	Low Gas Throughput	High Gas Throughput	Medium Gas Throughput	Low Gas Throughput
System Poles	-0.12	-0.07	-0.04	-0.23	-0.10	-0.05
	-0.62	-0.43	-0.36	-0.48	-0.36	-0.34
	-22.06±21.05i	-22.06±21.05i	-22.06±21.05i	-22.06±21.05i	-22.06±21.05i	-22.06±21.05i
	-27.86	-27.86	-27.86	-27.86	-27.86	-27.86
	-5.52±5.26i	-5.52±5.26i	-5.52±5.26i	-5.52±5.26i	-5.52±5.26i	-5.52±5.26i
	-6.97	-6.97	-6.97	-6.97	-6.97	-6.97
	-0.08	-0.06	-0.05	-0.10	-0.07	-0.05
	-4.41±4.21i	-4.41±4.21i	-4.41±4.21i	-11.03±10.53i	-11.03±10.53i	-11.03±10.53i
	-5.57	-5.57	-5.57	-13.93	-13.93	-13.93
	-0.06	-0.05	-0.05	-0.10	-0.07	-0.06
System Zeros	-4.41±4.20i	-4.41±4.20i	-4.41±4.21i	-15.33	-11.27±10.34i	-11.09±10.48i
	-5.57	5.52±5.26i	-5.57	-11.83±9.70i	-14.25	-14.01
	5.53±5.26i	6.97	5.52±5.26i	5.89±4.90i	5.61±5.16i	5.54±5.24i
	6.97	-5.57	6.97	6.18	6.77	6.92
	-0.06	-0.05	-0.05	-0.09	-0.07	-0.06
	-0.12	-0.07	-0.04	-0.21	-0.09	-0.05
	22.06±21.05i	22.06±21.05i	22.06±21.05i	22.06±21.05i	22.06±21.05i	22.06±21.05i
	27.86	27.86	27.86	27.86	27.86	27.86

I.2.2 MATLAB® Script for RGA Calculations

An example of the MATLAB® scripts used for the RGA calculations is provided below.

```
% Program RGA.m
% Calculates the RGA for CO2 train #1 at high gas throughput
%
clear
%
% Process gain, time constant and dead time matrices for SGC-RSF control structure
KpH1=[1.1695 -0.9885; 1.0881 -0.0262];
TpH1=[8.2231 13.1691; 1.6168 16.0241];
DTH1=[0.1667 0.6667; 0.1667 0.8333];
%
for i=1:2
    for j=1:2
        % 3rd order Pade approximations for dead times
        [DTH1num(i,:,j),DTH1den(i,:,j)]=pade(DTH1(i,j),3);
        %
        % Process transfer functions
        GpH1(i,j)=tf(KpH1(i,j)*DTH1num(i,:,j),conv([TpH1(i,j) 1],DTH1den(i,:,j)));
    end
end
%
% Steady-state RGA
RGAH1=KpH1.*inv(KpH1).';
%
% Calculate RGA over frequency range and print to text file
w = logspace(-5,2,100);
%
GpH1_w=freqresp(GpH1,w);
%
for i=1:length(w)
    RGAH1_w(:,:,i)=GpH1_w(:,:,i).*inv(GpH1_w(:,:,i)).';
end
%
for i=1:2
    RGAH1r1(i,:)=sign(RGAH1(1,i))*abs(RGAH1_w(1,i,:));
    RGAH1r2(i,:)=sign(RGAH1(2,i))*abs(RGAH1_w(2,i,:));
end
%
y=[w; RGAH1r1; RGAH1r2];
fid=fopen('RGAH1_w.txt','w');
fprintf(fid,'%12.8f %12.8f %12.8f %12.8f %12.8f\n',y);
fclose(fid);
```

I.2.3 MATLAB® Script for Stability Index Calculations

An example of the MATLAB® scripts used for the stability index calculations is provided below.

```
% Program StabilityIndices.m
% Completes variable pairing analysis for CO2 Train #1 at high gas throughput
% Calculates NI and MIC stability indices
%
clear
%
% Reordered process gain matrices for SGC-RSF control structure
% i.e. paired variables according to RGA along diagonal
KpH1=[-0.9885 1.1695; -0.0262 1.0881];
%
%
% Reordered process gain matrices with positive diagonal elements
KpH1p=[0.9885 1.1695; 0.0262 1.0881];
%
% Calculate NI values
NIH1=det(KpH1)/(KpH1(1,1)*KpH1(2,2))
%
% Determine eigenvectors and eigenvalues for positive diagonal gain matrices
[KpH1pEVec, KpH1pEVal] = eig(KpH1p);
%
% Calculate MIC values
MICH1=diag(KpH1pEVal)
```

I.3 Analysis of Diagonal Control Structure Performance

An example of the MATLAB® scripts used for the PRGA and CLDG calculations is provided below.

```

% Program PerformanceAnalysis.m
% Analyses performance of control structure for CO2 Train #1 at high gas throughput
% Calculates PRGA and CLDG
%
clear
%
% Reordered process gain, time constant and dead time matrices
% i.e. paired variables according to RGA along diagonal
KpH1=[-0.9885 1.1695; -0.0262 1.0881];
TpH1=[13.1691 8.2231; 16.0241 1.6168];
DTH1=[0.6667 0.1667; 0.8333 0.1667];
%
% Disturbance gain, time constant and dead time vectors
KdH1=[0.5757; -0.0735];
TpdH1=[6.1206; 3.4381];
DTdH1=[0.1667; 0.1667];
%
for i=1:2
    for j=1:2
        % 3rd order Pade approximations for dead times
        [DTH1num(i,:,j),DTH1den(i,:,j)]=pade(DTH1(i,j),3);
        [DTdH1num(i,:),DTdH1den(i,:)]=pade(DTdH1(i),3);
        %
        % Process and disturbance transfer functions
        GpH1(i,j)=tf(KpH1(i,j)*DTH1num(i,:,j),conv([TpH1(i,j) 1],DTH1den(i,:,j)));
        GdH1(i,1)=tf(KdH1(i)*DTdH1num(i,:),conv([TpdH1(i) 1],DTdH1den(i,:)));
    end
end
%
% Steady-state PRGA and CLDG
PRGAH1=diag(diag(KpH1))*inv(KpH1)
CLDGH1=PRGAH1*KdH1
%
% Frequency analysis
w=logspace(-5,2,100);
%
% Evaluate process and disturbance transfer functions over frequency range
GpH1_w=freqresp(GpH1,w);
GdH1_w=freqresp(GdH1,w);
%
% Calculate PRGA and CLDG over frequency range and print to text file
for i=1:length(w)
    % PRGA
    PRGAH1_w(:, :, i)=diag(diag(GpH1_w(:, :, i)))*inv(GpH1_w(:, :, i));
    %
    for j=1:2
        PRGAH1r1_w(j,i)=PRGAH1_w(1,j,i);
        PRGAH1r2_w(j,i)=PRGAH1_w(2,j,i);
    end
    %
    % CLDG
    CLDGH1_w(:,i)=PRGAH1_w(:, :, i)*GdH1_w(:, :, i);
end
y=[w; PRGAH1r1_w; PRGAH1r2_w
fid=fopen('PRGAH1_w.txt','w');
fprintf(fid,'%12.8f %12.8f %12.8f %12.8f %12.8f\n',y);
fclose(fid);
y=[w; CLDGH1_w];
fid=fopen('CLDGH1_w.txt','w');
fprintf(fid,'%12.8f %12.8f %12.8f\n',y);
fclose(fid);

```


I.4 BLT Tuning

An example of the MATLAB® scripts used to perform BLT tuning is provided below.

```
% Program BLT.m
% Performs BLT tuning for CO2 Train #1 at high gas throughput
%
clear
%
% Reordered process gain, time constant and dead time matrices
% i.e. paired variables according to RGA along diagonal
KpH1=[-0.9885 1.1695; -0.0262 1.0881];
TpH1=[13.1691 8.2231; 16.0241 1.6168];
DTH1=[0.6667 0.1667; 0.8333 0.1667];
%
% Ziegler-Nichols PI settings
KcZNH1=diag([-14.3942 7.2173]);
TiZNH1=diag([1.1883 0.2914]);
%
% Set up tuning parameters
i=sqrt(-1);
w=logspace(-3,2,500);
s=i*w;
f=2.1;
df=0.01;
loop=0;
flagm=-1;
flagp=-1;
dbmax=-100;
%
for i=1:2
    for j=1:2
        % 3rd order Pade approximations for dead times
        [DTH1num(i,:,j),DTH1den(i,:,j)]=pade(DTH1(i,j),3);
        [DTdH1num(i,:),DTdH1den(i,:)]=pade(DTdH1(i),3);
        %
        % Process transfer functions
        GpH1(i,j)=tf(KpH1(i,j)*DTH1num(i,:,j),conv([TpH1(i,j) 1],DTH1den(i,:,j)));
    end
end
%
% BLT tuning: vary f until dbmax=4 (because 2x2 system)
while abs(dbmax-4)>0.01
    KcH1=KcZNH1/f;
    TiH1=TiZNH1*f;
    %
    % Controller transfer function
    for i=1:2
        GcH1(i,i)=tf(KcH1(i,i)*[TiH1(i,i) 1],[TiH1(i,i) 0]);
    end
    %
    % Evaluate Gp and Gc over frequency range
    GpH1_w=freqresp(GpH1,w);
    GcH1_w=freqresp(GcH1,w);
    %
    % Calculate W function
    for i=1:length(w)
        WnyquistH1(i)=-1+det(eye(2)+GpH1_w(:, :, i)*GcH1_w(:, :, i));
        lc(i)=WnyquistH1(i)/(1+WnyquistH1(i));
        dbcl(i)=20*log10(abs(lc(i)));
    end
    %
    % Identify peak in closed-loop log modulus
    [dbmax,nmax]=max(dbcl);
    wmax=w(nmax);
    %
end
```

```
loop=loop+1;
if loop>50, break, end
%
% Test if +4 dB criterion is satisfied, if not get new value for f
if dbmax>4
    if flagp>0
        df=df/2;
    end
    flagm=1;
    f=f+df;
else
    if flagm>0
        df=df/2;
    end
    flagp=1;
    f=f-df;
    if f<1
        f=1;
    end
end
end
end
%
% Output to screen
loop, dbmax, f, KcH1, TiH1
%
% Output to text file
y=[w; real(WnyquistH1); imag(WnyquistH1)];
fid=fopen('WnyquistH1.txt','w');
fprintf(fid,'%12.8f %12.8f %12.8f\n',y);
fclose(fid);
```

I.5 Diagonal Control Structure Dynamic Simulations

I.5.1 MATLAB® Script for Dynamic Simulations

An example of the MATLAB® scripts used to perform the dynamic simulations of the RGF-RSF diagonal control structure is provided below.

```
% DynSim1.m
% Performs dynamic simulations for CO2 train #1 at high gas throughput
%
clear
%
% Reordered process gain, time constant and dead time matrices
% i.e. paired variables according to RGA along diagonal
KpH1=[-0.9885 1.1695; -0.0262 1.0881];
TpH1=[13.1691 8.2231; 16.0241 1.6168];
DTH1=[0.6667 0.1667; 0.8333 0.1667];
%
% Disturbance gain, time constant and dead time vectors
KdH1=[0.5757; -0.0735];
TpdH1=[6.1206; 3.4381];
DTdH1=[0.1667; 0.1667];
%
% BLT tuned controller settings for reordered system
% Include settings for medium and low gas throughput
KcH1=diag([-6.7578 3.3884]);
KcM1=diag([-7.5029 4.1056]);
KcL1=diag([-8.1480 4.3767]);
TiH1=diag([2.5311 0.6207]);
TiM1=diag([2.9964 0.7399]);
TiL1=diag([3.3639 0.8320]);
%
for i=1:2
    for j=1:2
        % 3rd order Pade approximations for dead times
        [DTH1num(i,:,j),DTH1den(i,:,j)]=pade(DTH1(i,j),3);
        [DTdH1num(i,:),DTdH1den(i,:)]=pade(DTdH1(i),3);
        %
        % Process, disturbance and controller transfer functions
        GpH1(i,j)=tf(KpH1(i,j)*DTH1num(i,:,j),conv([TpH1(i,j) 1],DTH1den(i,:,j)));
        GdH1(i,1)=tf(KdH1(i)*DTdH1num(i,:),conv([TpdH1(i) 1],DTdH1den(i,:)));
        GcH1(i,i)=tf(KcH1(i,i)*[TiH1(i,i) 1],[TiH1(i,i) 0]);
        GcM1(i,i)=tf(KcM1(i,i)*[TiM1(i,i) 1],[TiM1(i,i) 0]);
        GcL1(i,i)=tf(KcL1(i,i)*[TiL1(i,i) 1],[TiL1(i,i) 0]);
    end
end
%
w=logspace(-5,2,100);
%
% Evaluate process, disturbance and controller transfer functions over frequency
range
GpH1_w=freqresp(GpH1,w);
GdH1_w=freqresp(GdH1,w);
GcH1_w=freqresp(GcH1,w);
GcM1_w=freqresp(GcM1,w);
GcL1_w=freqresp(GcL1,w);
%
% Calculate system loop transfer functions and output to text file
for i=1:length(w)
    for j=1:2
        % Using H controller settings
        LH1H_w(j,i)=GcH1_w(j,j,i)*GpH1_w(j,j,i);
        %
        % Using M controller settings
        LH1M_w(j,i)=GcM1_w(j,j,i)*GpH1_w(j,j,i);
    end
end
```

```

        %
        % Using L controller settings
        LH1L_w(j,i)=GcL1_w(j,j,i)*GpH1_w(j,j,i);
    end
end
y=[w; LH1H_w];
fid=fopen('LH1H_w_v4.txt','w');
fprintf(fid,'%12.8f %12.8f %12.8f\n',y);
fclose(fid);
y=[w; LH1M_w];
fid=fopen('LH1M_w_v4.txt','w');
fprintf(fid,'%12.8f %12.8f %12.8f\n',y);
fclose(fid);
y=[w; LH1L_w];
fid=fopen('LH1L_w_v4.txt','w');
fprintf(fid,'%12.8f %12.8f %12.8f\n',y);
fclose(fid);
%
% Consider step response to unit setpoint change
% Closed-loop transfer functions with H controller settings
GclH1H=inv(eye(2)+GpH1*GcH1)*GpH1*GcH1;
%
% Closed-loop transfer functions with M controller settings
GclH1M=inv(eye(2)+GpH1*GcM1)*GpH1*GcM1;
%
% Closed-loop transfer functions with L controller settings
GclH1L=inv(eye(2)+GpH1*GcL1)*GpH1*GcL1;
%
T=[0:0.05:60];
%
% H controller settings
[YH1H,T]=step(GclH1H,T);
%
% M controller settings
[YH1M,T]=step(GclH1M,T);
%
% L controller settings
[YH1L,T]=step(GclH1L,T);
%
for i=1:length(T)
    for j=1:2
        YH1Hr1(j,i)=YH1H(i,1,j);
        YH1Hr2(j,i)=YH1H(i,2,j);
        %
        YH1Mr1(j,i)=YH1M(i,1,j);
        YH1Mr2(j,i)=YH1M(i,2,j);
        %
        YH1Lr1(j,i)=YH1L(i,1,j);
        YH1Lr2(j,i)=YH1L(i,2,j);
    end
end
end
%
% Output to text file
y=[T; YH1Hr1; YH1Hr2];
fid=fopen('StepH1H.txt','w');
fprintf(fid,'%12.8f %12.8f %12.8f %12.8f %12.8f\n',y);
fclose(fid);
y=[T; YH1Mr1; YH1Mr2];
fid=fopen('StepH1M.txt','w');
fprintf(fid,'%12.8f %12.8f %12.8f %12.8f %12.8f\n',y);
fclose(fid);
y=[T; YH1Lr1; YH1Lr2];
fid=fopen('StepH1L.txt','w');
fprintf(fid,'%12.8f %12.8f %12.8f %12.8f %12.8f\n',y);
fclose(fid);
%
% Consider step response to unit disturbance
% Closed-loop transfer functions with H controller settings

```

```
GcldH1H=inv(eye(2)+GpH1*GcH1)*GdH1;
%
% Closed-loop transfer functions with M controller settings
GcldH1M=inv(eye(2)+GpH1*GcM1)*GdH1;
%
% Closed-loop transfer functions with L controller settings
GcldH1L=inv(eye(2)+GpH1*GcL1)*GdH1;
%
T=[0:0.05:60];
%
% H controller settings
[YdH1H,T]=step(GcldH1H,T);
%
% M controller settings
[YdH1M,T]=step(GcldH1M,T);
%
% L controller settings
[YdH1L,T]=step(GcldH1L,T);
%
for i=1:length(T)
    for j=1:2
        YdH1Hr1(j,i)=YdH1H(i,j);
        YdH1Mr1(j,i)=YdH1M(i,j);
        YdH1Lr1(j,i)=YdH1L(i,j);
    end
end
%
% Output to text file
y=[T'; YdH1Hr1];
fid=fopen('StepdH1H.txt','w');
fprintf(fid,'%12.8f %12.8f %12.8f\n',y);
fclose(fid);
y=[T'; YdH1Mr1];
fid=fopen('StepdH1M.txt','w');
fprintf(fid,'%12.8f %12.8f %12.8f\n',y);
fclose(fid);
y=[T'; YdH1Lr1];
fid=fopen('StepdH1L.txt','w');
fprintf(fid,'%12.8f %12.8f %12.8f\n',y);
fclose(fid);
```

I.5.2 Step Response Curves

The step response curves for the RGF-RSF diagonal control structure for CO₂ trains #1 and #7 at the medium and low gas throughput conditions are given below.

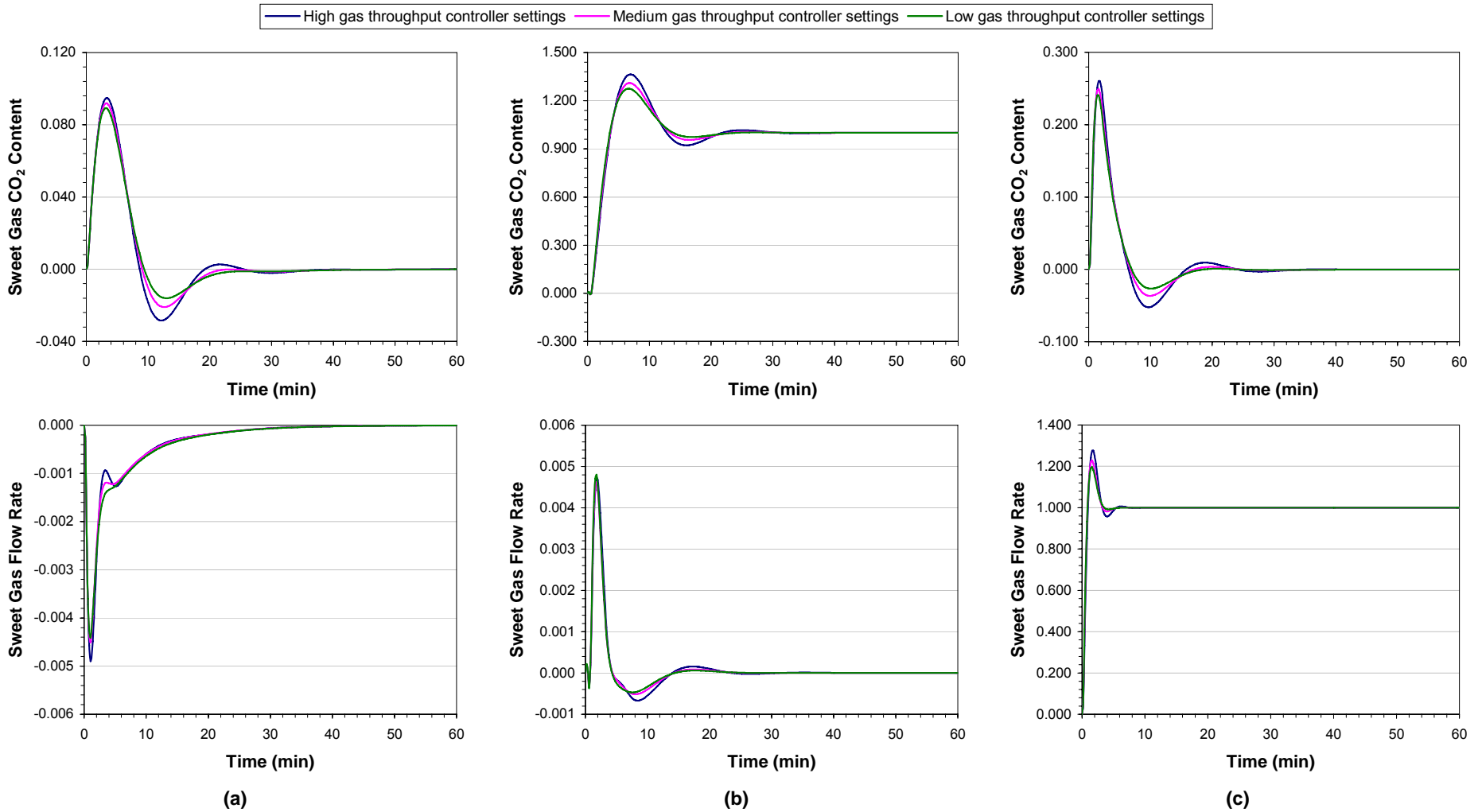


Figure I.5.1: CO₂ train #1 closed-loop step response curves at the medium gas throughput conditions. (a) Unit magnitude change in the raw gas CO₂ content at 0 min. (b) Unit magnitude change in the sweet gas CO₂ content setpoint at 0 min. (c) Unit magnitude change in the sweet gas flow rate setpoint at 0 min.

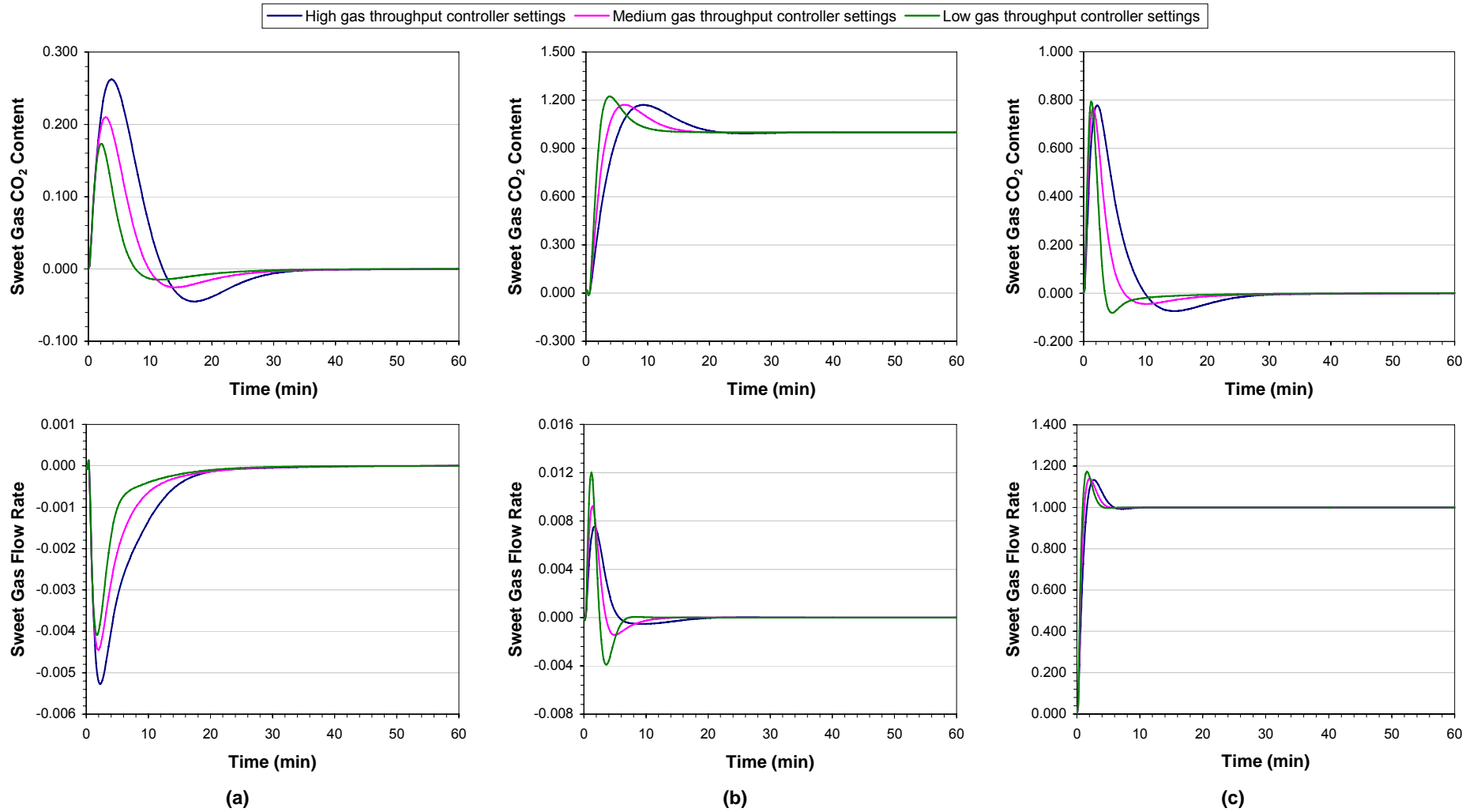


Figure I.5.2: CO₂ train #7 closed-loop step response curves at the medium gas throughput conditions. (a) Unit magnitude change in the raw gas CO₂ content at 0 min. (b) Unit magnitude change in the sweet gas CO₂ content setpoint at 0 min. (c) Unit magnitude change in the sweet gas flow rate setpoint at 0 min.

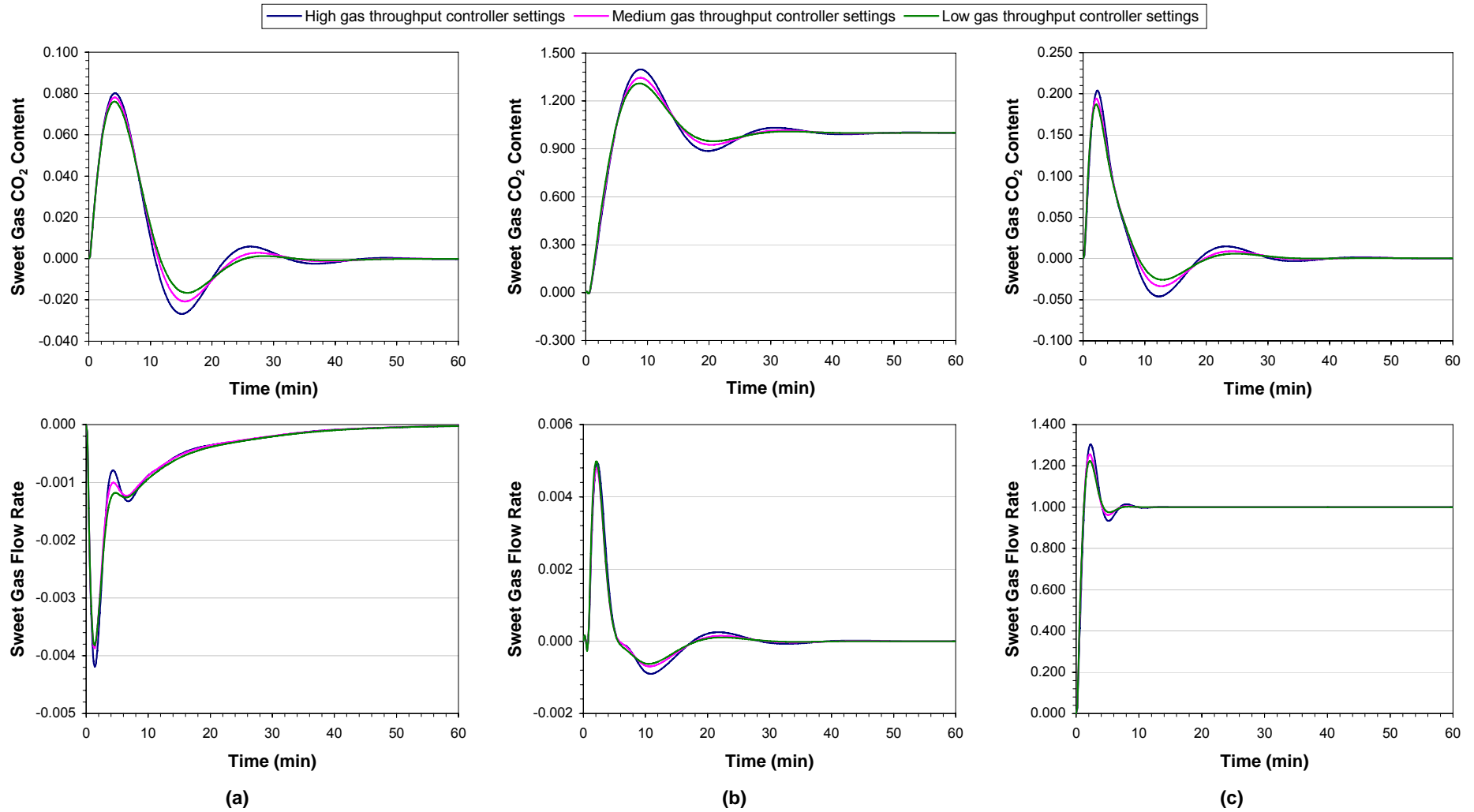


Figure I.5.3: CO₂ train #1 closed-loop step response curves at the low gas throughput conditions. (a) Unit magnitude change in the raw gas CO₂ content at 0 min. (b) Unit magnitude change in the sweet gas CO₂ content setpoint at 0 min. (c) Unit magnitude change in the sweet gas flow rate setpoint at 0 min.

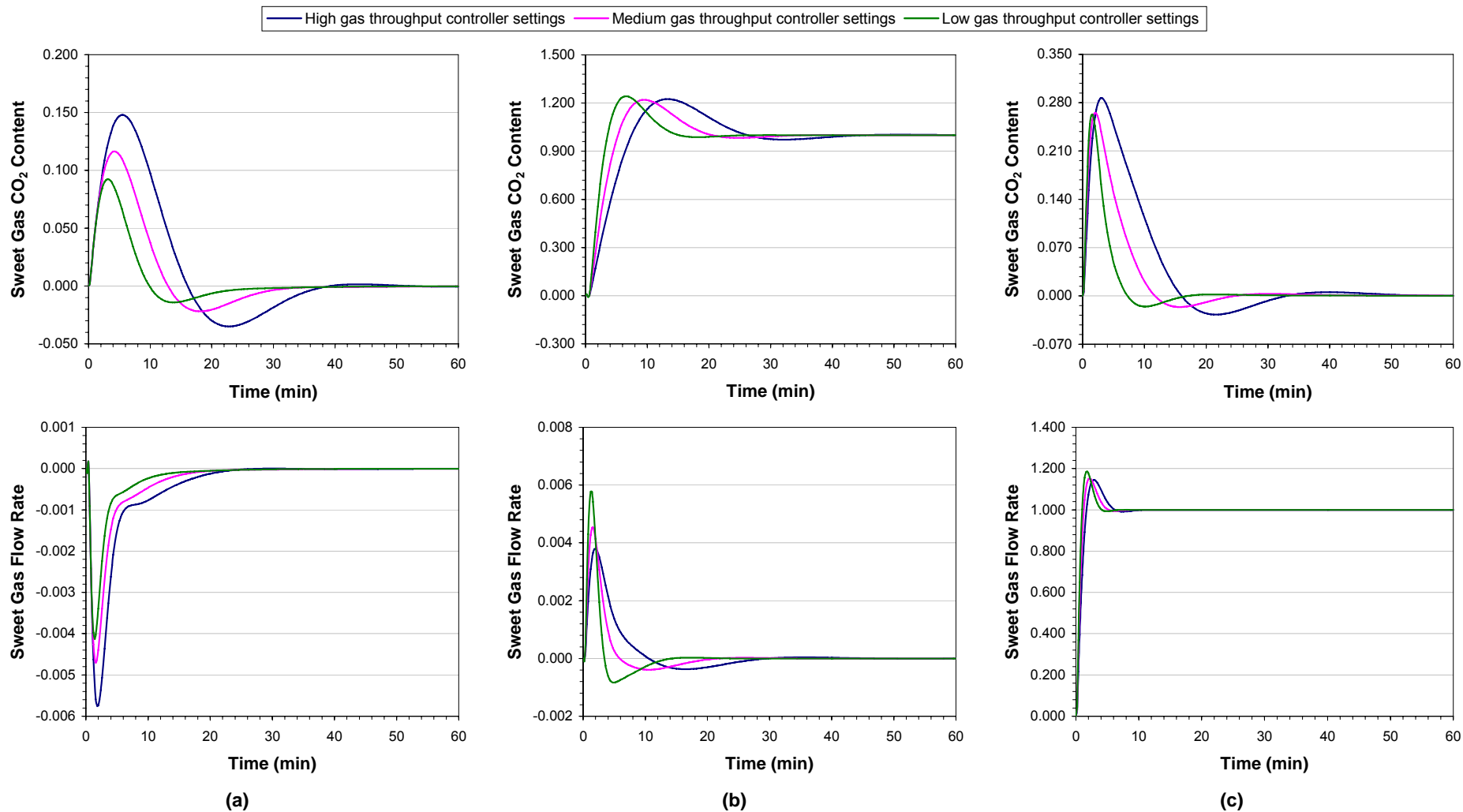


Figure I.5.4: CO₂ train #7 closed-loop step response curves at the low gas throughput conditions. (a) Unit magnitude change in the raw gas CO₂ content at 0 min. (b) Unit magnitude change in the sweet gas CO₂ content setpoint at 0 min. (c) Unit magnitude change in the sweet gas flow rate setpoint at 0 min.